

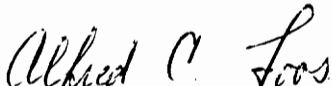
**A FINITE ELEMENT CURE MODEL AND CURE CYCLE OPTIMIZATION
FOR COMPOSITE STRUCTURES**

by

Nagendra Somanath

Thesis submitted to the Faculty of the
Virginia Polytechnic Institute and State University
in partial fulfillment of the requirements for the degree of
Master of Science
in
Engineering Mechanics


APPROVED:



Alfred C. Loos, Chairman



Charles E. Knight Jr



Scott L. Hendricks



Zafer Gurdal

26 October 1987.

Blacksburg, Virginia

2

LD
5655
V855
1987
S422
C. 2

A FINITE ELEMENT CURE MODEL AND CURE CYCLE OPTIMIZATION FOR COMPOSITE STRUCTURES

by

Nagendra Somanath

Alfred C. Loos, Chairman

Engineering Mechanics

(ABSTRACT)

A one-dimensional cylindrical cure model was developed to describe the curing process of an axisymmetric filament wound composite structure. For a specified cure cycle, the cure model can be used to calculate the temperature distribution, the degree of cure of the resin, and the resin viscosity inside the composite case. Solutions to the cylindrical cure model were obtained numerically using the finite element technique.

The cylindrical cure model was verified by measuring the temperature distribution in a small 5.75 inch graphite - epoxy test bottle. The data were compared with the results calculated with the computer code for conditions employed in the tests. Good agreement was found between the data and the results of the computer code. The error between the experimental data and the results of the computer code was less than 10 %.

A cure cycle optimization problem is formulated for the curing process using a calculus of variations approach. The optimum cure cycle should tailor the temperature in the composite such that a uniform temperature and degree of cure distribution is achieved in the composite while minimizing the reaction exotherms and thermal lag.

Cure simulations of an one inch thick graphite - epoxy composite case predict a minimization of the reaction exotherms and the thermal lag. The the final process time needed to achieve uniform degree of cure and uniform temperature distribution in the composite is also predicted. The resultant cure cycle appears to approach the boundary temperatures specified as limits on the cure cycle temperature.

Acknowledgements

I owe many thanks to my advisor, Dr. Alfred Loos, whose advice and active support has been invaluable throughout my graduate career. I would like to thank Dr C.E. Knight Jr, Dr S.L. Hendricks and Dr Z. Gurdal for serving on my committee and for making several helpful suggestions. I would like to take this opportunity to thank all my friends for their help and advice.

This material is based on work supported by the Virginia Center for Innovative Technology Grant # MAT - 85 - 013 - 03 and Morton Thiokol, Inc., (Aerospace Group), Ogden, Utah.

Table of Contents

CHAPTER 1 2

INTRODUCTION 2

 1.1 Curing Process Modeling of Epoxy Matrix Composites 3

 1.2 Curing Process Control & Optimization 5

 1.3 Objectives 7

CHAPTER 2 9

CURING PROCESS - PROBLEM IDENTIFICATION 9

 2.1 Winding Process 9

 2.2 Preparation For Cure 10

 2.3 Curing Process 13

 2.4 Processing Cycle Identification 13

 2.5 Cylindrical Cure Model - Analysis 15

 2.6 Cylindrical Cure Model - Submodel Identification 16

 2.7 Submodel - I : HEAT TRANSFER MODEL 17

 2.8 Submodel - II : CURE KINETICS MODEL 18

 2.9 Submodel - III : VISCOSITY MODEL 20

2.10 Spatial Boundary Conditions	21
2.11 Initial Conditions	22
2.12 Material Properties	23
2.13 Method of Solution	27
CHAPTER 3	28
FINITE ELEMENT FORMULATION	28
3.1 Domain Discretization	29
3.2 Variational Formulation	31
3.3 Shape Functions and Finite Element Discretization	34
3.4 Direct Time Integration	37
3.5 Degree of Cure Estimation	39
3.6 Numerical Solution Procedure	39
CHAPTER 4	41
COMPARISON STUDIES & VALIDATION	41
4.1 Comparison Studies	42
4.2 Axisymmetric Cure Model	42
4.3 Experimental	46
4.4 Results	52
4.5 Cure Simulation Model Results	54
CHAPTER 5	77
CURING PROCESS OPTIMAL CONTROL	77
5.1 Effects of Processing Environment	78
5.2 State, Co-state & Control Variables	79
5.3 Constraints & Stopping Conditions	80
5.4 Constraint Specifications	81

CHAPTER 6	91
OPTIMAL CURE CYCLE IDENTIFICATION	91
6.1 Equation Of State For Control	92
6.2 Co-state Equation	95
6.3 Initial Conditions	95
6.4 Hamiltonian Functions	96
6.5 Transversality Conditions	98
6.3 Minimum Principle	104
6.4 First Order Gradient Method	105
6.5 Computational Algorithm	106
 CHAPTER 7	 117
OPTIMUM CURE CONTROL CYCLE	117
7.1 Optimal Control : Linear Diffusion Problem	118
7.2 Cure Cycle Optimization	121
7.3 Design Cure Window	125
7.4 Optimal Cure Simulation : Case - 1	127
7.5 Optimal Cure Simulation : Case - 2	142
7.6 Optimal Cure Simulation : Case - 3	156
7.7 Optimal Cure Simulation : Case - 4	164
 CHAPTER 8	 170
IN CONCLUSION	170
8.1 Curing Process in Filament Wound Composites	170
8.2 Curing Process Optimal Control	172
8.3 Future Research	174
 BIBLIOGRAPHY	 175

Appendix A. VARIATION OF REACTION RATE 181

Appendix B. CURE RATE DERIVATIVES 184

Appendix C. VARIATION OF VISCOSITY 186

Appendix D. CLASSICAL HEAT TRANSFER 188

Vita 191

List of Illustrations

Figure 1. LATHE TYPE FILAMENT WINDER. 11

Figure 2. FILAMENT WOUND COMPOSITE - Geometry 12

Figure 3. FILAMENT WOUND COMPOSITE - End View 14

Figure 4. BLOCK DIAGRAM OF FWC CYLINDRICAL CURE MODEL 24

Figure 5. FINITE ELEMENT MODEL - Domain Discretization 30

Figure 6. FINITE ELEMENT MODEL - Generalized Coordinates 32

Figure 7. GEOMETRY and FINITE ELEMENT MESH 44

Figure 8. AXISYMMETRIC HEAT TRANSFER 45

Figure 9. MANDREL SCHEMATIC 47

Figure 10. FWC ASSEMBLY (END VIEW) 50

Figure 11. FINITE ELEMENT MESH and BOUNDARY CONDITIONS 51

Figure 12. AXISYMMETRIC CURE MODEL - Temperature vs Time (5.75 in Bottle) 53

Figure 13. AXISYMMETRIC CURE MODEL - Degree of Cure vs Time 55

Figure 14. AXISYMMETRIC CURE MODEL - Log Viscosity vs Time (5.75 in Bottle) 56

Figure 15. CURE CYCLE 59

Figure 16. AXISYMMETRIC CURE MODEL - Temperature vs Time (Thin Case) .. 62

Figure 17. TEMPERATURE DROP ACROSS THE CASE 63

Figure 18. AXISYMMETRIC CURE MODEL - Degree of Cure vs Time (Thin Case) 64

Figure 19. AXISYMMETRIC CURE MODEL - Degree of Cure vs Normalized Radius 65

Figure 20. AXISYMMETRIC CURE MODEL - Log Viscosity vs Time (Thin Case) . .	66
Figure 21. AXISYMMETRIC CURE MODEL - Temperature vs Time (Thick Case) .	68
Figure 22. TEMPERATURE DROP ACROSS THE CASE	69
Figure 23. AXISYMMETRIC CURE MODEL - Temperature vs Normalized Radius .	70
Figure 24. AXISYMMETRIC CURE MODEL - Degree of Cure vs Time (Thick Case)	71
Figure 25. AXISYMMETRIC CURE MODEL - Degree of Cure vs Normalized Radius	72
Figure 26. AXISYMMETRIC CURE MODEL - Log Viscosity vs Time (Thick Case) .	74
Figure 27. COMPARISON STUDIES - Degree of Cure vs Time	75
Figure 28. COMPARISON STUDIES - Log Viscosity vs Time	76
Figure 29. EXOTHERM REGION - Temperature vs Time	87
Figure 30. LAG REGION - Temperature vs Time	89
Figure 31. OPTIMAL CURE - Flow Chart	115
Figure 32. LINEAR DIFFUSION PROBLEM - Temperature vs Normalized Radius	120
Figure 33. LINEAR DIFFUSION PROBLEM - Control Cycle vs Time	122
Figure 34. LINEAR DIFFUSION PROBLEM - Objective vs Iterations	123
Figure 35. EXOTHERM MINIMIZATION - Temperature vs Time	129
Figure 36. EXOTHERM MINIMIZATION - Cure Cycles	131
Figure 37. EXOTHERM MINIMIZATION - Degree of Cure vs Time.	134
Figure 38. EXOTHERM MINIMIZATION - Temperature vs Normalized Radius. . .	135
Figure 39. EXOTHERM MINIMIZATION - Degree of Cure vs Normalized Radius.	136
Figure 40. EXOTHERM MINIMIZATION - Degree of Cure vs Time	138
Figure 41. EXOTHERM MINIMIZATION - Log Viscosity vs Time	139
Figure 42. EXOTHERM MINIMIZATION - Cure Rate Sensitivity Derivative vs Time	140
Figure 43. EXOTHERM MINIMIZATION - Cure Rate Sensitivity Derivative vs Time	141
Figure 44. EXOTHERM MINIMIZATION - Objective $J(r,t)$ vs Iterations	143
Figure 45. EXOTHERM & LAG MINIMIZATION - Temperature vs Time	145

Figure 46. EXOTHERM & LAG MINIMIZATION - Cure Cycles	146
Figure 47. EXOTHERM & LAG MINIMIZATION - Degree of Cure vs Time.	148
Figure 48. EXOTHERM & LAG MINIMIZATION - Log Viscosity vs Time.	149
Figure 49. EXOTHERM & LAG MINIMIZATION - Temperature vs Normalized Radius.	151
Figure 50. EXOTHERM & LAG MINIMIZATION - Degree of Cure vs Normalized Radius.	152
Figure 51. EXOTHERM & LAG MINIMIZATION - Degree of Cure vs Time	153
Figure 52. EXOTHERM & LAG MINIMIZATION - Log Viscosity vs Time	154
Figure 53. EXOTHERM & LAG MINIMIZATION - Cure Rate Sensitivity Derivative vs Time	155
Figure 54. EXOTHERM & LAG MINIMIZATION - Cure Rate Sensitivity Derivative vs Time	157
Figure 55. EXOTHERM & LAG MINIMIZATION - Objective $J(r,t)$ vs Iterations ...	158
Figure 56. DOUBLE STEP CURE CYCLE - Temperature vs Time	159
Figure 57. DOUBLE STEP CURE CYCLE - Cure Cycle	161
Figure 58. DOUBLE STEP CURE CYCLE - Degree of Cure vs Time	162
Figure 59. DOUBLE STEP CURE CYCLE - Log Viscosity vs Time	163
Figure 60. AL 6061 MANDREL - Temperature vs Time	165
Figure 61. AL 6061 MANDREL - Cure Cycle	166
Figure 62. AL 6061 MANDREL - Degree of Cure vs Time	168
Figure 63. AL 6061 MANDREL - Log Viscosity vs Time	169

List of Tables

Table 1. STEP BY STEP INTEGRATION PROCEDURE. 40

Table 2. MATERIAL PROPERTIES FOR 5.75" BOTTLE. 43

Table 3. INPUT PARAMETERS FOR PROGRAM "FEMCURE" 57

Table 4. MATERIAL PROPERTIES FOR 18" BOTTLE 58

Table 5. INPUT PARAMETERS FOR PROGRAM "CUREOPT". 116

Table 6. REACTION RATE CONSTANTS FOR FIBERITE 976. 183

Table 7. VISCOSITY CONSTANTS FOR FIBERITE 976. 187

To my parents, teachers and friends

CHAPTER 1

INTRODUCTION

The need for structural materials with greater strength - to - weight ratios has led to the development of fiber-reinforced composites. One technique that is commonly used to fabricate advanced composites is filament winding.

Filament winding technology is a manufacturing methodology wherein composite structures having shapes of bodies of revolution can be fabricated. This technique has been successfully used in the production of high strength, light weight tactical motor cases and pressure vessels. Some of the most recent achievements in filament winding technology include the reusable composite solid rocket motor case for the NASA Space Shuttle and the graphite / epoxy launch tubes for the MX missiles.

The advent of high specific strength prepregs with low coefficients of thermal expansion, [1,2], have lead to weight savings without compromising on structural performance. This was found highly attractive by the aerospace industry which placed stringent demands on precision, repeatability, and quality control of the finished product [3].

The principles underlying the fabrication of thin walled filament wound composite structures have been fairly well understood. However, recent attempts at producing large thick walled filament wound structures has seen little success. The primary reason for this failure lies in the most crucial yet least understood area of the manufacturing process, namely the relationship between winding process variables, the curing process, and the final mechanical performance of the structure.

1.1 Curing Process Modeling of Epoxy Matrix Composites

In order to comprehend the classical phenomena that forms the key to the manufacturing process it is of utmost importance to have a mathematical model that can effectively portray the thermal, physical, and chemical processes occurring during the cure. Pioneering work in this field was carried out by Springer [4,5] who proposed a fairly accurate characterization of the material behavior during the curing process of epoxy matrix composites. Significant contributions by Loos and Springer [6,7,8] have lead to the now often used Loos - Springer model. An integral part of the Loos -

Springer model is the kinetic and rheological studies carried out for the specific resin used in the composite. Lee et al.[9] and the more recent study by Dusi et al.[10] have contributed significantly towards the understanding of the resin behavior during curing. Earlier an attempt at understanding the transport processes of composites in the subcured state was carried out by Blankenship [11].

Needless to say, as the emphasis of composite research is shifted towards processing in order to improve composite properties and reliability, a clear understanding of the transport phenomena occurring during cure is essential.

The mechanical properties of a composite (i.e., interlaminar strength, compressive strength, fatigue performance, and shear modulus) depend to a great extent on the type of resin and fiber used for the composite, as well as, on the processing cycle. Johnson and Owston [12] studied the effect of cure cycle on mechanical properties using Weibull analysis. They concluded that the mechanical properties of a composite system depend on the cure cycle, and in order to obtain an optimum value of a particular mechanical property, there is an optimum curing time for any curing temperature. The effect of the matrix resin on composite on composite processing studied by Hayes [13]. Aylward et al.[14] analyzed the effects of undercure and thermal degradation in pultruded laminate processing. Young and Lloyd [15] and Munjal [1,2] studied the characterization of filament wound composites, with specific emphasis on the use of fiber - reinforced composites in the rocket motor industry. Munjal et al.[3] identified from empirical studies, the effects of composite geometry on processing. It was concluded from available data, that property degradation due to geometry changes and scaling was very apparent and affected the structural performance of large composite structures. It was recognized by Young and Lloyd

[15] that the quality of high performance pressure vessels, and other aerospace composite components are highly process dependent.

Almost all studies revealed the fact that the effect of processing on fiber dominated properties like tensile strength and elastic modulus, was very small. On the other hand, the effect of improper processing on resin dominated properties like transverse tensile strength, compressive strength, and shear strength, resulted in higher degradation.

1.2 Curing Process Control & Optimization

Process methodology for filament wound composite structures is still in its infancy. Present day methods are highly empirical. Processing cycles are often chosen by an educated guess or by trial and error experimentation using small subscale parts. Experience has shown that large filament wound composite structures processed by using cure cycles developed for subscale parts are often cured nonuniformly with a high void content resulting in degradation of mechanical properties.

Of particular interest is the search for an optimal processing cycle capable of producing a composite that has the desired properties satisfying the stringent demands placed on the dimensional stability, strength, and final structural performance. This has been an aspect of composite processing that has been largely neglected.

The phenomena of heat transfer in a solid is described by the well known Fourier heat conduction equation. The heat transfer process, described by a parabolic type of partial differential equation, is governed by regulating the temperature at one or more spatial boundaries. Systems described by partial differential equations, with two or more variables are called distributed parameter systems (DPS).

Scant attention has been paid to optimization problems in distributed parameter systems where the state of the system is a function of two or more variables. The state of the system, namely the temperature, is space and time dependent. Little has been done to extend the pioneering work of Butkovskii [17] and Sakawa [18] on optimal control in distributed parameter systems. Denn et al.[19] used the calculus of variations approach to generate Green's functions to address the Sakawa boundary control problem. Denn [20] also applied a Green's function approach to optimize the mass diffusion process of a nonlinear distributed system consisting of a packed, tubular reactor with radial diffusion and a single reversible reaction. Chen and Seinfeld [21] and Seinfeld [22] addressed the estimation and identification of parameters in systems governed by parabolic partial differential equations using a dynamic programming approach. Tzafestas and Nightingale [23] developed a direct, distributed stochastic control theory based on a version of Pontryagin's minimum principle, and derived the Hamilton - Jacobi equation. Recently, Nakamichi and Washizu [24] applied the finite element method to solve a typical optimal control problem by applying a stationary variational principle. Ray and Gupta [25] extended the ideas of Denn [19,26] applied to optimal control in packed tubular reactors by considering process end point constraints and stopping conditions.

Surprisingly, only a few papers treated the nonlinear optimal boundary control problem in distributed parameter systems, and no papers were found in the literature addressing the optimal boundary control and estimation problem in distributed parameter systems having state constraints, variable properties, and constraints on the control.

1.3 Objectives

The current challenge is to make advanced composites having desired prespecified properties and improve our understanding of fabrication of filament wound composite structures. The motivation for this study arises from two significant and challenging aspects of composite processing. First, an increased emphasis on understanding the curing process of filament wound composites. Second, to try and seek a logical method of analysis and design of an optimal processing cycle.

The objectives of this study can be summarized as :

1. To seek a better understanding of the phenomena of curing in filament wound composite structures.
2. To develop a mathematical model to simulate the thermal, physical, and chemical behavior of filament wound composites during cure.

3. To develop a design strategy to achieve prespecified properties in the composite on completion of the curing process.
4. To minimize and control reaction exotherms in thick-section composites during cure.
5. To develop a processing cycle that will enable us to achieve an optimally cured filament wound composite in the minimum process time.

CHAPTER 2

CURING PROCESS - PROBLEM IDENTIFICATION

To clearly understand the curing process, it is of primary interest to formulate the problem in terms that are amenable to the construction of mathematical models of individual sub phenomenon that occur at different stages of the process.

2.1 Winding Process

Consider a mandrel - insulator assembly mounted on a shaft of a computer controlled, multiaxis, general purpose lathe type filament winder (Figure 1) rotating at a predetermined angular velocity " ω ". The composite case is formed by winding con-

tinuous bands of resin impregnated fibers over the surface of an elastomeric insulator [27,28]. The feed head (Figure 1) moves back and forth along a path parallel to the axis of the mandrel, with a controlled speed " V ". The winding pattern depends on the predetermined controlled motion of the carriage drive, mandrel angular velocity, and mandrel geometry.

Initially the resin is uncured. However, upon exposure to ambient temperature during the winding process, the fiber bands preimpregnated with resin begin to cure. On completion of the winding process two material phases, the solid fibers and the soft partially cured resin, coexist in the composite case.

2.2 Preparation For Cure

After winding the case, the entire mandrel - insulator - case assembly is prepared for curing by wrapping a porous release cloth and a porous breather cloth (the outer layer shown in Figure 2) around the outer surface of the case.

The entire assembly is then encased in a vacuum bag. When the vacuum system is activated, the bag is drawn tightly around the entire assembly allowing for the compaction of the outer layers of the case.

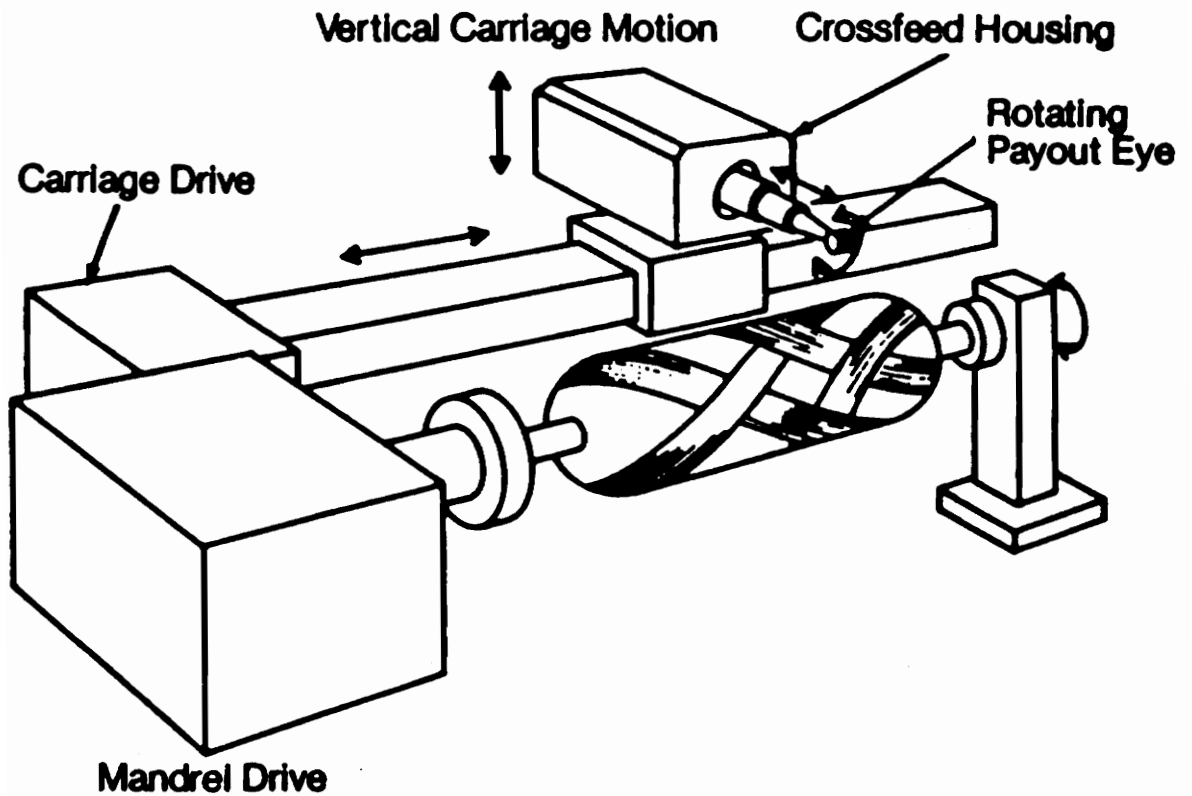


Figure 1. LATHE TYPE FILAMENT WINDER:

A computer controlled, multiaxis lathe type filament winder. The horizontal and vertical carriage drives can be numerically controlled allowing for various winding patterns and shapes of the FWC structure.

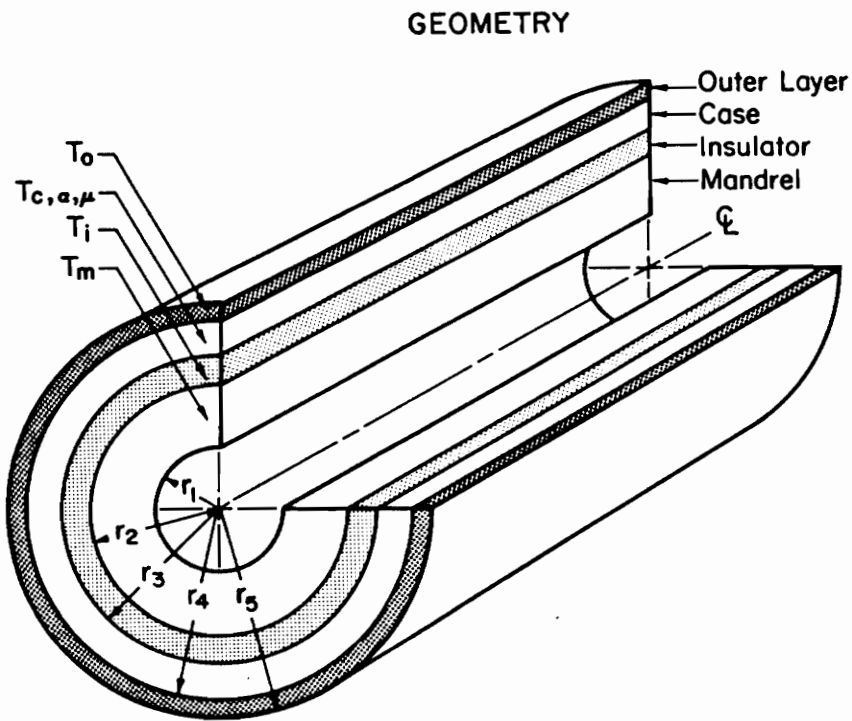


Figure 2. FILAMENT WOUND COMPOSITE - Geometry:

Schematic of the FWC assembly. The individual layers and the radial distances with respect to the axis of symmetry are indicated.

2.3 Curing Process

The entire bagged assembly comprising of the mandrel - insulator - case - outer layer is placed in a forced air oven or an autoclave and cured for a specific length of time. The cure temperature $T_{\infty}(t)$, may vary with time in an arbitrary manner. The most significant event during the curing process [7] is the heat initiated exothermic chemical reaction occurring in the composite matrix resin caused by the interaction of the heated oven fluid with the assembly at one or more spatial boundaries (Figure 3). The matrix chemical reactions play a critical role in determining the thermal and material properties of the composite case at any instant of the processing cycle.

Thus, the objective is to develop a comprehensive model which can be used to select the cure temperature which results in a composite case that is cured uniformly and completely in the shortest possible time.

2.4 Processing Cycle Identification

The elevated temperature to which the assembly is subjected to is referred to as the cure or processing cycle [8]. The magnitude and duration of the temperatures applied during the curing process significantly affect the performance of the finished product. Therefore, the cure cycle must be logically designed and not arbitrarily chosen for each particular application.

Some of the major constraints which an optimum cure cycle should satisfy are :

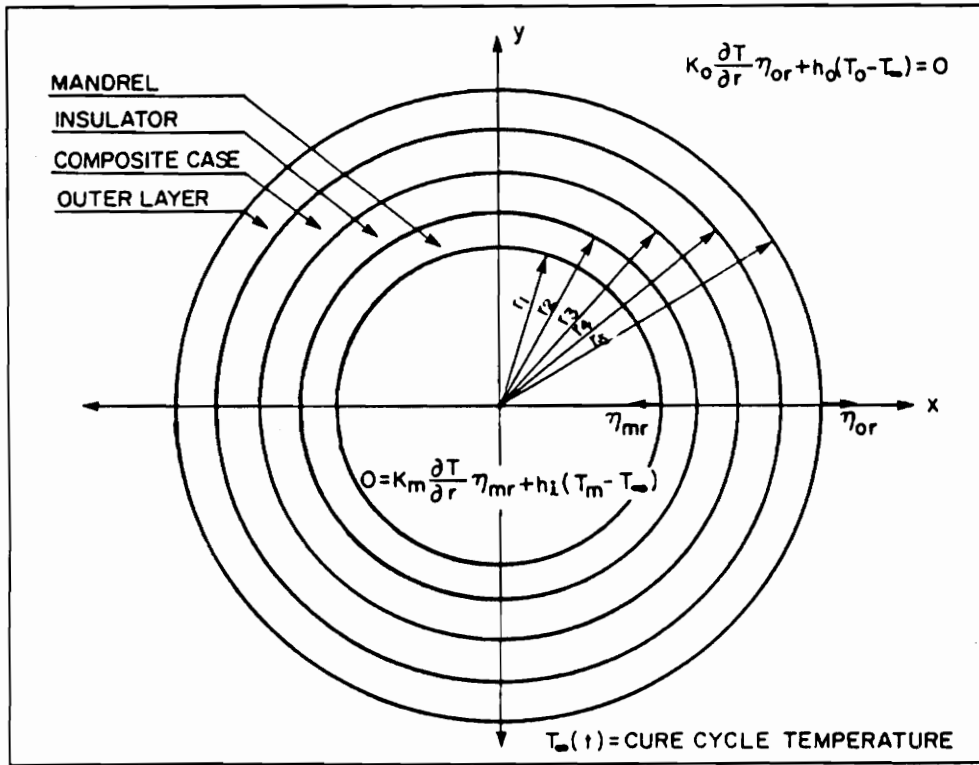


Figure 3. FILAMENT WOUND COMPOSITE - End View:

The FWC assembly (hollow mandrel) cured in an oven with heat transfer coefficient h_i (on the inner surface) and h_o on the outer surface. The convective boundary conditions are indicated where $T_m(r,t)$ is the temperature of the inner surface of the mandrel and $T_o(r,t)$ is the temperature of the outer surface of the outer layer and $T_\infty(t)$ is the oven temperature. η_{mr} and η_{or} are the outward drawn normals at the inner boundary surface of the mandrel and the outer surface of the outer layer.

1. The temperature inside the composite case should not exceed a preset maximum value at any time during the cure.
2. Towards the end of the process, the composite should have attained uniform and complete cure.
3. The curing process is achieved in the shortest possible time.

2.5 Cylindrical Cure Model - Analysis

Consider the mandrel - insulator - composite case - outer layer assembly (denoted as FWC assembly) pictured in Figure 2, having a fiber - reinforced thermosetting matrix composite case of thickness, t_{case} , inner radius, r_3 , and outer radius, r_4 . The FWC assembly can be treated as infinitely long concentric cylinders such that the heat flow through the walls is in the radial direction only. Thus, the filament winding process problem is modeled as being dominated by changes in the spatial direction " r " only.

In formulating the cure model the following simplifications can be considered :

1. The effects of layer compaction and resin displacement due to fiber tension, vacuum bagging, and external pressure are neglected.

2. The winding pattern, while important in determining the strength and stiffness of the case, has no direct effect on the model except in calculation of the winding time.
3. It is assumed that the thickness of the vacuum bag is small as compared to the thickness of the breather cloth. Hence the temperature drop across the bag can be neglected.

2.6 Cylindrical Cure Model - Submodel Identification

The comprehensive cure model for filament wound composites is comprised of three specific submodels, which effectively portray the following phenomena :

1. The HEAT TRANSFER MODEL which models the heat transfer process.
2. Curing of the resin inside the composite, due to the effects of the thermal process and exothermic chemical reactions is simulated by the CURE - KINETICS MODEL.
3. Resin viscosity is characterized by the VISCOSITY MODEL.

In the analysis, the FWC assembly is treated as infinitely long concentric cylinders. Furthermore, this simplification leads to a model having temperature, degree of cure, and viscosity variations in a single domain in space (i.e., the radial direction).

In the following sections governing equations and the associated boundary and initial conditions for the three submodels will be established.

2.7 Submodel - I : HEAT TRANSFER MODEL

The entire spatial domain $r \in [r_1, r_5]$ (Figure 3) is divided into subdomains for each individual section of the assembly. Since the outer surface of the outer layer and the inner surface of the mandrel (for a hollow mandrel) interact with the fluid (Figure 3) the boundary flux needs to be specified. At the interfacial points of the individual subdomains, the conservation of energy dictates the equality of temperature and heat flux [29,30]. The initial conditions for the process have to be specified for each of the models at time, $t = 0$. The explicit set of equations and boundary conditions are outlined below.

Governing Equations

The classical governing equations for the transient heat transfer analysis in the coaxial cylinder assembly (Figure 2) for all times, $t \geq 0$ are :

$$\rho_m C_m \frac{\partial T_m}{\partial t} = \frac{K_m}{r} \frac{\partial}{\partial r} \left(r \frac{\partial T_m}{\partial r} \right) \quad \forall \quad r \in [r_1, r_2] \quad (2.1a)$$

$$\rho_i C_i \frac{\partial T_i}{\partial t} = \frac{K_i}{r} \frac{\partial}{\partial r} \left(r \frac{\partial T_i}{\partial r} \right) \quad \forall \quad r \in [r_2, r_3] \quad (2.1b)$$

$$\rho_o C_o \frac{\partial T_o}{\partial t} = \frac{K_o}{r} \frac{\partial}{\partial r} \left(r \frac{\partial T_o}{\partial r} \right) \quad \forall \quad r \in [r_4, r_5] \quad (2.1c)$$

where subscripts m, i, and o identify the mandrel, insulator and the outer layer, respectively. ρ is the density, C is the specific heat, and K is the thermal conductivity. T is the temperature, r is the radial coordinate and t is time.

The one-dimensional unsteady heat conduction equation for the composite case (Figure 3) which includes a term representing the rate of heat generation due to exothermic chemical reactions is written as [7,8,31]

$$\frac{\partial(\rho_c C_c T_c)}{\partial t} = \frac{1}{r} \frac{\partial}{\partial r} (K_c r \frac{\partial T_c}{\partial r}) + \rho_c \dot{H} \quad \forall \quad r \in [r_3, r_4] \quad (2.1d)$$

where ρ_c and C_c are the density and specific heat of the composite, respectively, and K_c is the thermal conductivity of the composite perpendicular to the direction of heat flow (normal to the radial direction). \dot{H} is the rate of heat generated by chemical reactions and is obtained from the kinetics model.

2.8 Submodel - II : CURE KINETICS MODEL

The kinetics of the chemical reactions occurring inside the composite case are resin dependent [11,14].

If the assumption is made that the rate of heat generation during the cure is proportional to the rate of the cure reaction, then the degree of cure of the resin $\alpha(t)$ may be defined as

$$\alpha(t) = \frac{H(t)}{H_R} \quad (2.2)$$

where $H(t)$ is the amount of the heat evolved from the beginning of the reaction to some intermediate time, t , and H_R , is the total or ultimate heat of reaction during the cure. $\alpha(t)$ is zero initially and for a completely cured resin approaches unity. By differentiating the expression for the degree of cure Eq.(2.2) with respect to time and rearranging we get an expression for the rate of heat generation.

$$\dot{H}(t) = \frac{d\alpha(t)}{dt} H_R \quad (2.3)$$

where $d\alpha(t)/dt$, is defined as the reaction rate or cure rate. The functional representation of the dependence of the cure rate on the temperature and degree of cure of the resin may be written as

$$\frac{d\alpha(t)}{dt} = f_1(T, \alpha) \quad (2.4)$$

The exact functional form of the cure rate, along with the value of the heat of reaction, depends on the matrix resin used in the composite case and must be determined experimentally. The most frequently used technique, that has the advantage of simultaneously measuring both the heat of reaction and the cure rate, is the differential scanning calorimetry (DSC) [7,8,9,10]. Empirical expressions for the cure rate along with values of the heat of reaction are give in Appendix A for several commonly used epoxy resin systems.

If the diffusion of the chemical species is neglected, the degree of cure at each point inside the case can be determined by integrating the expression for the cure rate with respect to time in the following manner.

$$\alpha(t) = \int_0^t \frac{d\alpha(t)}{dt} dt \quad (2.5)$$

The cure kinetics model provides the relationships necessary to calculate the rate at which heat is generated by the chemical reactions in the composite, $\dot{H}(t)$, the cure rate, $d\alpha/dt$, and the degree of cure of the matrix resin in the composite case.

2.9 Submodel - III : VISCOSITY MODEL

In order to calculate the fiber motion and resin displacement in the composite case during cure, the resin viscosity must be known as a function of position and time. The shear viscosity of a thermosetting resin is a complex function of temperature, degree of cure (or time), and shear rate. However, a reasonably good approach to this complex problem is to assume that the resin viscosity is independent of shear rate and to measure the resin viscosity at very low shear rates. A mathematical expression which has been used to describe the changes in the viscosity of thermosetting resins [8] during cure can be written as :

$$\mu(T, \alpha) = \mu_{\infty} e^{\left(\frac{U}{RT} + K_{\mu} \alpha\right)} \quad (2.6)$$

where μ_{∞} , is the isothermal viscosity constant for the resin system, U is the activation energy for viscous flow, K_{μ} is the constant which accounts for the effects of the

chemical reaction on the viscosity, R is the universal gas constant, and α , is determined from the cure kinetics model. The constants in Eq.(2.6) can be determined from isothermal viscosity data as demonstrated in reference 9. The constants in the viscosity model for a commonly used epoxy resin system are reported in Appendix C.

2.10 Spatial Boundary Conditions

The spatial boundary conditions are the dirchlet type or mixed type of boundary conditions specifying the flux at the boundaries of the subdomains. The boundary conditions are valid for all times, $t \geq 0$. The equality of heat flux at the interfaces and the flux boundary conditions at the inner and outer surfaces of the FWC assembly interacting with the oven fluid (see Figure 3) are written as

$$\begin{aligned}
 K_m \frac{\partial T_m}{\partial r} \eta_{mr} + h_i (T_m - T_\infty) &= 0 & \text{at } r = r_1 \\
 K_m \frac{\partial T_m}{\partial r} \eta_{mr} + K_i \frac{\partial T_i}{\partial r} \eta_{ir} &= 0 & \text{at } r = r_2 \\
 K_i \frac{\partial T_i}{\partial r} \eta_{ir} + K_c \frac{\partial T_c}{\partial r} \eta_{cr} &= 0 & \text{at } r = r_3 \\
 K_c \frac{\partial T_c}{\partial r} \eta_{cr} + K_o \frac{\partial T_o}{\partial r} \eta_{or} &= 0 & \text{at } r = r_4 \\
 K_o \frac{\partial T_o}{\partial r} \eta_{or} + h_o (T_o - T_\infty) &= 0 & \text{at } r = r_5
 \end{aligned} \tag{2.7}$$

and, the temperature continuity boundary conditions at the interfacial points of the subdomains (Figure 3) can be expressed as

$$\begin{aligned}
 T_m(r_2, t) &= T_i(r_2, t) & \text{at } r &= r_2 \\
 T_i(r_3, t) &= T_c(r_3, t) & \text{at } r &= r_3 \\
 T_c(r_4, t) &= T_o(r_4, t) & \text{at } r &= r_4
 \end{aligned} \tag{2.8}$$

where η_{ij} is the outward drawn normal of the subdomain i at location j , h_i is the inner surface convective heat transfer coefficient, h_o is the outer surface convective heat transfer coefficient, and $T_\infty(t)$ is the ambient temperature of the fluid in the oven or autoclave.

2.11 Initial Conditions

The initial conditions require that initial temperature distributions inside the mandrel, insulator, composite case, and outer layer be specified at the beginning of the curing process. In addition, the cure kinetics model requires that the initial degree of cure distribution in the composite case upon completion of the winding process, (i.e., $t \leq 0$) be specified. The initial conditions are written as follows :

$$\begin{aligned}
 T_m(r, 0) &= \dot{T}_m(r) & \forall \quad r &\in [r_1, r_2] \\
 T_i(r, 0) &= \dot{T}_i(r) & \forall \quad r &\in [r_2, r_3] \\
 T_c(r, 0) &= \dot{T}_c(r) & \forall \quad r &\in [r_3, r_4] \\
 T_o(r, 0) &= \dot{T}_o(r) & \forall \quad r &\in [r_4, r_5] \\
 \alpha(r, 0) &= \dot{\alpha}(r) & \forall \quad r &\in [r_3, r_4]
 \end{aligned} \tag{2.9}$$

where, $T_m^*(r)$, $T_i^*(r)$, $T_c^*(r)$, and $T_o^*(r)$, are the initial temperatures (at $t = 0$) of the mandrel, insulator, case, and outer layer, respectively. $\alpha^*(r)$ is the initial degree of cure distribution in the case. The three submodels describing separate phenomena are solved concurrently and describe the thermo-chemical behavior occurring inside the FWC assembly. The solutions to Eqs (2.1) and (2.3 - 2.6) yield the temperature distributions inside the mandrel, insulator, composite case, and outer layer, and the cure rate, degree of cure, and resin viscosity as functions of position and time inside the composite case. The comprehensive cure model and the interdependence of the individual submodels is outlined in Figure 4.

2.12 Material Properties

The thermal and mechanical properties of composites are fundamental to the analysis and design of composite structures. Composite micromechanics relates the properties of the fiber and the matrix to the final mechanical properties of the composite using the now familiar, "rule of mixtures" approach [32,33,34]. One of the basic assumptions on which property estimation of the composite is based is that the interaction of the fiber with the matrix is purely mechanical. The chemical reaction of the resin does not affect the micromechanics estimation of the pertinent property [34].

Solution of the cylindrical cure model, requires that the density ρ , specific heat capacity C , and thermal conductivity K of the mandrel, insulator, composite case, and the outer layer be known. In addition, the heat of reaction of the composite case must

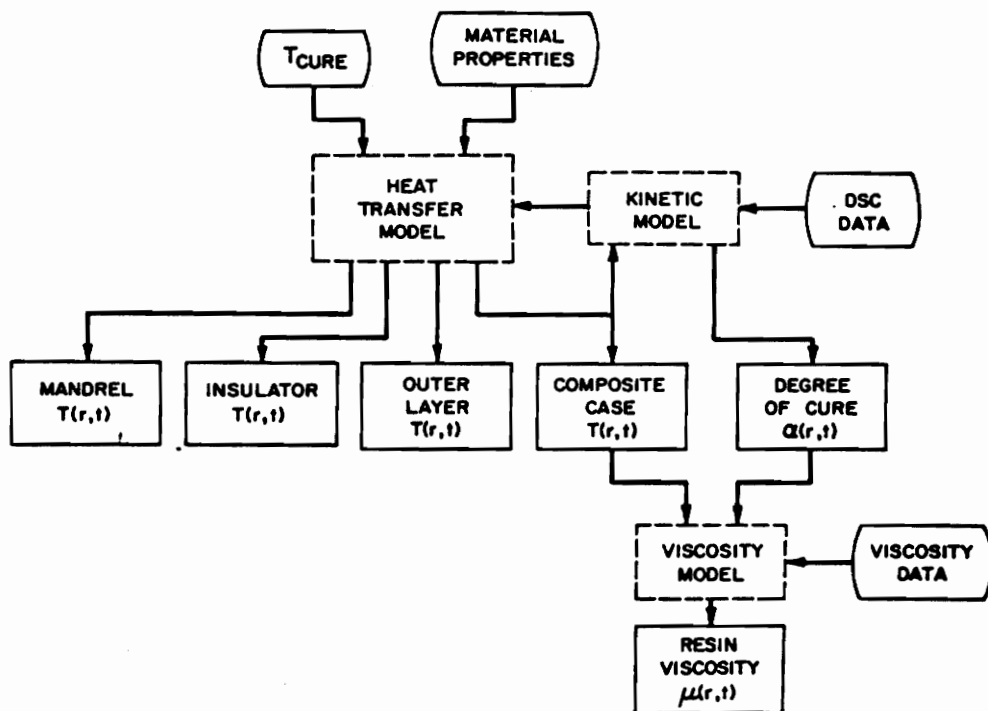


Figure 4. BLOCK DIAGRAM OF FWC CYLINDRICAL CURE MODEL:

The individual submodels (i.e., the heat transfer, cure-kinetics and the viscosity models) form the comprehensive cure model and correlate the boundary temperatures with the thermal, chemical and the physical process occurring within the composite.

be specified. In the present analysis, it is assumed that the density, specific heat, and thermal conductivity of the mandrel, insulator, and outer layer do not vary significantly with temperature. Therefore, these material properties will be treated as constants and room temperature values will be used.

The density, specific heat, thermal conductivity, and heat of reaction of the composite case depends on the temperature, degree of cure of the resin, and the fiber and resin volume fractions. In general, the variations in these properties with temperature and degree of cure are not known and cannot be readily determined.

The "rule of mixtures" model requires that the constituent properties of the resin and the fiber, and resin mass fraction be prespecified. Applying the "rule of mixtures" model, we can calculate the resin volume fraction, v_r , of the composite as

$$v_r = \frac{1.0}{1.0 + \left(\frac{1.0}{m_r} - 1.0\right) \frac{\rho_r}{\rho_f}} \quad (2.10)$$

where m_r is the resin mass fraction, ρ_r is the resin density, and ρ_f is density of the fiber. The resin mass fraction is usually specified for a prepreg roving or tape.

The density of the composite ρ_c , can be written as

$$\rho_c = \rho_f + (\rho_r - \rho_f)v_r \quad (2.11)$$

Eq.(2.11) assumes that the sum of the volume fractions of the resin and the fiber is unity. The specific heat capacity of the composite, C_c , can be derived as

$$C_c = C_f + (C_r - C_f)m_r \quad (2.12)$$

where C_f is the specific heat capacity of the fiber and, C_r , the specific heat capacity of the resin.

The heat of reaction for the composite can be expressed as

$$H_R = m_r H_r = \frac{\rho_r}{\rho_c} v_r H_r \quad (2.13)$$

where H_R is the heat of reaction per unit mass for the composite and H_r is the heat of reaction per unit mass for the resin system. H_r is usually determined from DSC data of neat resin samples.

The thermal conductivity of the composite normal to the fibers (r - direction) may be calculated from the relationship derived by Tsai and Springer [32] for a cylindrical filament in a square packed array

$$K_c = K_r \left(1 - 2 \left(\frac{v_f}{\pi} \right)^{0.5} \right) + \frac{K_r}{\beta_k} \left[\pi - \frac{4}{\left(1 - \left(\beta_k^2 \frac{v_f}{\pi} \right) \right)^{0.5}} \tan^{-1} \left(\frac{\left(\frac{1 - \beta_k^2 v_f}{\pi} \right)^{0.5}}{\left(1 + \beta_k \left(\frac{v_f}{\pi} \right)^{0.5} \right)} \right) \right] \quad (2.14)$$

where β_k is defined as,

$$\beta_k = 2.0 \left(\frac{K_r}{K_f} - 1.0 \right) \quad (2.15)$$

v_f the fiber volume fraction is expressed as,

$$v_f = 1.0 - v_r \quad (2.16)$$

and K_r and K_f , are the thermal conductivities of the resin and the fibers, respectively.

2.13 Method of Solution

Solution of the cylindrical cure model must be obtained by numerical methods. A standard finite element approach is adopted to model and solve the cure model.

CHAPTER 3

FINITE ELEMENT FORMULATION

One dimensional field problems can be solved by effectively subdividing the region into finite domains or elements. The field variables within each element are approximated by separate interpolation functions, which have common values at the nodes of the elements in the mesh. Material properties can be different for each element, and in general mixed boundary conditions can be easily handled.

The sequence of steps adopted in the finite element analysis procedure are :

1. Identification of a mathematical model that describes the phenomena.

2. Development of a discrete model, computational strategy, and numerical algorithm to approximate the mathematical model.
3. Develop and assemble the software to implement the strategy and numerical scheme.
4. Postprocessing and interpretation of the predictions of the computational model.

The mathematical model was identified as the three submodels of Chapter 2. In the following sections the discretization of the model and the solution strategy will be discussed.

3.1 Domain Discretization

The domain $r \in [r_1, r_5]$ of the FWC assembly (Figure 2) is divided into individual subdomains identified by the mandrel, insulator, composite case and outer layer as described in Section 2.7. Individual subdomains are discretized into isoparametric finite elements. The discretized domain may be modeled by a uniform or a nonuniform set of finite elements. A typical example of a discretized domain for the FWC assembly is shown in Figure 5.

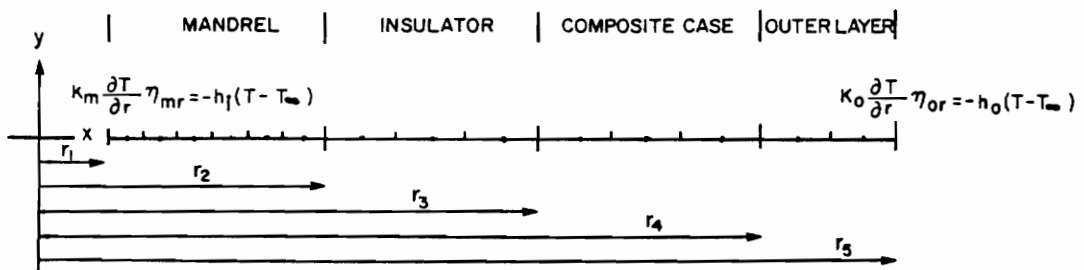
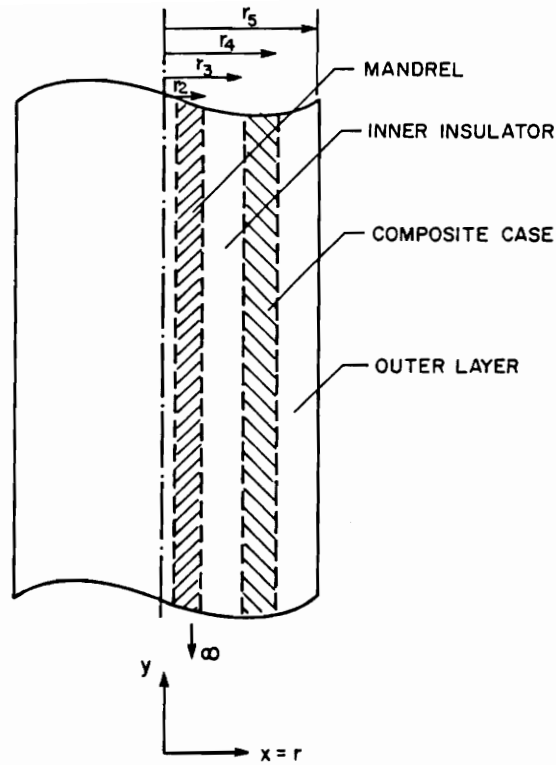


Figure 5. FINITE ELEMENT MODEL - Domain Discretization:

The FWC assembly is divided into individual subdomains comprising of the individual layers of the assembly. The finite element model is made up of an unsymmetric or symmetric mesh of axisymmetric finite elements.

3.2 Variational Formulation

Consider a generalized one-dimensional unsteady heat conduction equation in radial coordinates with heat generation,

$$\frac{\partial(\rho_j C_j T_j)}{\partial t} = \frac{1}{r} \frac{\partial}{\partial r} (K_j r \frac{\partial T_j}{\partial r}) + \rho_j \dot{H} \quad \forall \quad r \in [r_e, r_{e+1}] \quad (3.1)$$

where ρ_j , C_j , and, K_j are the density, specific heat capacity, and the thermal conductivity, respectively of the region described by the specific element, $r \in [r_e, r_{e+1}]$. $T_j(r,t)$ and H are the temperature and the rate of heat generation over the domain modeled by the element. r_e and r_{e+1} are the radial coordinates of the element as shown in Figure 6.

The generalized heat flux boundary conditions for the element can be written as

$$K_j \frac{\partial T_j}{\partial r} \eta_e + h_e (T_j(r,t) - T_\infty(t)) = 0 \quad \text{at } r = r_e \quad (3.2)$$

and

$$K_j \frac{\partial T_j}{\partial r} \eta_{e+1} + h_{e+1} (T_j(r,t) - T_\infty(t)) = 0 \quad \text{at } r = r_{e+1} \quad (3.3)$$

where η_e and η_{e+1} are the outward pointing normals at r_e and r_{e+1} , respectively. The heat transfer coefficients at r_e and r_{e+1} are denoted by h_e and h_{e+1} . $T_\infty(t)$ is the cure cycle temperature.

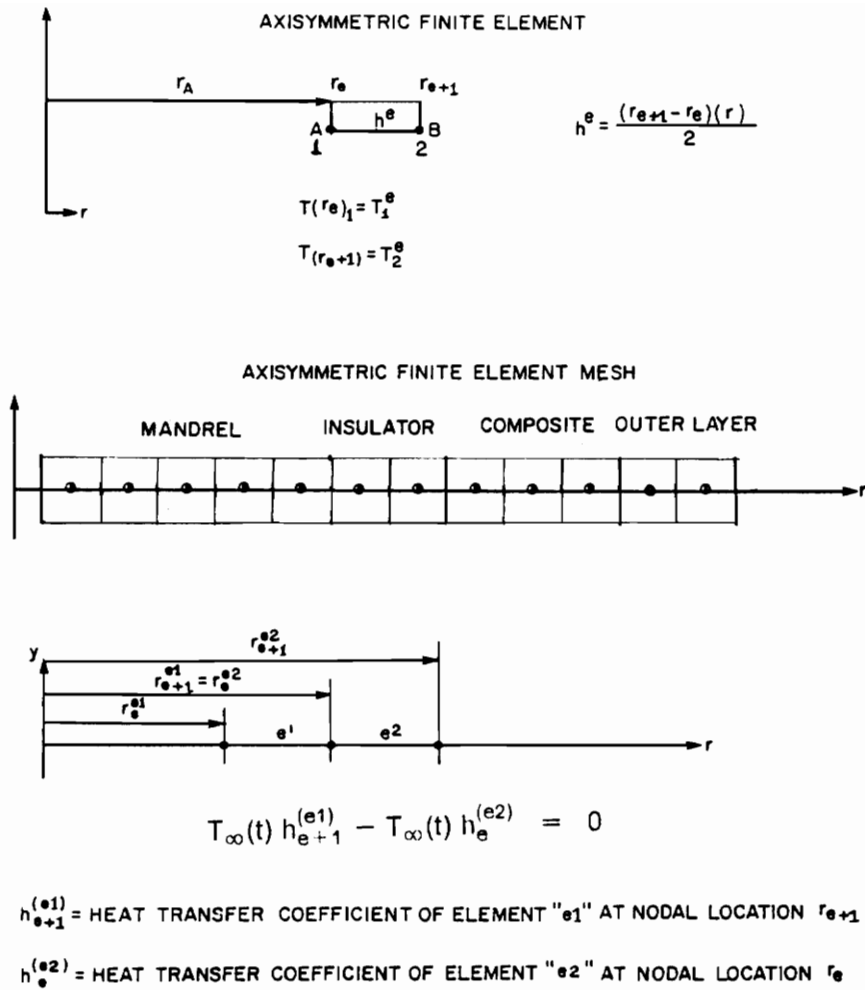


Figure 6. FINITE ELEMENT MODEL - Generalized Coordinates:

The domain is modeled using axisymmetric finite elements. The element mesh and the interactions at the nodal points are shown above.

If the properties ρ_j , C_j , and, K_j are constant over the domain modeled by the specific element $r \in [r_e, r_{e+1}]$ then Eq.(3.1) can be written as :

$$\rho_j C_j \frac{\partial T_j}{\partial t} - \frac{K_j}{r} \frac{\partial}{\partial r} \left(r \frac{\partial T_j}{\partial r} \right) - \rho_j \dot{H} = 0 \quad (3.4)$$

Multiplying Eq.(3.4) by an arbitrary test function $q(r)$ and integrating the expression by parts results in the general variational form of the heat conduction expression over the element $r \in [r_e, r_{e+1}]$.

$$0 = \int_{r_e}^{r_{e+1}} \rho_j C_j q(r) \frac{\partial T_j}{\partial t} r dr + \int_{r_e}^{r_{e+1}} K_j \frac{\partial q(r)}{\partial r} \frac{\partial T_j}{\partial r} r dr - \int_{r_e}^{r_{e+1}} \rho_j \dot{H} q(r) r dr + \left[q(r) \left(-r K_j \frac{\partial T_j}{\partial r} \right) \right]_{r_e}^{r_{e+1}} \quad (3.5)$$

Substituting Eq.(2.3) for H into Eq.(3.5), the general variational equation can be written at the elemental level as

$$0 = \int_{r_e}^{r_{e+1}} \rho_j C_j q(r) \frac{\partial T_j}{\partial t} r dr + \int_{r_e}^{r_{e+1}} K_j \frac{\partial q(r)}{\partial r} \frac{\partial T_j}{\partial r} r dr - \int_{r_e}^{r_{e+1}} \rho_j H_R \frac{d\alpha}{dt} q(r) r dr + \left[q(r) \left(-r K_j \frac{\partial T_j}{\partial r} \right) \right]_{r_e}^{r_{e+1}} \quad (3.6)$$

Note that Eq.(3.6) is valid for an element $r \in [r_e, r_{e+1}]$ at a particular time, t and is the exact variational equation for the elements in the composite case. However, the governing equations for heat transfer in the mandrel, insulator, and outer layer subdomains do not include the heat generation term. (see Section 2.7). Thus, the general variational form of the heat conduction equation for elements in the mandrel, insulator, and outer layer subdomains follows a similar development as Eq.(3.6) without the heat generation term.

3.3 Shape Functions and Finite Element Discretization

Interpolation functions or shape functions are the primary method of approximating the finite element solution over the domain modeled by the element. The primary variable $T_j(r,t)$ and the test function $q(r)$ can be approximated over the domain $r \in [r_e, r_{e+1}]$ by the following expressions

$$T_j^{(e)}(r,t) = \sum_{p=1}^m \psi_p^{(e)}(r) T_p^{(e)}(t) \quad (3.7)$$

$$q^{(e)}(r) = \sum_{i=1}^m \psi_i^{(e)}(r) \quad (3.8)$$

where $\psi_i^{(e)}(r)$ and $\psi_p^{(e)}(r)$ are the shape functions and m is the total number of nodes in each element.

Substituting the generalized boundary conditions (Eq.(3.2) and Eq.(3.3)) into Eq.(3.6) and taking into consideration the proper signs on the outward pointing normal at the boundary points of the element, Eq.(3.6) can be written as

$$\begin{aligned} 0 = \int_{r_e}^{r_{e+1}} \rho_j C_j q(r) \frac{\partial T_j}{\partial t} r dr + \int_{r_e}^{r_{e+1}} K_j \frac{\partial q(r)}{\partial r} \frac{\partial T_j}{\partial r} r dr - \int_{r_e}^{r_{e+1}} \rho_j H_R \frac{d\alpha}{dt} q(r) r dr \\ + [q(r) h_{e+1} r (T_j(r,t) - T_\infty(t))] |_{r_{e+1}} \\ + [q(r) h_e r (T_j(r,t) - T_\infty(t))] |_{r_e} \end{aligned} \quad (3.9)$$

Substituting Eq.(3.7) for the test functions and Eq.(3.8) for the temperature distribution into Eq.(3.9) yields

$$\begin{aligned}
0 = & \int_{r_e}^{r_{e+1}} \sum_{i=1}^m \sum_{p=1}^m \rho_j C_j \psi_i^{(e)} \psi_p^{(e)} r \frac{\partial T_p^{(e)}(t)}{\partial t} dr \\
& + \int_{r_e}^{r_{e+1}} \sum_{i=1}^m \sum_{p=1}^m K_j \frac{\partial \psi_i^{(e)}}{\partial r} \frac{\partial \psi_p^{(e)}}{\partial r} T_p^{(e)}(t) r dr \\
& - \int_{r_e}^{r_{e+1}} \sum_{i=1}^m \rho_j H_R \frac{d\alpha}{dt} \psi_i^{(e)} r dr \\
& + \sum_{i=1}^m \sum_{p=1}^m [\{\psi_i^{(e)}(r_{e+1}) \psi_p^{(e)}(r_{e+1}) h_{e+1} r_{e+1}\} T_p^{(e)}(t)] \\
& + \sum_{i=1}^m \sum_{p=1}^m [\{\psi_i^{(e)}(r_e) \psi_p^{(e)}(r_e) h_e r_e\} T_p^{(e)}(t)] \\
& - \sum_{i=1}^m [\{\psi_i^{(e)}(r_{e+1}) r_{e+1} h_{e+1}\} T_\infty(t)] \\
& - \sum_{i=1}^m [\{\psi_i^{(e)}(r_e) r_e h_e\} T_\infty(t)] \tag{3.10}
\end{aligned}$$

Interchanging the order of integration and summation and rearranging Eq.(3.10) gives the following expression.

$$\begin{aligned}
& \sum_{i=1}^m \sum_{p=1}^m \int_{r_e}^{r_{e+1}} \rho_j C_j \psi_i^{(e)} \psi_p^{(e)} \frac{\partial T_p^{(e)}(t)}{\partial t} r dr \\
& + \sum_{i=1}^m \sum_{p=1}^m \int_{r_e}^{r_{e+1}} K_j \frac{\partial \psi_i^{(e)}}{\partial r} \frac{\partial \psi_p^{(e)}}{\partial r} T_p^{(e)}(t) r dr
\end{aligned}$$

$$\begin{aligned}
& + \sum_{i=1}^m \sum_{p=1}^m [\{\psi_i^{(e)}(r_{e+1}) \psi_p^{(e)}(r_{e+1}) h_{e+1} r_{e+1}\} T_p^{(e)}(t)] \\
& + \sum_{i=1}^m \sum_{p=1}^m [\{\psi_i^{(e)}(r_e) \psi_p^{(e)}(r_e) h_e r_e\} T_p^{(e)}(t)] \\
& = \sum_{i=1}^m \int_{r_e}^{r_{e+1}} \rho_j H_R \frac{d\alpha}{dt} \psi_i^{(e)} r dr \\
& + \sum_{i=1}^m [\{\psi_i^{(e)}(r_{e+1}) r_{e+1} h_{e+1}\} T_{\infty}(t)] \\
& + \sum_{i=1}^m [\{\psi_i^{(e)}(r_e) r_e h_e\} T_{\infty}(t)] \tag{3.11}
\end{aligned}$$

Eq.(3.11) results in a set of simultaneous equations for the element and can be written in matrix notation as

$$[C_{ip}^{(e)}] \{\dot{T}_p^{(e)}\} + [K_{ip}^{(e)}] \{T_p^{(e)}\} = \{F_i^{(e)}\} \tag{3.12}$$

where $\{\dot{T}_p^{(e)}\}$ is the vector containing the rate of change of temperature derivatives, $\{T_p^{(e)}\}$ is the vector containing the temperature, $[C_{ip}^{(e)}]$ is the heat capacitance matrix, $[K_{ip}^{(e)}]$ is the thermal conductivity matrix, and $\{F_i^{(e)}\}$ is the thermal load vector. From Eq.(3.11) the heat capacitance and thermal conductivity matrices and the thermal load vector are defined as follows

$$C_{ip}^{(e)} = \int_{r_e}^{r_{e+1}} \rho_j C_j \psi_i^{(e)}(r) \psi_p^{(e)}(r) r dr \tag{3.13}$$

$$\begin{aligned}
K_{ip}^{(e)} = \int_{r_e}^{r_{e+1}} K_j \frac{\partial \psi_i^{(e)}}{\partial r} \frac{\partial \psi_p^{(e)}}{\partial r} r dr & + h_{e+1} r_{e+1} \psi_i^{(e)}(r_{e+1}) \psi_p^{(e)}(r_{e+1}) \\
& + h_e r_e \psi_i^{(e)}(r_e) \psi_p^{(e)}(r_e) \tag{3.14}
\end{aligned}$$

$$F_i^{(e)} = \int_{r_e}^{r_{e+1}} \rho_r H_r v_r \frac{d\alpha}{dt} \psi_i^{(e)} r dr + h_{e+1} r_{e+1} \psi_i^{(e)}(r_{e+1}) T_\infty(t) + h_e r_e \psi_i^{(e)}(r_e) T_\infty(t) \quad (3.15)$$

Since Eq.(3.12) was derived for an arbitrary element, it holds for any element in the finite element mesh. The assembly of individual finite elements is based on the idea that the quadratic functional (or the variational formulation) associated with the problem is equal to the sum of the quadratic functional of each element [37]. If there are N elements in the mesh, assembly of the elements in the domain results in the following expression

$$0 = \sum_{e=1}^N \sum_{i=1}^m \left[\sum_{p=1}^m C_{ip}^{(e)} \dot{T}_p^{(e)} + \sum_{p=1}^m K_{ip}^{(e)} T_p^{(e)} - F_i^{(e)} \right] \quad (3.16)$$

Eq.(3.16) is a set of simultaneous equations which can be written in matrix form as

$$[C] \{\dot{T}\} + [K] \{T\} = \{F\} \quad (3.17)$$

3.4 Direct Time Integration

In direct time integration [35], the set of algebraic equations in Eq.(3.17) are solved numerically without further transformation in the time domain. A 'θ' family of approximation is used to approximate the time derivative of the dependent variable $T_j(r,t)$ at two consecutive time steps t and $t + \Delta t$ by linear interpolation [37],

$$\theta \{\dot{T}\}_{n+1} + (1 - \theta) \{\dot{T}\}_n = \frac{\{T\}_{n+1} - \{T\}_n}{\Delta t_{n+1}} \quad (3.18)$$

where $\Delta t_{n+1} = t_{n+1} - t_n$ is the $(n + 1)$ st time step. The parameter ' θ ' varies between 0 and 1.0 and determines the difference scheme adopted for the time integration. Substituting Eq.(3.18) into Eq.(3.17) and rearranging gives

$$[\bar{C}] \{T\}_{n+1} = [\bar{K}] \{T\}_n + \{F\}_{n,n+1} \quad (3.19a)$$

where $[\bar{C}]$ is the modified effective capacitance matrix, $[\bar{K}]$ is the modified thermal conductivity matrix, and $\{F\}_{n,n+1}$ is the modified thermal load vector defined as

$$[\bar{C}] = [C] + \theta \Delta t_{n+1} [K] \quad (3.19b)$$

$$[\bar{K}] = [C] - (1 - \theta) \Delta t_{n+1} [K] \quad (3.19c)$$

$$\{F\}_{n,n+1} = \Delta t_{n+1} [\theta \{F\}_{n+1} + (1 - \theta) \{F\}_n] \quad (3.19d)$$

From Eq.(3.19 a) we get the solution at time step $t = t_{n+1}$ in terms of the solution known at time $t = t_n$ as follows

$$\{T\}_{n+1} = [\bar{C}]^{-1} [\bar{K} \{T\}_n + \{F\}_{n,n+1}] \quad (3.20)$$

At $t=0$, the solution is known from the initial conditions and Eq.(3.20), can be solved at $t = \Delta t$.

In order to reduce the computational effort involved in the simulation of the composite curing process it was necessary to utilize large time steps. The stability analysis carried out by Bathe and Wilson [38] for the heat transfer equations identical to Eq.(3.19a) indicated that a suitable value for the parameter " θ " was 0.5, which corresponded to a Crank - Nicholson type of interpolation. Furthermore, an accuracy analysis for $\theta = 0.5$ shows that the solution was second order accurate [35 - 38].

3.5 Degree of Cure Estimation

The degree of cure $\alpha(r,t)$, can be calculated from the expression defined in Eq.(2.5),

$$\alpha(r,t) = \int_{t=0}^{t=t} \frac{d\alpha}{dt} dt \quad \forall \quad r \in [r_3, r_4] \quad (3.21)$$

where the cure rate $\frac{d\alpha}{dt}$ can be calculated from the Eq.(2.4) and the expression in Appendix A. An Euler type numerical scheme was adopted to calculate the value of $\alpha^{n+1}(r,t)$ from $\alpha^n(r,t)$ of the previous time step.

$$\alpha^{n+1}(r,t) = \alpha^n(r,t) + f_1[\alpha^n(r,t), T^n(r,t)] \Delta t \quad (3.22)$$

The degree of cure for the next time integration can be estimated from the value of the degree of cure of the previous time step.

3.6 Numerical Solution Procedure

A Fortran computer program named "FEMCURE" was developed to implement the numerical procedures described in Sections 3.1 - 3.5. An overview of the step by step integration procedures for the FWC curing process developed and utilized in Program "FEMCURE" is given in Table 1.

Table 1. STEP BY STEP INTEGRATION PROCEDURE.

The step by step integration procedure for the curing process developed and utilized in program "FEMCURE" is as follows :-

1. Set up the finite element mesh and read in the initial conditions and time independent domain constants (i.e., the individual layer properties and fiber and matrix properties)
2. Calculate all properties of the composite necessary for the process using micromechanics relationships between fiber and matrix.
3. Form the thermal conductivity matrix $[K]$, the heat capacitance matrix $[C]$ and calculate the thermal load vector $\{F\}$.
4. Read in the time control parameter θ and calculate the associated parameters for the time integration.
5. Read in the initial conditions for the process and the heat transfer coefficients for the surfaces in contact with the environment.
6. Calculate the effective thermal conductivity matrix $[\bar{K}]$, the effective heat capacitance matrix $[\bar{C}]$ and the effective force vector $\{F\}_{n,n+1}$
7. Solve for the nodal point temperatures at time $t + \Delta t$ knowing all values at time t using

$$\{T\}_{n+1} = [\bar{C}]^{-1} [\bar{K}\{T\}_n + \{F\}_{n,n+1}]$$

8. Calculate the degree of cure from the relationship

$$\alpha^{n+1}(r,t) = \alpha^n(r,t) + f_1[\alpha^n(r,t), T^n(r,t)] \Delta t$$

9. Calculate the resin viscosity at time $t + \Delta t$ using the nodal temperatures and the degree of cure at that time.
10. Check if the required degree of cure has been achieved using a search procedure across the composite thickness. Simultaneously store the minimum degree of cure and the maximum viscosity at that particular instant of time
11. Reiterate for the next time step if the required degree of cure has not been achieved across the composite.

CHAPTER 4

COMPARISON STUDIES & VALIDATION

The cure model described in Chapter 2 and the associated assumptions have to be verified before proceeding to the optimization and optimal control of the curing process. The cure model is based on the heat transfer model, the cure kinetics model, and the viscosity model described earlier.

The heat transfer model will be compared with the classical solution for the transient convective heat transfer outlined in Appendix D for an infinitely long cylinder available in literature [29,30,40]. Then, the heat transfer model, with exothermic heat generation due to reaction kinetics of the matrix resin, will be compared with the experimental results carried out at Morton Thiokol Inc.

4.1 Comparison Studies

The finite element solution was compared with the classical solution for an infinitely long solid wrought aluminum cylinder of outside diameter 0.4723 m (Figure 7). The material properties used for the simulation are presented in Table 2. The simulation studies were carried out for the cylinder having an initial temperature of 21.11°C and suddenly subjected to a convective environment at 176.6°C. The heat transfer coefficient was 100 W/m² – K.

A symmetric mesh of quadratic axisymmetric finite elements [36] was utilized to simulate the heat transfer characteristics of the cylinder. The co-ordinates and the schematic of the mesh is presented in Figure 7. The classical transient heat transfer solution obtained by the method of separation of variables was compared with the solution of the finite element model. Temperature versus time results were compared at 3 radial positions. These included the centerline temperature (i.e., temperature along axis of symmetry, $r = 0.0$), one arbitrarily chosen internal point and the outermost point in contact with the environment. The comparisons are plotted in Figure 8. There is excellent agreement between the classical solution and the finite element simulation.

4.2 Axisymmetric Cure Model

The validated heat transfer model was extended to include heat generation due to chemical reactions, resin cure kinetics, and resin viscosity. Based on the assump-

Table 2. MATERIAL PROPERTIES FOR 5.75" BOTTLE.

Material Properties 5.75 in bottle.

	Material	Density	Heat Capacity	Thermal Conductivity	Thickness
		ρ	C_p	K	r
		kg/m^3	$J/kg K$	$W/m K$	m
MANDREL	Al 6061 ASTM	0.2800×10^4	0.9600×10^3	171.00	0.9525×10^{-2}
INSULATOR	30% SiO_2 NBR	0.1220×10^4	1.5062×10^3	0.2765	0.6096×10^{-2}
CASE - FIBER	T-300	0.1790×10^4	0.7117×10^3	25.97	0.9550×10^{-2}
CASE - MATRIX	FIBERITE 976	0.1260×10^4	1.256×10^3	0.1674	
OUTER LAYER	POLYESTER	0.1370×10^4	1.0460×10^3	0.1507	0.3175×10^{-2}

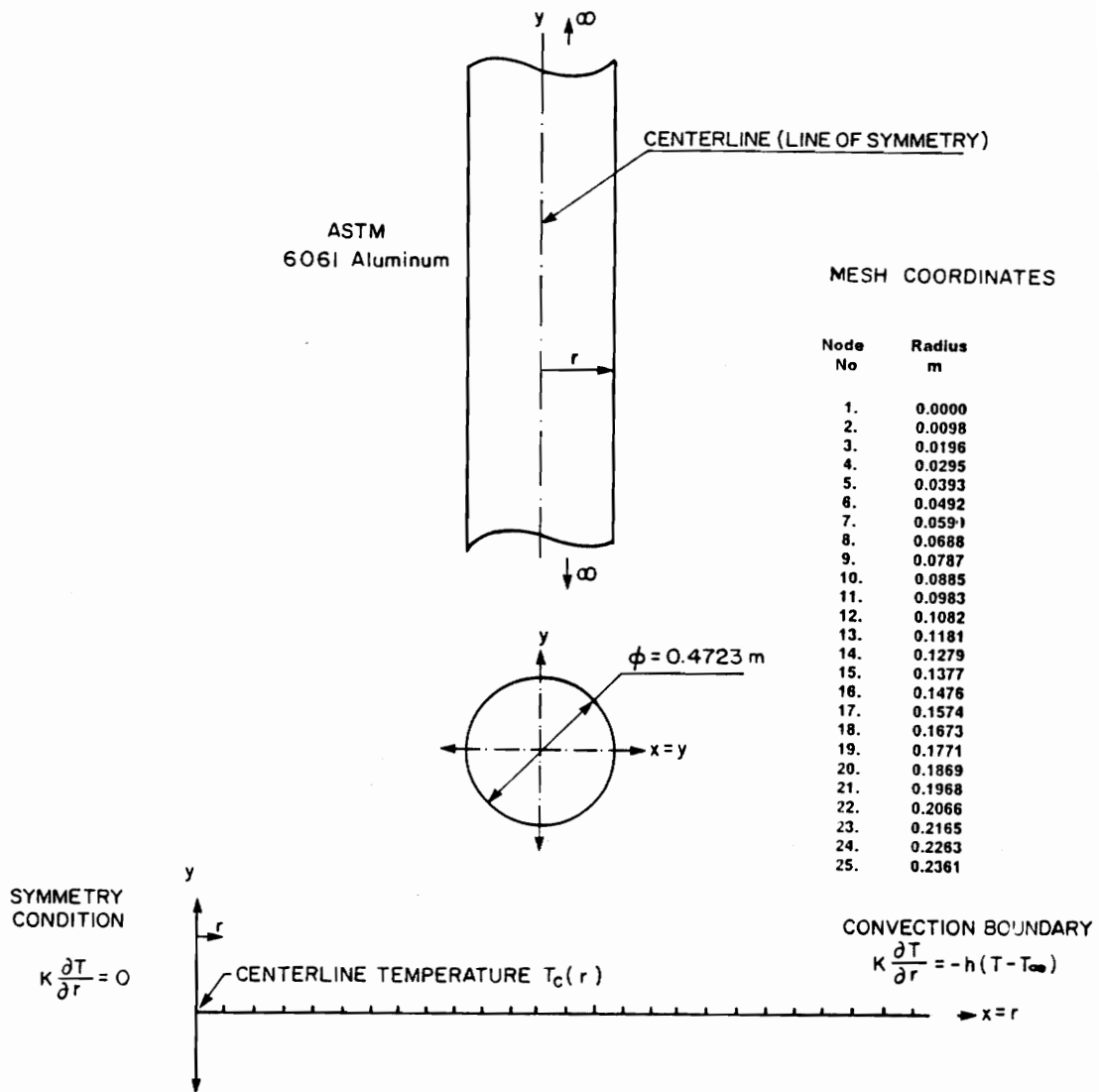


Figure 7. GEOMETRY and FINITE ELEMENT MESH:

The Al 6061 cylinder of diameter 0.4723 m is subjected to a convective environment of heat transfer coefficient $h_o = 100 \text{ W/m}^2 - \text{K}$. The finite element mesh of axisymmetric finite elements and the mesh co-ordinates are also shown.

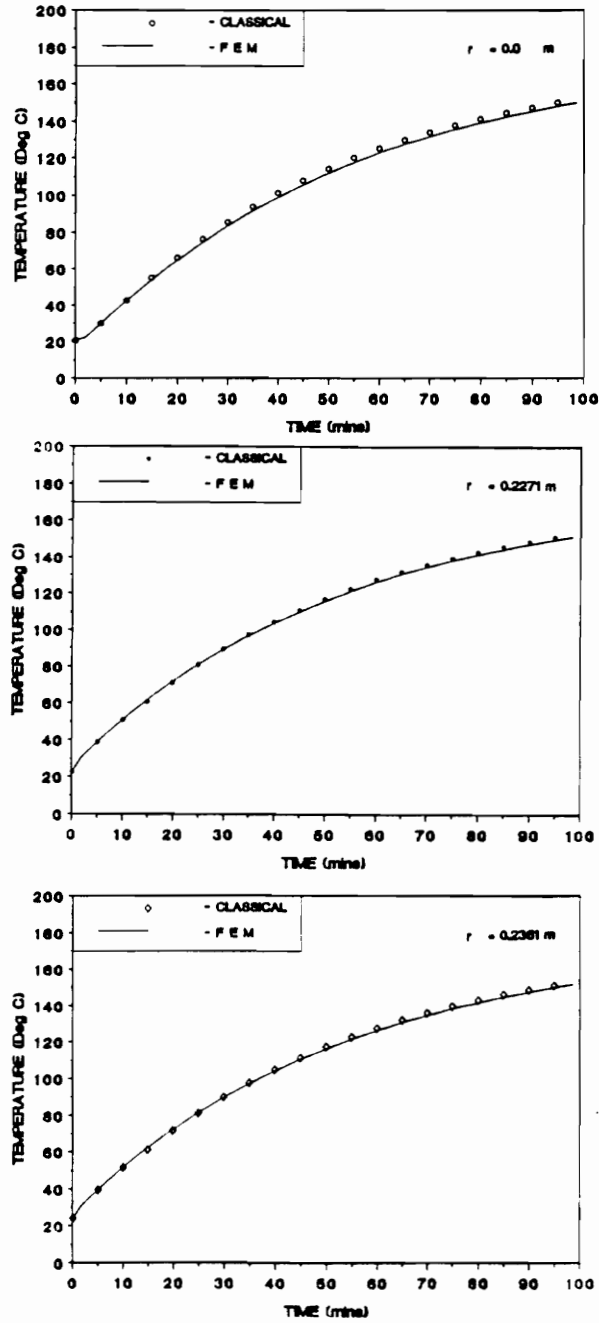


Figure 8. AXISYMMETRIC HEAT TRANSFER:

The comparison between the classical solution and the finite element solution for an Al 6061 cylinder is carried out at $r = 0.0 \text{ m}$ (i.e., the centerline), an arbitrary point $r = 0.2271 \text{ m}$ and the boundary point $r = 0.2361 \text{ m}$ subjected to a heat transfer coefficient $h_0 = 100.0 \text{ W/m}^2 \cdot \text{K}$.

tions and the mathematical relations outlined in Chapter 2, the resulting cure model is a comprehensive cure model for the filament wound composite case. The cure model is developed as a computer program named "FEMCURE".

Due to the complexity of the physical phenomena and the lack of temperature data measured during cure of a filament wound case in literature, Morton Thiokol Inc., agreed to wind a composite cylinder and measure the temperature distribution in the case during cure.

4.3 Experimental

A cylindrical composite bottle was wound using T300 / Fiberite 976 prepreg roving. The properties of the prepreg are listed in Table 2. Fiberite 976 is a 350°F curing system with a glass transition temperature T_g of 410°F. The resin is used for temperature aerospace applications.

1. MATERIALS

a. MANDREL

The mandrel was an ASTM 6061 wrought aluminum pipe, of outer diameter 0.14605 m (5.75 in.), having a total end to end length of 0.1799 m (7.683 in.). Both the ends of the cylindrical pipe were covered with end caps made of the same material. A schematic of the mandrel is shown in Figure 9.

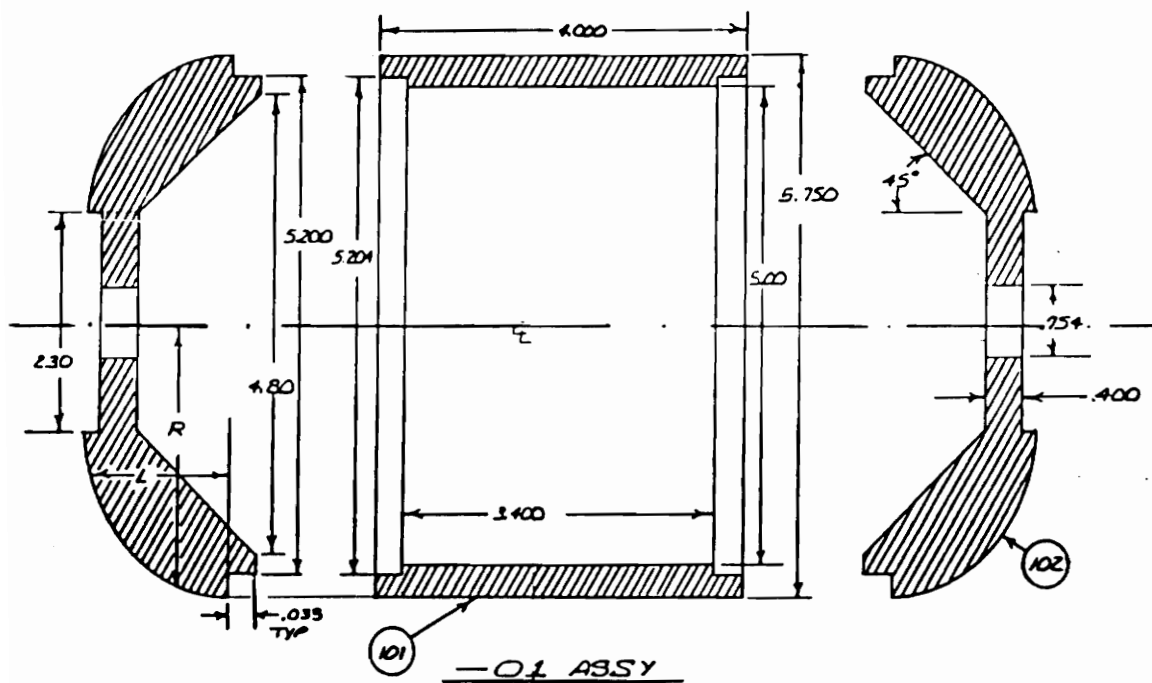


Figure 9. MANDREL SCHEMATIC:

The 5.75 inch Al 6061 mandrel is shown in schematic. The mandrel has two Al 6061 endcaps which are placed at either ends. All dimensions are in inches. [Courtesy : Morton Thiokol Inc - (Wasatch Division)]

b. INSULATOR

The mandrel was wrapped with an elastomeric insulator made up of 30 % filled silicon dioxide, nitrile butadiene rubber (NBR), having a nominal thickness of $6.096 \times 10^{-3} \text{ m}$ (0.24 in.).

c. COMPOSITE CASE

The composite case was formed by winding the prepreg in a helical pattern at 24.2° with respect to the longitudinal axis of the mandrel. The applied winding tension was measured to be approximately $7.997 \times 10^7 \text{ N/m}^2$. The preconsolidated roving thickness was measured to be $3.048 \times 10^{-4} \text{ m}$ (0.012 in.), the resin weight percentage was 30 %, and the case thickness was measured to be $0.9550 \times 10^{-2} \text{ m}$ (0.376 in.).

d. OUTERLAYER

The outer layer comprised of a perforated FEP film, Airweave breather cloth, and a silicon vacuum bag for a total thickness of $3.175 \times 10^{-3} \text{ m}$ (0.125 in.). Only the thermal resistance of the breather cloth was used in the calculations.

The properties of the materials as well as the geometric thicknesses used in the simulation are summarized in Table 2.

2. TEMPERATURE MEASUREMENT

The temperature measurements were carried out using 18 type J thermocouples embedded at various radial locations in the composite cylinder. Additional

thermocouples were placed on the inner and outer surfaces of the cylinder as well as above the assembly. All the thermocouples were connected to a Molitek recorder which was programmed to convert and record the sensor information onto a strip chart plotter at time intervals of 5 minutes.

All thermocouples were measured to be at ambient temperature (21.11°C) before the heating cycle was switched on. An endview of the thermocouple locations is presented in Figure 10.

3. CURE CYCLE

The temperature data measured from thermocouple number 0 and thermocouple number 17 indicate that the oven was heated at a constant rate of 5° F/ min from an ambient temperature of 21.11°C to the final hold temperature of 176.6°C. The oven was held at 176.6°C for a period of 300 minutes.

The measurements of the strip chart plotter were reduced and used for the validation of the finite element model. The total time of the process used in the finite element simulations was approximately 2 hours. The finite element model of the FWC assembly used an unsymmetric mesh modeled by axisymmetric quadratic finite elements. The finite element mesh and the associated boundary conditions are illustrated in Figure 11.

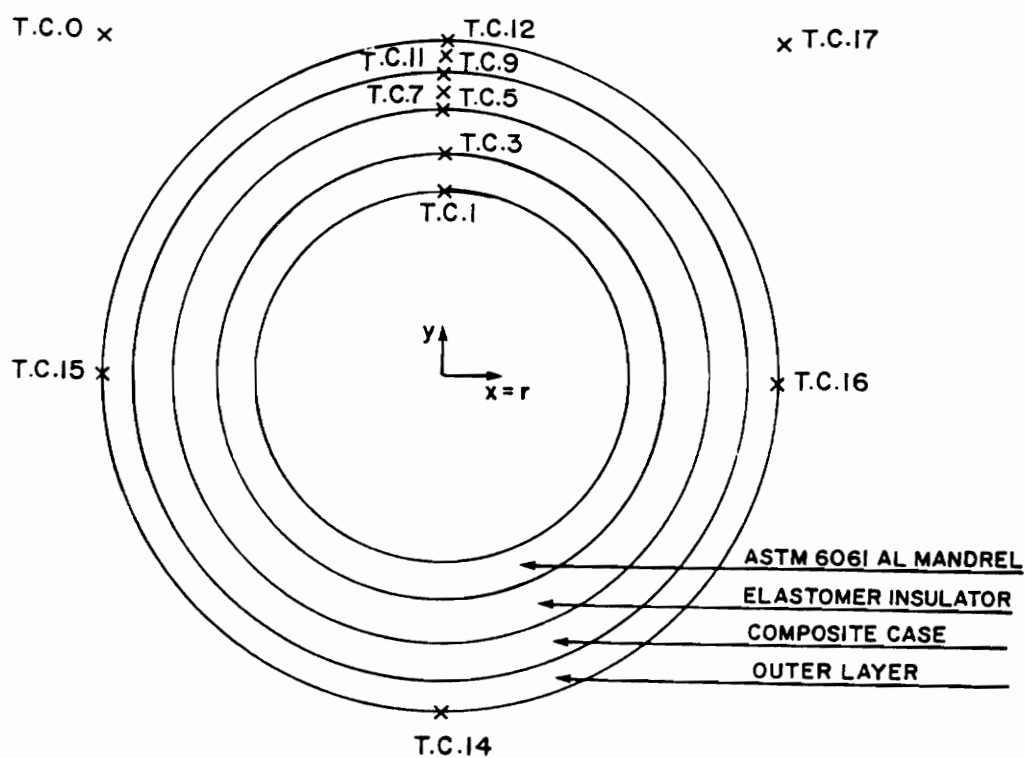
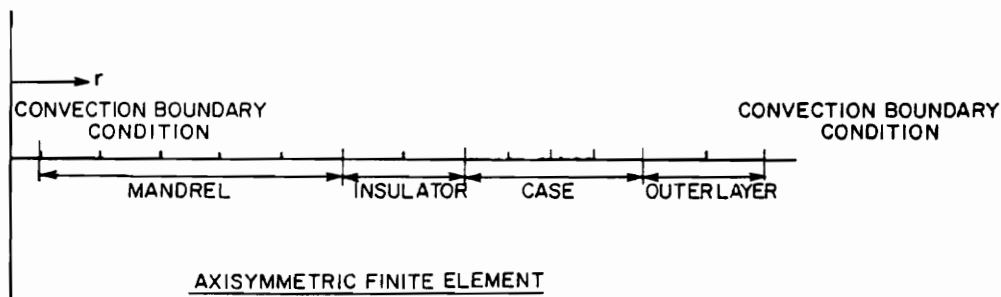


Figure 10. FWC ASSEMBLY (END VIEW):

18 J type thermocouples are placed to sense the temperature at 16 locations across the FWC assembly and at 2 locations in the autoclave. Thermocouple number 0 and thermocouple number 17 measure the autoclave heating cycle.



MESH COORDINATES

Node No	Radius m
1.	0.1524
2.	0.1599
3.	0.1673
4.	0.1748
5.	0.1823
6.	0.1897
7.	0.1972
8.	0.2047
9.	0.2121
10.	0.2196
11.	0.2271
12.	0.2275
13.	0.2278
14.	0.2282
15.	0.2286
16.	0.2318
17.	0.2350
18.	0.2381
19.	0.2413
20.	0.2445
21.	0.2477
22.	0.2508
23.	0.2540
24.	0.2548
25.	0.2556
26.	0.2564
27.	0.2572

Figure 11. FINITE ELEMENT MESH and BOUNDARY CONDITIONS:

The 5.75 inch bottle is modeled using an unsymmetric mesh of axisymmetric finite elements. The dirchlet type of boundary conditions are also indicated.

4.4 Results

The finite element solution and the experimental temperature data were compared at 5 relevant points (Figure 10) namely:

1. The inner surface temperature of the hollow mandrel measured by the thermocouple number 1.
2. The mandrel - insulator interface which was measured by the thermocouple number 3
3. The insulator - case interface which was measured by the thermocouple number 5
4. The case - outer layer interface which was measured by the thermocouple number 9
5. The outer layer surface temperature measured by thermocouple number 12.

The temperature vs time plots of the comparisons are presented in Figure 12. The FEM calculations were performed using a heat transfer coefficient of $5 \text{ W/m}^2\text{K}$ on the inner surface of the hollow mandrel and $45 \text{ W/m}^2\text{K}$ on the outer surface in contact with the oven fluid. The inner surface heat transfer coefficient is much lower than that of the outer surface heat transfer coefficient because the inner surface of the mandrel does not have direct contact with the oven fluid due to the integrally wound end closures.

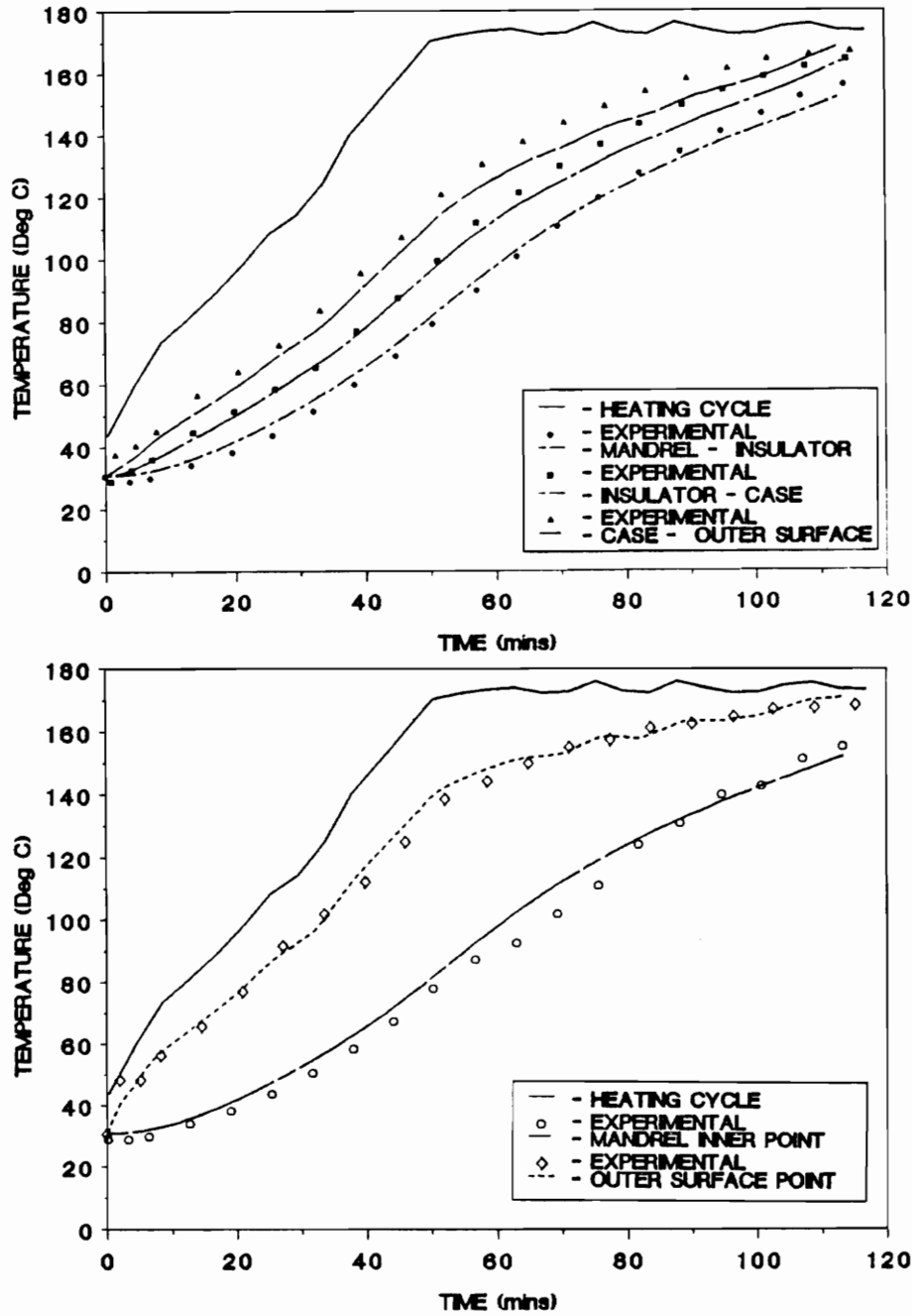


Figure 12. AXISYMMETRIC CURE MODEL - Temperature vs Time:

The experimental data and the finite element analysis results are plotted as a function of time. The inner surface heat transfer coefficient, h_i is $5 \text{ W/m}^2 - \text{K}$ and the outer surface heat transfer coefficient h_o is $45 \text{ W/m}^2 - \text{K}$. The symbols indicate the experimental data provided by Morton Thiokol Inc.

The temperature vs time plots at the different locations indicate that a very good correlation between the finite element model and the experiment exists. The temperature drop across any individual layer can be determined from the distributions plotted in Figure 12. The degree of cure vs time plot for the center of the case and the minimum degree of cure at any arbitrary point inside the case (shown in Figure 13) indicates that the case cures uniformly. The viscosity behavior at the center of the case and the maximum viscosity as a function of time are shown in Figure 14. However, since the degree of cure and the viscosity were not measured experimentally, no experimental data were available for comparison.

4.5 Cure Simulation Model Results

The axisymmetric cure model was used to simulate the curing process of two sample filament wound composite cases to illustrate the type of information that can be generated by the model and the associated FORTRAN computer code "FEMCURE". The input parameters required by the FEMCURE program are outlined in Table 3. Cure simulations were performed for composite cases fabricated from Fiberite T300 / 976 prepreg rovings and wound on an 18 inch sand PVA mandrel. The properties of EPDM rubber were used for the insulator and polyester was used as the outer layer material. The thickness and properties of each layer used in the finite element simulations are given in Table 4.

The calculations were performed using the cure cycle shown in Figure 15. The cure temperature was increased at a constant heating rate of 2.8°C/ min (5°F/min) from

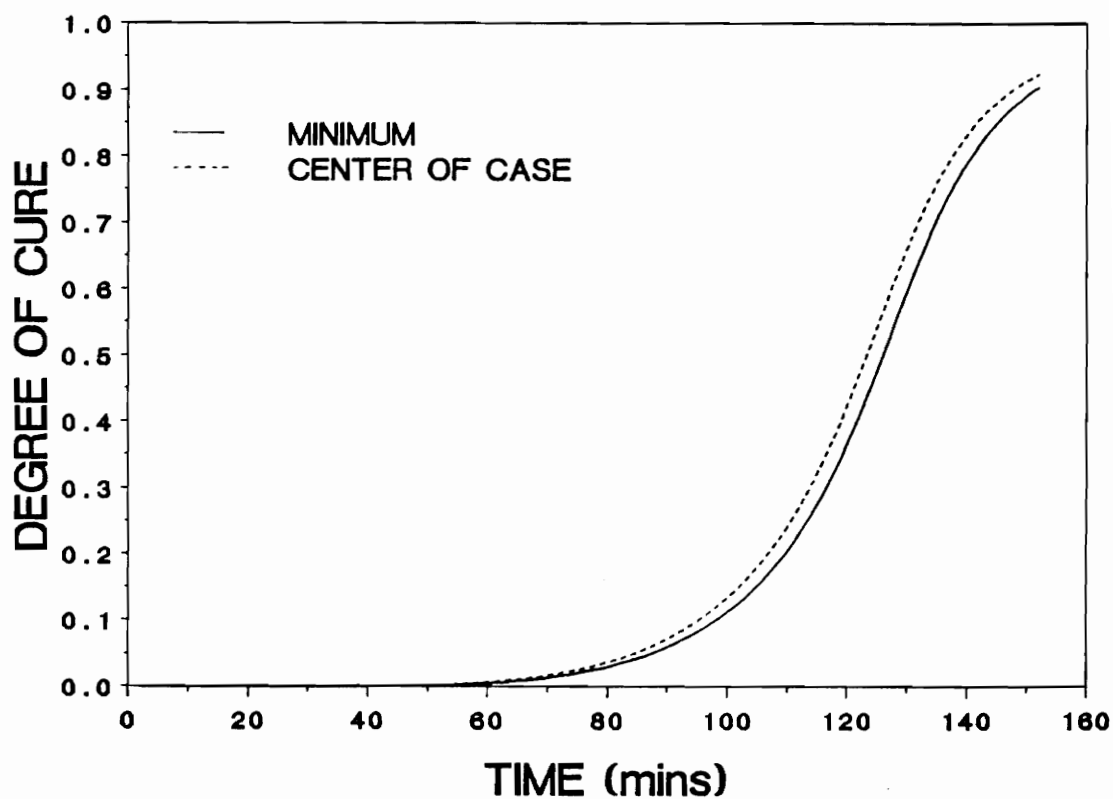


Figure 13. **AXISYMMETRIC CURE MODEL - Degree of Cure vs Time (5.75 in Bottle):**

The degree of cure at the center of the case and the minimum degree of cure are plotted as a function of time. The prepreg being used is the FIBERITE 976 / T300 which cures to an acceptable degree of 0.95 in 150 mins.

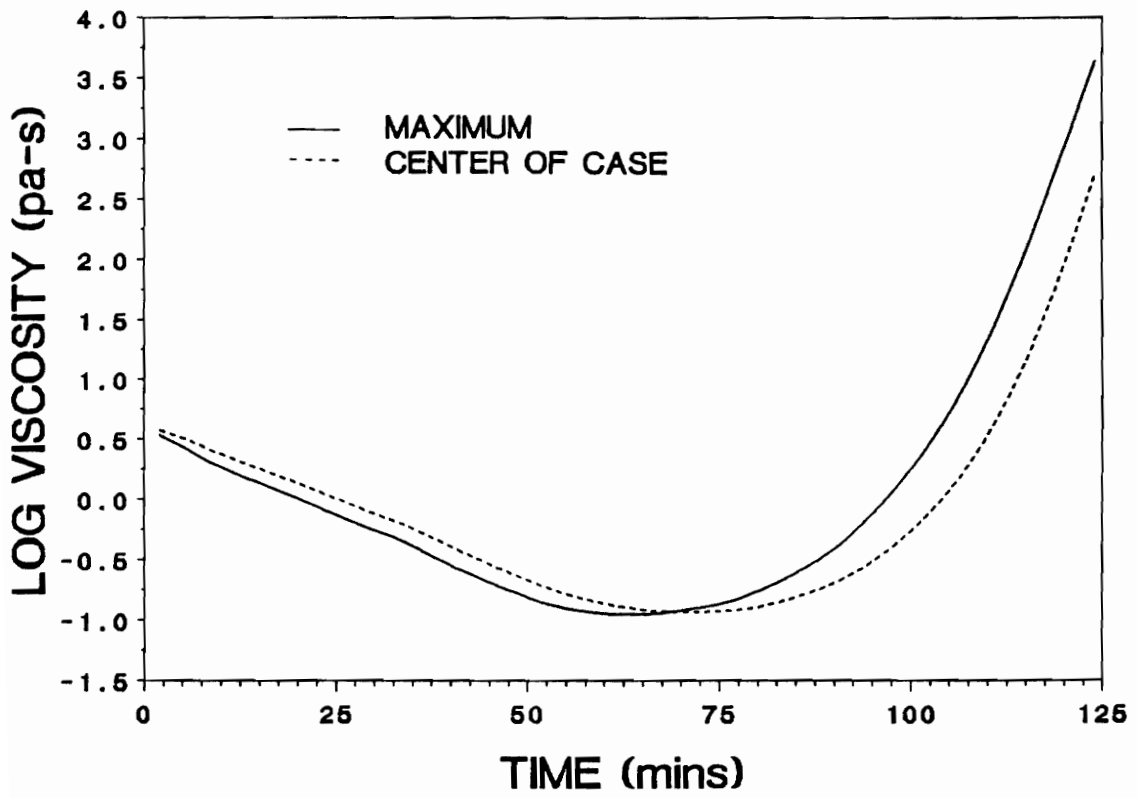


Figure 14. AXISYMMETRIC CURE MODEL - Log Viscosity vs Time (5.75 in Bottle):

The viscosity at the center of the case and the maximum viscosity are plotted as a function of time.

Table 3. INPUT PARAMETERS FOR PROGRAM "FEMCURE"

- | | |
|--|--|
| <p>1. GEOMETRY</p> <ul style="list-style-type: none"> a. Shape of the structure. b. Number of layers. c. Thickness of individual layers. <p>2. MANDREL PROPERTIES</p> <ul style="list-style-type: none"> a. Density. b. Specific Heat Capacity. c. Thermal Conductivity. <p>3. INSULATOR PROPERTIES</p> <ul style="list-style-type: none"> a. Density. b. Specific Heat Capacity. c. Thermal Conductivity. <p>4. PREPREG PROPERTIES</p> <ul style="list-style-type: none"> a. Initial resin mass fraction. b. Type of fiber being used. c. Type of resin being used in the composite. <p>5. RESIN PROPERTIES</p> <ul style="list-style-type: none"> a. Density. b. Specific Heat Capacity. c. Thermal Conductivity. d. Heat of Reaction. e. Relationship between cure rate, temperature and degree of cure. f. Relationship between viscosity, temperature and degree of cure. | <p>6. FIBER PROPERTIES</p> <ul style="list-style-type: none"> a. Density. b. Specific Heat Capacity. c. Thermal Conductivity. <p>7. OUTER LAYER PROPERTIES</p> <ul style="list-style-type: none"> a. Density. b. Specific Heat Capacity. c. Thermal Conductivity. <p>8. FINITE ELEMENT MESH PARAMETERS</p> <ul style="list-style-type: none"> a. Type of element being used. b. Type of mesh - symmetric or unsymmetric. c. Number of elements in the mesh. d. Number of nodes in the mesh. e. Number of elements modeling each subdomain. f. Time step parameter θ g. Time step h. Boundary nodes for convective heat transfer. <p>9. INITIAL AND BOUNDARY CONDITIONS</p> <ul style="list-style-type: none"> a. Initial temperature distribution in the composite. b. Initial degree of cure distribution in the composite. c. Cure cycle temperature as a function of time. |
|--|--|

Table 4. MATERIAL PROPERTIES FOR 18" BOTTLE

Material Properties 18 in bottle.

	Material	Density	Heat Capacity	Thermal Conductivity	Thickness
		ρ	C_p	K	r
		kg/m^3	$J/kg\ K$	$W/m\ K$	m
MANDREL	SAND PVA	0.2234×10^4	0.8373×10^3	1.851	0.7468×10^{-1}
INSULATOR	EPDM RUBBER	0.1100×10^4	0.1758×10^4	0.2077	0.1524×10^{-2}
CASE - FIBER	T - 300	0.1790×10^4	0.7117×10^3	25.97	0.4343×10^{-2}
CASE - MATRIX	FIBERITE 976	0.1260×10^4	1.2560×10^3	0.1674	
OUTER LAYER	POLYESTER	0.1370×10^3	1.0460×10^3	0.1507	0.3175×10^{-2}

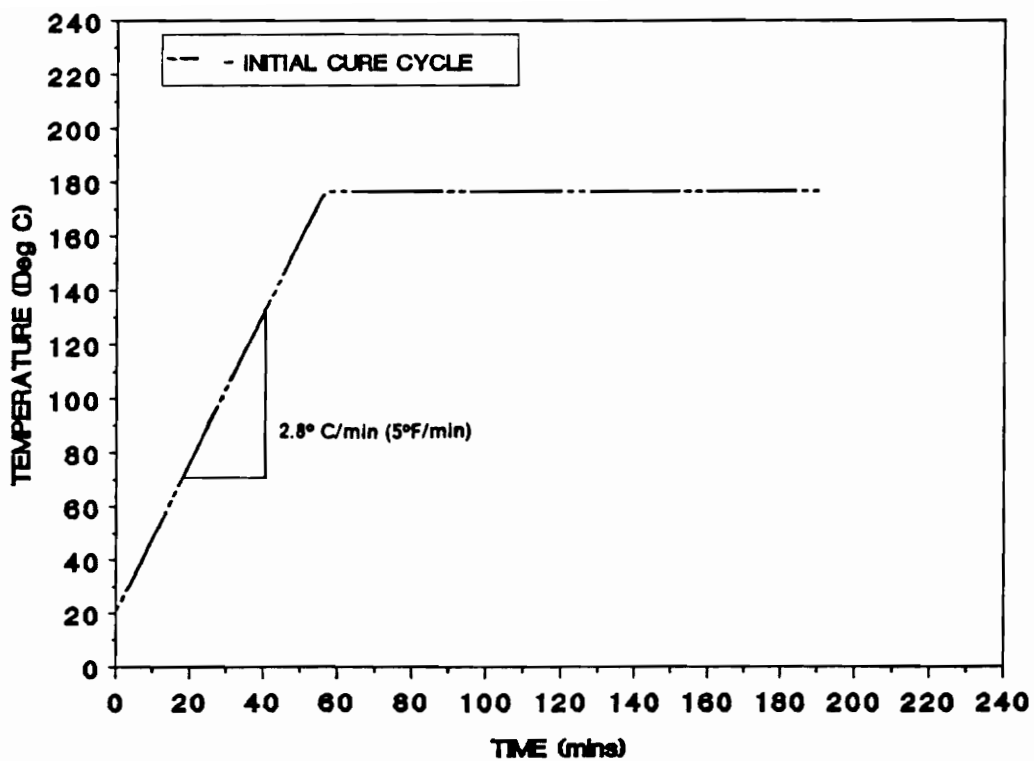


Figure 15. CURE CYCLE:

The cure temperature was increased at a constant heating rate of 2.8° C/min (5°F/min) from room temperature of 21.1°C until a maximum cure temperature of 177°C (350°F) was reached.

room temperature until a maximum cure temperature of 177°C (350°F) was reached. The temperature was held at 177°C until every point inside the composite case reached a degree of cure of 0.99.

For all calculations, it was assumed that the convective heat transfer coefficients were the same for the inner surface of the mandrel and the outer surface of the outer layer and remained constant throughout the cure. In general the convective heat transfer coefficient is a complex function of the geometry of the FWC assembly, the velocity and the physical properties of the autoclave fluid, and the temperature difference between the solid surface and the fluid, and must be determined experimentally. An assumed value for h_i and h_o was taken to be 100 W/m²K and used in the numerical analysis.

Thin Case

1. TEMPERATURE

The temperature distribution for a 0.4343×10^{-2} m (0.171 in.) thick case is presented in Figure 16. The temperature as a function of time at five selected locations inside the FWC assembly is shown in Figure 16. It is observed that the largest temperature drop occurs across the polyester breather cloth used as the outer layer material. The temperature difference across the composite case (Figure 17) is small and the case is curing uniformly. It is also noted that the temperatures at the inner surface of the mandrel and outer surface of the outer layer are quite different even though the oven temperature and the convective heat transfer coefficient were assumed to be the same. This could be attributed

to the curvature effects and the different material properties in the FWC assembly.

2. DEGREE OF CURE

The degree of cure $\alpha(r,t)$ of the resin in the composite case as a function of time is shown in Figure 18. Since the case is thin only the degree of cure at the center of the case and the minimum degree of cure at any point inside the case were plotted. The cure time for the composite case can be estimated from the time required for the degree of cure at any point in the composite to reach a pre-specified value of 0.99 which is observed to be approximately 205 minutes. The degree of cure as a function of the normalized radius is shown in Figure 19.

3. RESIN VISCOSITY

The viscosity of the resin in the composite case is plotted as a function of time in Figure 20. The maximum viscosity at any point inside the composite case at any time can be used to estimate the location and time when the resin begins to gel.

Thick Case

1. TEMPERATURE

The cure simulation was repeated for a thick composite case with a wall thickness of $0.254 \times 10^{-1} \text{m}$ (1.0 in.). The temperature as a function of time is presented

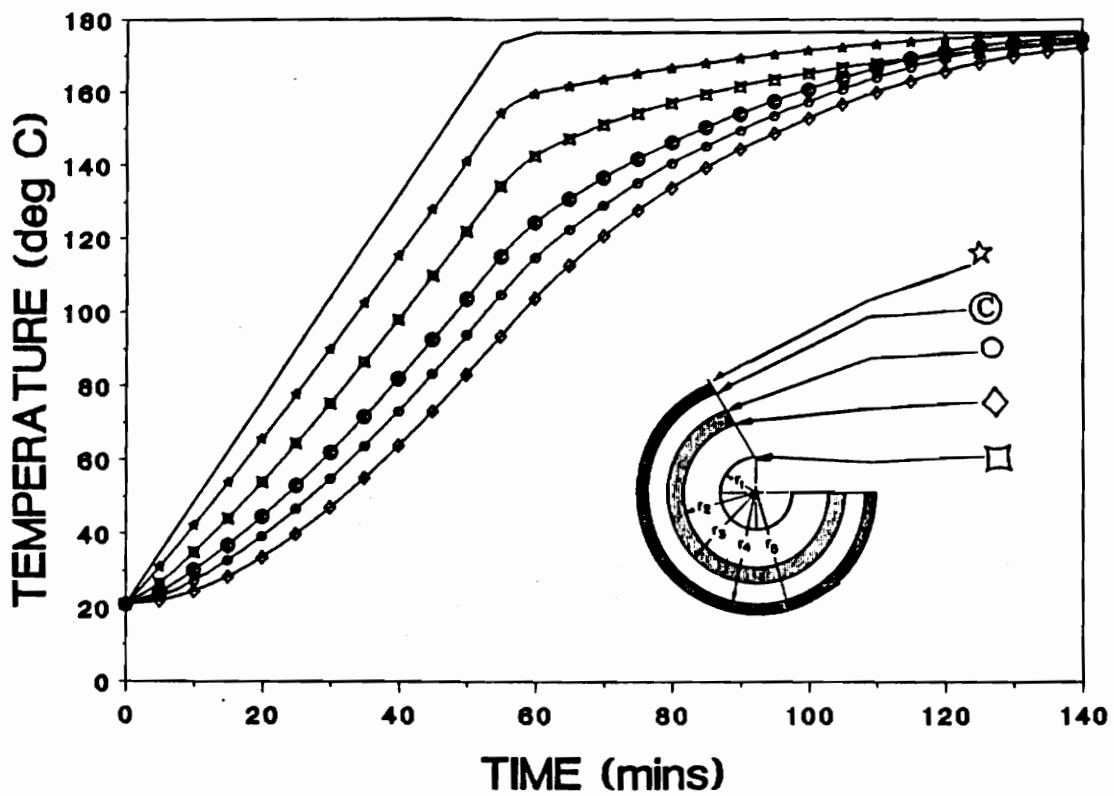


Figure 16. AXISYMMETRIC CURE MODEL - Temperature vs Time (Thin Case):

The temperature distributions at:- (a). the inner surface of the mandrel $r = r_1$, (b). the mandrel - insulator interface $r = r_2$, (c). the insulator - case interface $r = r_3$, (d). the case - outer layer interface $r = r_4$, and (e). the outer surface point $r = r_5$, are plotted as function of time for an 18 inch bottle with a 0.171 inch thick case. The heat transfer coefficients at the inner and outer surfaces were $100 \text{ W/m}^2\text{K}$

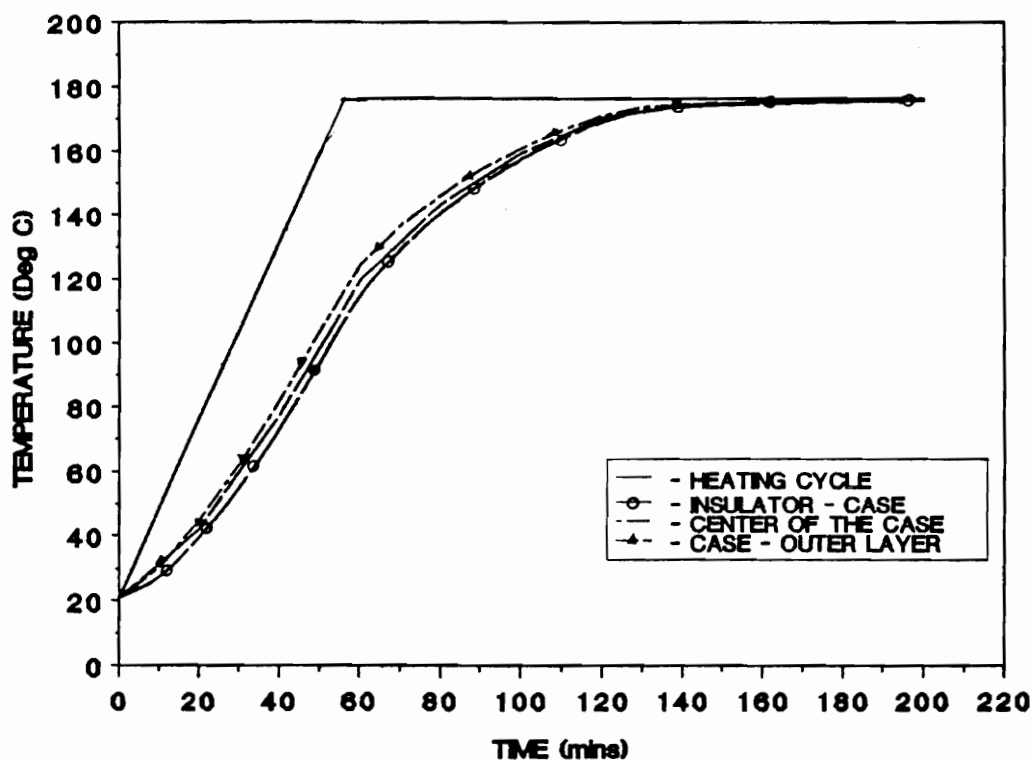


Figure 17. TEMPERATURE DROP ACROSS THE CASE:

The temperature distribution across the case and the temperature of the case center are plotted as a function of time for the 0.171 inch case.

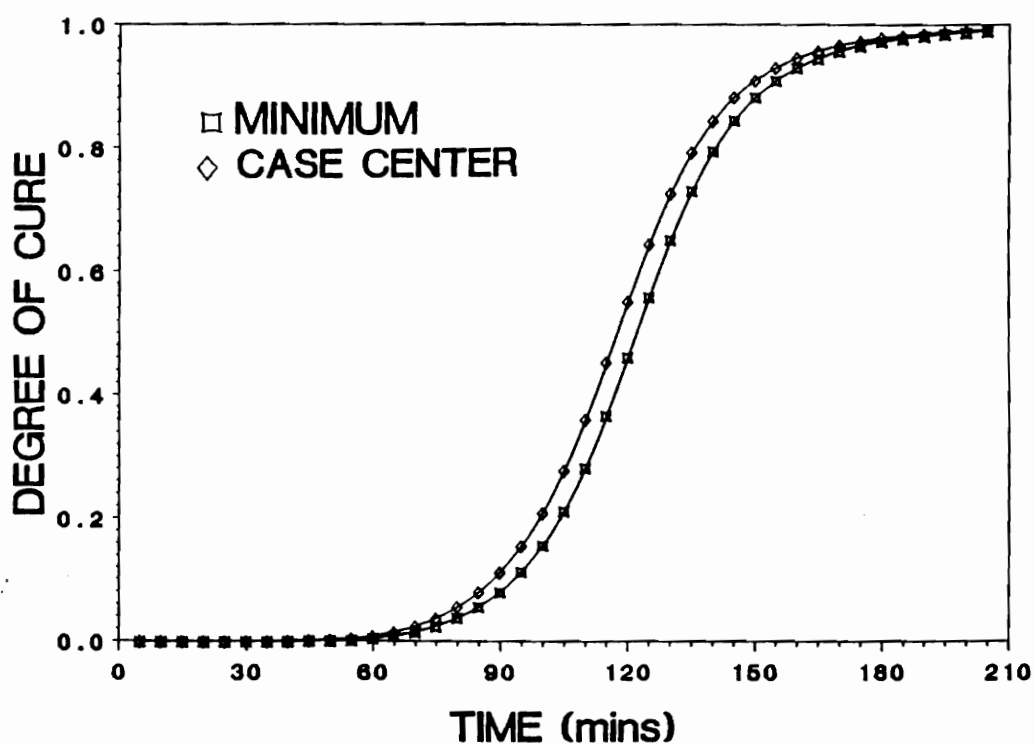


Figure 18. AXISYMMETRIC CURE MODEL - Degree of Cure vs Time (Thin Case):

The degree of cure at the case center and the minimum degree of cure are plotted as a function of time for the 0.171 inch case.

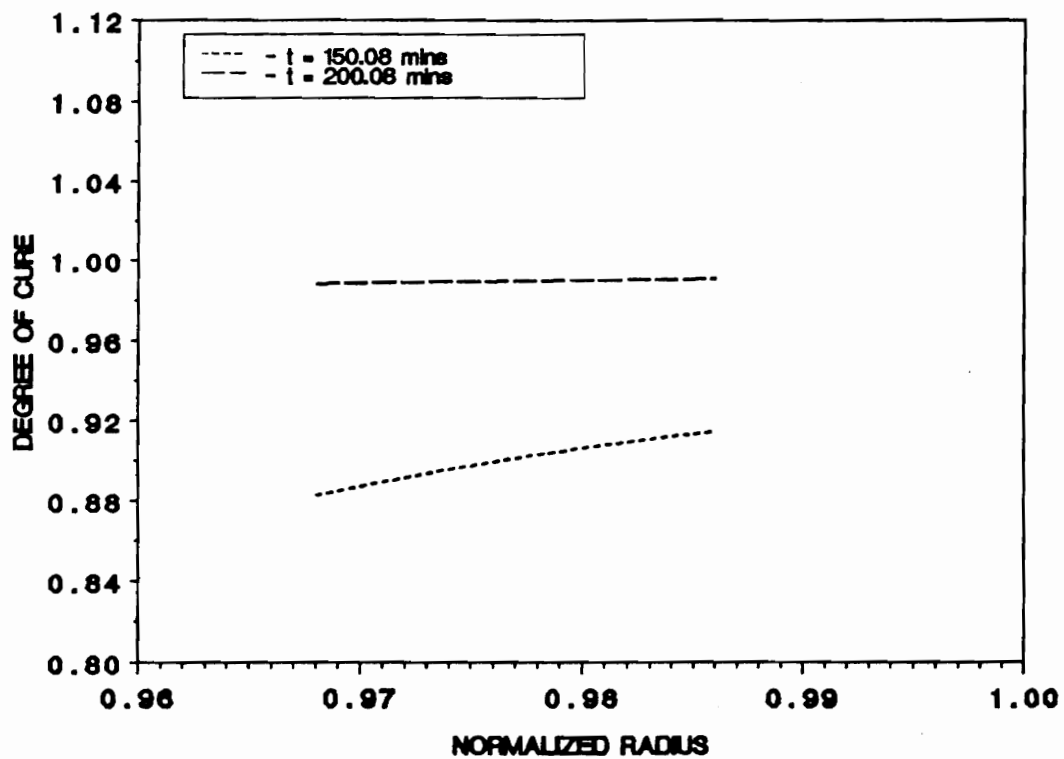


Figure 19. AXISYMMETRIC CURE MODEL - Degree of Cure vs Normalized Radius:

The degree of cure variation across the FWC assembly for a 0.171 inch case is plotted at two different times.

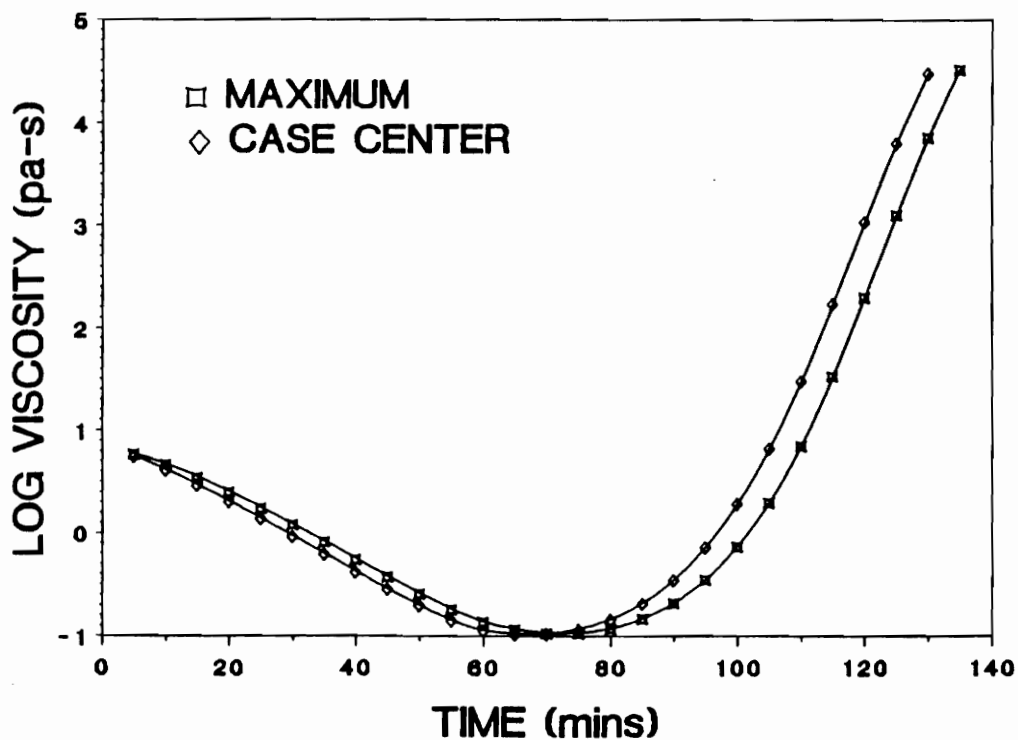


Figure 20. AXISYMMETRIC CURE MODEL - Log Viscosity vs Time (Thin Case):

The viscosity at the center of the case and the maximum viscosity are plotted as a function of time.

in Figure 21. As expected the increased wall thickness results in a substantial temperature drop across the case thickness. At 120 minutes into the cure, the temperature at the outer surface of the case actually exceeds the cure temperature by almost 10°C. The temperature overshoot occurs due to runaway reactions causing heat to be generated at a rate higher than it can be dissipated. The overshoot reaches a peak value of 228.3°C at a time of 133.3 minutes. As the cure progresses the the temperature begins to fall and converges to the hold temperature as the specified degree of cure is achieved across the composite thickness. The temperature drop across the case is shown in Figure 22. The peak overshoot occurs at the case - outer layer interface. The temperature drop across the case in the lag region is fairly uniform until the exotherm occurs. The temperature distribution in the FWC assembly with the thick case is shown in Figure 23. Due to the presence of exotherms the temperature distribution in the FWC assembly is nonuniform.

2. DEGREE OF CURE

The degree of cure as a function of time is shown in Figure 24. Due to the nonuniformity in the temperature distribution it would be expected that the case is being cured nonuniformly as shown in Figure 25. The degree of cure behavior as a function of the normalized radius is shown in Figure 25. At $t = 120.08$ mins and $t = 140.08$ mins the composite is curing nonuniformly as expected due to the nonuniform temperature distribution in the case.

3. RESIN VISCOSITY

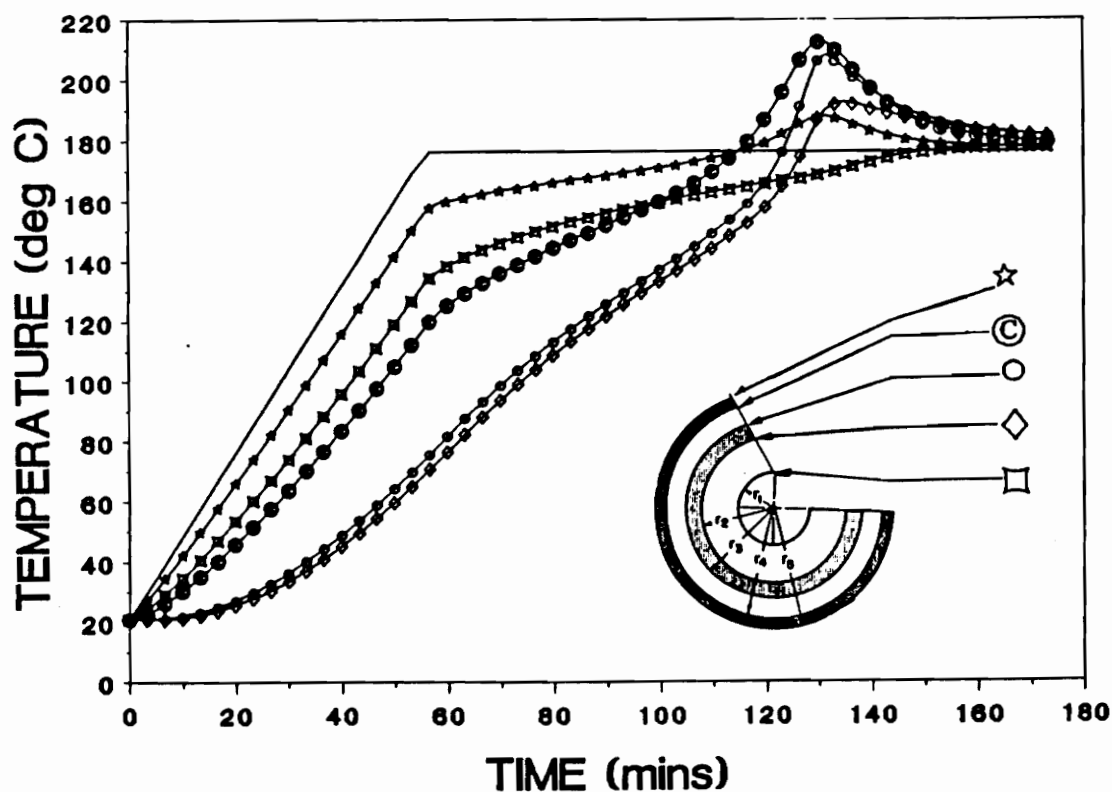


Figure 21. AXISYMMETRIC CURE MODEL - Temperature vs Time (Thick Case):

The temperature distributions at: (a). the inner surface of the mandrel $r = r_1$, (b). the mandrel - insulator interface $r = r_2$, (c). the insulator - case interface $r = r_3$, (d). the case - outer layer interface $r = r_4$, and (e). the outer surface point $r = r_5$, are plotted as function of time for an 18 inch bottle with a 1.0 inch thick case. The heat transfer coefficients at for the inner and outer surfaces were $100 \text{ W/m}^2\text{K}$

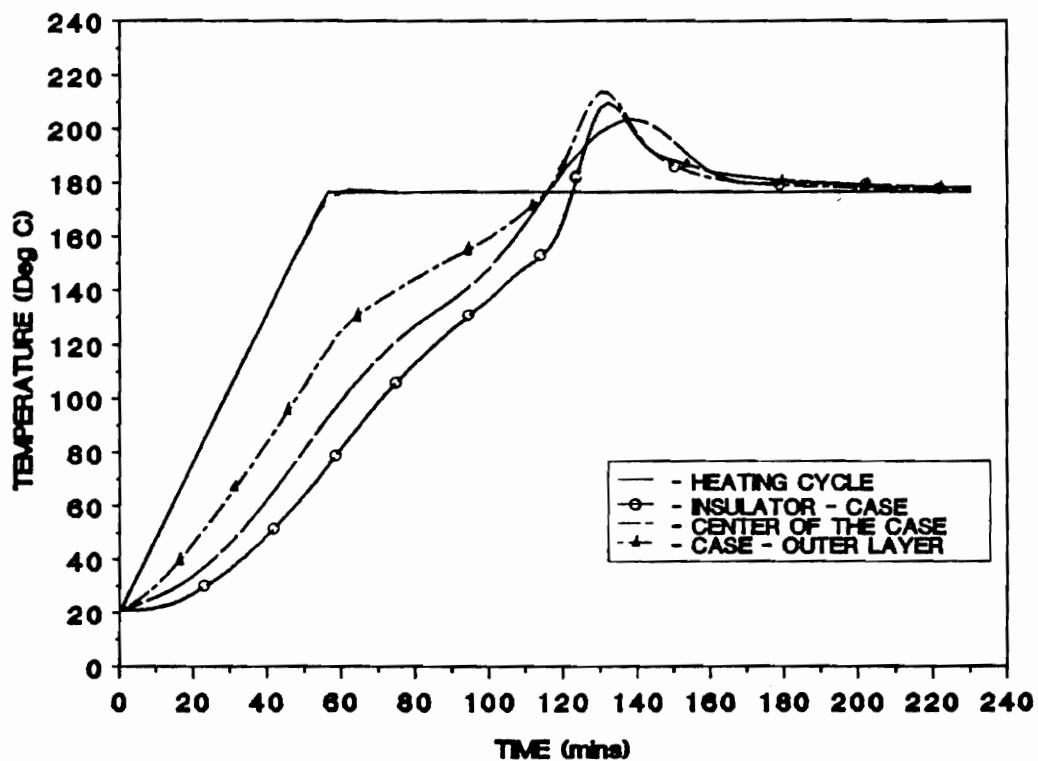


Figure 22. TEMPERATURE DROP ACROSS THE CASE:

The temperature at the insulator - case interface, the center of the case and the case - outer layer interface is plotted as a function of time. The beginning of the reaction exotherm can be identified

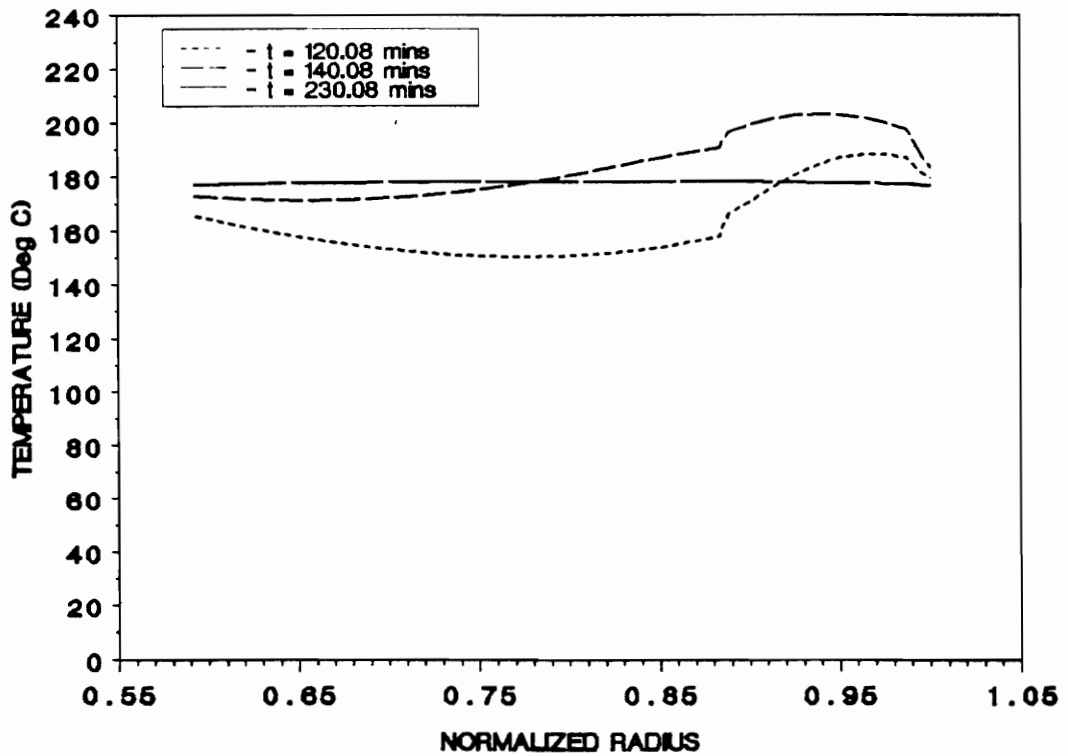


Figure 23. AXISYMMETRIC CURE MODEL - Temperature vs Normalized Radius:

The temperature distribution of the FWC assembly plotted at three different times: (a). $t = 120.08$ mins, a time before the temperature overshoot peaks, (b). $t = 140.08$ mins, a time after the temperature overshoot peak has been reached, (c). $t = 230.08$ mins, a time when desired degree of cure is achieved in the composite.

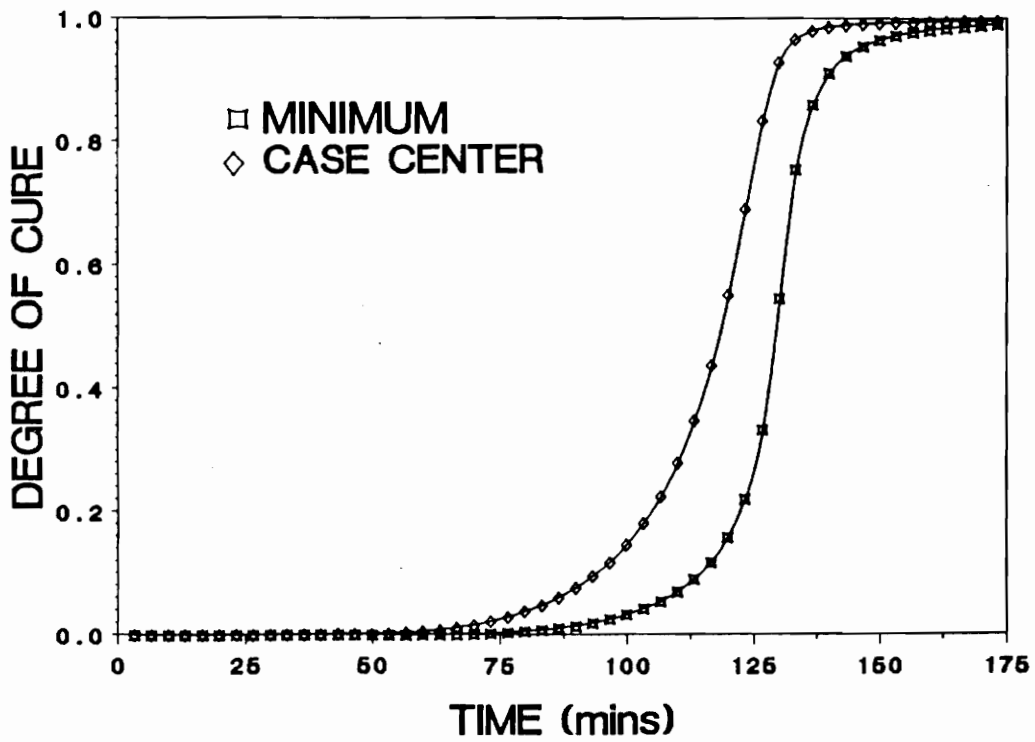


Figure 24. AXISYMMETRIC CURE MODEL - Degree of Cure vs Time (Thick Case):

The minimum degree of cure and the degree of cure at the center of the case are plotted as a function of time for a 1.0 inch thick composite case.

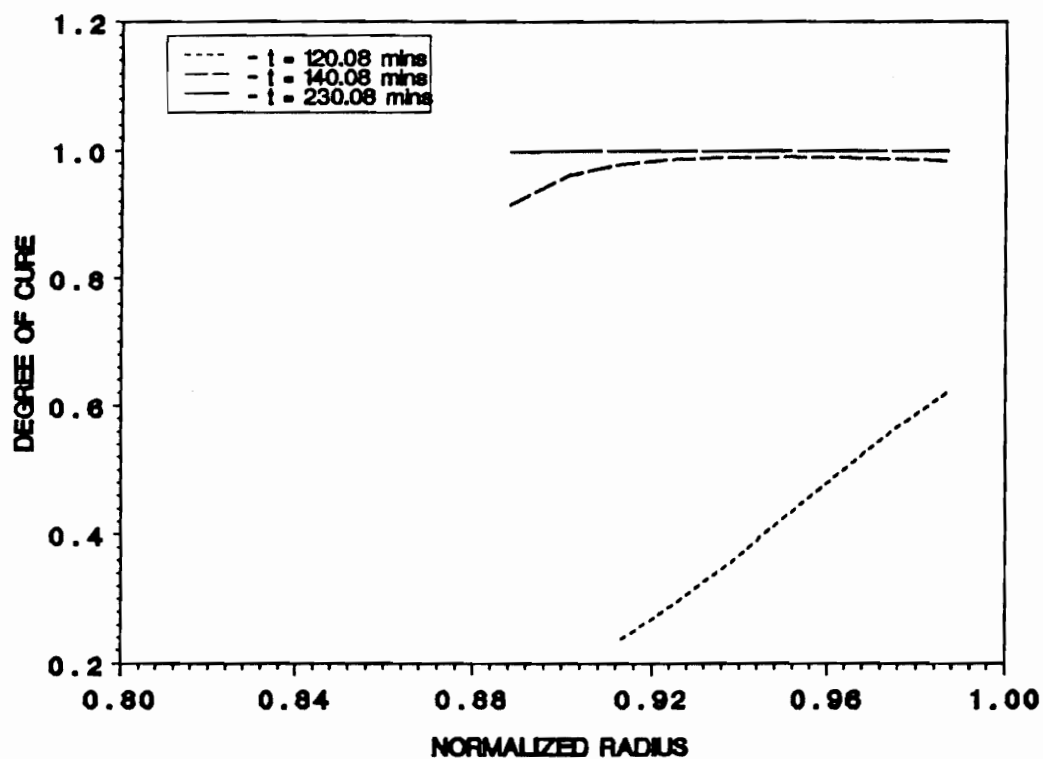


Figure 25. AXISYMMETRIC CURE MODEL - Degree of Cure vs Normalized Radius:

The degree of cure across the thickness of the FWC assembly is plotted at three different times.

The resin viscosity as a function of time and the viscosity distribution for the thick case are shown in Figure 26. As expected the viscosity distribution is nonuniform and the resin in the outside layers of the composite gels quickly. Premature gelation may lead to poor matrix properties and decrease in the strength of the composite.

Comparison Between Thin and Thick Cases

A comparison between the degree of cure at the center of the 0.171 inch case and at the center of the 1.0 inch case is shown in Figure 27. Curing of the thin section composite is gradual as compared to curing of the thick section composite which is rapid due to reaction exotherms. The viscosity at the center of the case for the 0.171 inch case and the 1.0 inch case is compared in Figure 28. It is observed that the thick section composite gels easily which in turn reduces the time for compaction and flow.

The process modeling problem analyzed thus far gives the initial estimate on the time required for the composite to achieve a prespecified degree of cure of 0.99. For the thin section composite it is estimated that all the points within the composite will achieve a prespecified degree of cure in 180 - 200 minutes. In the case of the thick section composite the final time to achieve the same degree of cure it takes 230 - 240 minutes.

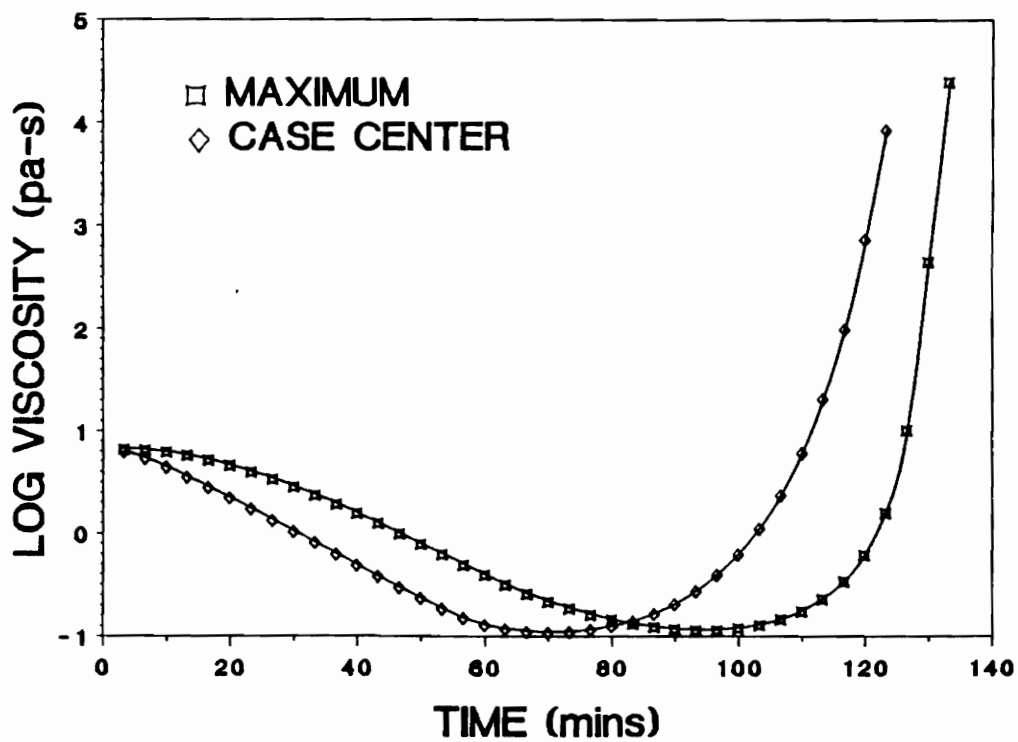


Figure 26. AXISYMMETRIC CURE MODEL - Log Viscosity vs Time (Thick Case):

The maximum viscosity and the viscosity at the case center for a 1.0 inch thick composite case are plotted as a function of time.

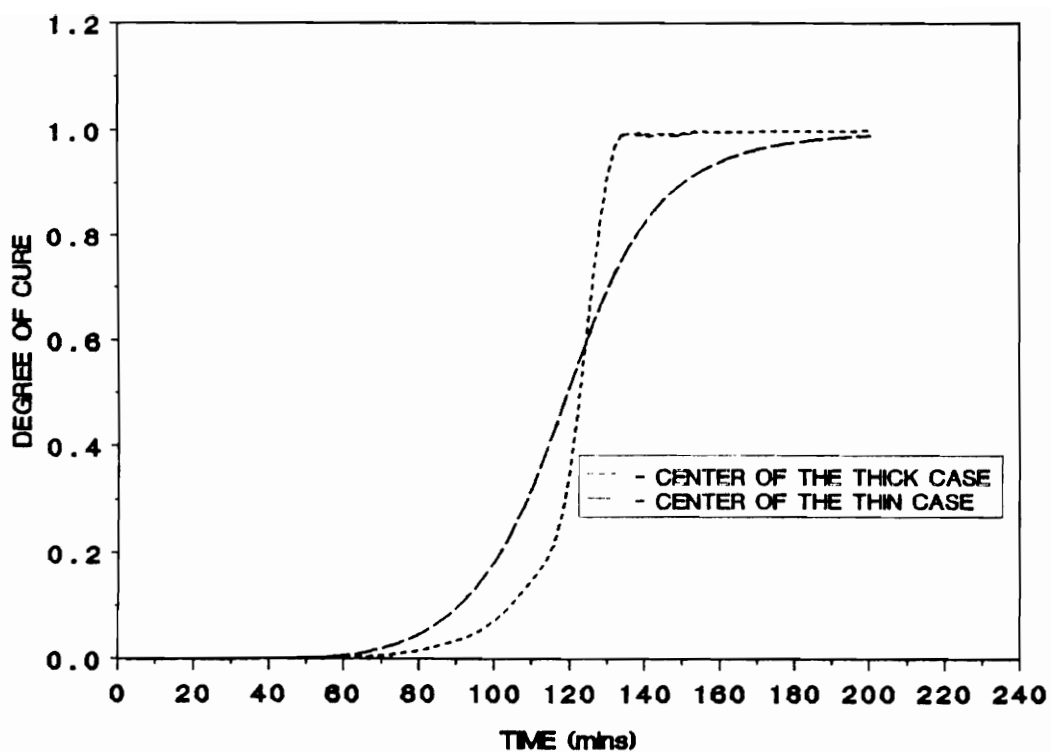


Figure 27. COMPARISON STUDIES - Degree of Cure vs Time:

The degree of cure of the thick section composite and the thin section composite is compared at the center of the case as a function of time.

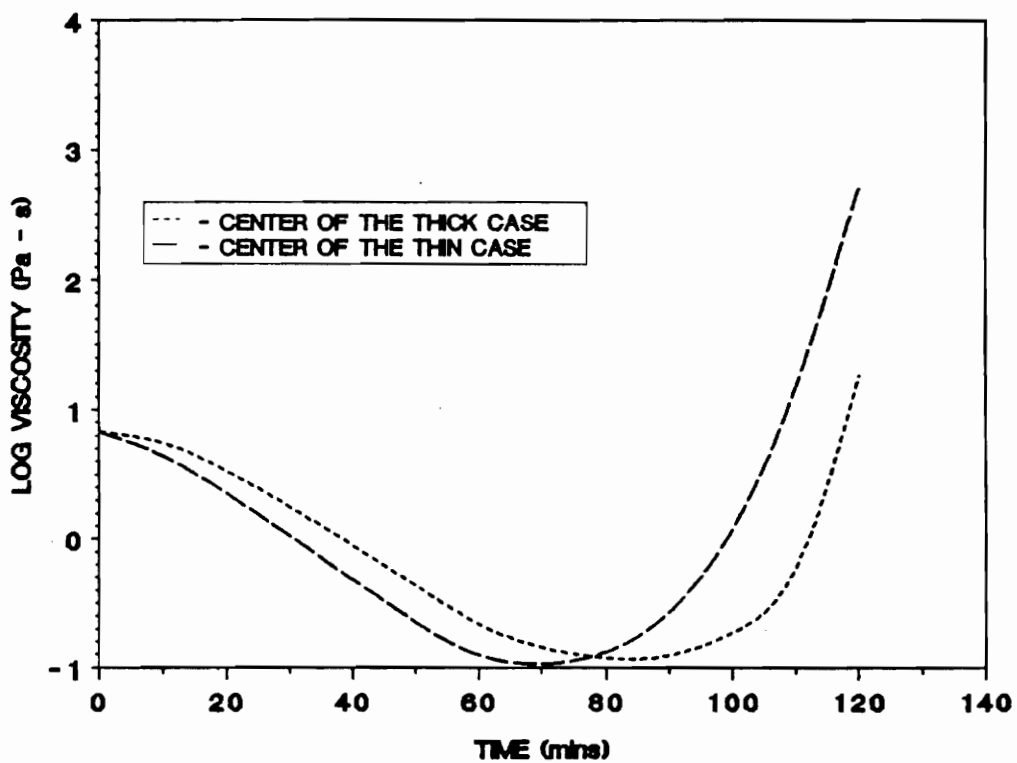


Figure 28. COMPARISON STUDIES - Log Viscosity vs Time:

The viscosity of the thick section composite and the thin section composite is compared at the center of the case as a function of time.

CHAPTER 5

CURING PROCESS OPTIMAL CONTROL

The curing process of filament wound composites was modeled and validated with available experimental data for a predetermined cure cycle. No attempt was made to optimize the cure cycle. It was also demonstrated in Section 4.5 that curing of thick section composites using cure cycles developed for thin laminates results in a non-uniformly cured structure.

It has been of primary interest that a technique be determined in order to eliminate the costly and time consuming trial and error procedure for determining the optimum cure cycle for a given application. The cure cycle process variables, namely the autoclave (or oven) temperature and applied pressure, significantly influence the mechanical performance of the cured composite. Thus, it is imperative that we fully

understand the effects of the processing cycle used to cure a filament wound composite.

5.1 Effects of Processing Environment

In a thermoset composite, the matrix resin when subjected to an autoclave processing environment of elevated temperature undergoes a transition from a soft uncured material to a hard, brittle, insoluble, and infusible material through exothermic chemical reactions. A fully cured resin does not melt upon application of heat. However, thermosetting resins have an effective upper use temperature [42 - 44] beyond which they suffer a loss in stiffness. This temperature is defined as the heat distortion temperature or the resin glass transition temperature. The glass transition temperature depends on the state of cure of the resin.

It has been demonstrated experimentally that the cure or reaction rate for thermosetting resins used in polymer based composites depends on the degree of cure and temperature [6 - 9] at any instant of time. A typical functional relationship for epoxy resins is given in Appendix A. The exothermic chemical reactions generate heat which can affect the temperature in the composite. It has been observed (Figure 23), that the generation of heat can lead to the temperature overshoots or runaway reactions [43]. This is particularly true for thick filament wound composites and laminates [2,43,45].

Observations of the viscosity variations with respect to time (Figure 28) indicates that upon initial heating the viscosity decreases and as the reaction progresses the

viscosity rises and resin gels. It was shown in Section 2.9 that both the degree of cure and temperature determine the viscosity of the resin in the composite.

The temperature plays a major role in determining the extent of the cure reaction and the uniformity of cure in the composite. Thus, the cure temperature must be carefully selected for a given application.

5.2 State, Co-state & Control Variables

Recognition of the fact that temperature plays a dominant role in the curing process enables us to realize that if the temperature of the processing environment is properly controlled then we can control the thermal, chemical, and physical processes occurring during cure of the composite. Careful control of the curing process coupled with a fundamental understanding of the curing process will allow the final properties of the composite to be optimized. The goal of this investigation is to develop a technique which can be used to select the optimal cure cycle for the filament wound composite case.

The mandrel - insulator - composite case - outer layer (FWC assembly, Figure 3), placed in the autoclave and subjected to the cure cycle temperature becomes the system to be optimized. The governing partial differential equations for conduction heat transfer given in Eqs.(2.1a) - (2.1d) are the equations used to determine the state of the system (i.e., temperature as a function of space and time). In effect the parabolic PDE's describe the unsteady, nonlinear heat transfer process in the FWC assembly.

Influence of the processing cycle enters through the boundary conditions Eq.(2.7). The internal temperature distributions can be controlled by adjusting the cure temperature on the inner and outer surfaces of the FWC assembly. Thus, the cure cycle temperature ($T_{\infty}(t)$) is the primary control variable and determines the state (temperature distribution) of the system.

The reaction rate occurring in the composite, having a functional form described by Eq.(2.4), is temperature dependent and affects the rate of heat generation, degree of cure, and resin viscosity. Since the cure reaction determines the total process time, the degree of cure defined in Eq.(2.5) will be considered as an active co-state of the system. The resin viscosity depends entirely on the degree of cure and temperature within the composite and is considered as a passive co-state and is not used directly in the optimization.

5.3 Constraints & Stopping Conditions

A distributed parameter system has constraints related to both the distributions in the spatial domain as well as the time domain. The control variable $T_{\infty}(t)$ is constrained to lie within a decision space governed by the physical limitations of the autoclave. The autoclave has limitations on the rate of heating and cooling, as well as, on the maximum operating temperature. All of these factors have to be considered as the limiting bounds of the decision space as well as bounds on the control variable $T_{\infty}(t)$.

The temperature and degree of cure distributions in the composite are constrained to lie within bounds governed by the material system used. Ideally it is desired that

the composite would attain prespecified acceptable properties within the shortest possible time. Also, it is important to control the temperature inside the composite in such a manner that the temperature overshoots due to runaway exothermic chemical reactions are controlled and minimized.

The trial and error method of guessing or choosing a cure cycle based on empiricism can be eliminated by utilizing a dynamic programming approach [47 - 49] to monitor the curing process variables and incorporate the constraints on the system by defining an error (objective) function to be minimized. This approach will enable us to determine the optimal cure cycle and ensure that the composite will cure within a specified time or reaches a specified stopping condition. The stopping condition terminates the curing process upon attaining a prespecified degree of cure and provides an estimate of the final process time t_f . Also, the stopping condition will ensure that the cured composite has the desired prespecified properties.

5.4 Constraint Specifications

The constraints specify the boundaries of the decision space within which the optimal cure cycle temperature can lie. The constraints which are pertinent to the optimal cure process control problem are identified below :

1. CONSTRAINT ON CONTROL VARIABLE - CURE CYCLE TEMPERATURE

The cure cycle is physically constrained to lie within the upper or lower temperature bounds of the autoclave (or oven).

$$U_L(t) \leq T_{\infty}(t) \leq U_U(t) \quad (5.1)$$

Here, $U_L(t)$ is the lower bound of the autoclave temperature (usually room temperature) and $U_U(t)$ is the upper bound temperature defined as the maximum temperature that can be applied to the material being cured in the autoclave. The upper bound temperature can also be governed by the performance characteristics of the autoclave (i.e., fluid viscosity, flow characteristics, thermal load).

2. CONSTRAINT ON THE EXTENT OF THE REACTION

The degree of cure $\alpha(r,t)$ (defined as the co-state), which characterizes the extent of polymerization and thermally induced crosslinking, is constrained to lie within prespecified bounds. The thermo-kinetic model of the chemical reaction gives the degree of cure at any instant in the process. If the cure cycle heating rate or temperature is very high, excessive temperatures can develop in the interior of the composite resulting in thermolysis and gradual degradation of the stiffness properties of the resin matrix. It is thus necessary to control the reaction such that resin polymerization is achieved uniformly in the composite without damage or degradation of the matrix.

The lower bound on the extent of cure is the initial degree of cure of the composite at the inception of the process $\alpha^*(r)$.

$$\alpha_L(r,t) = \alpha^*(r) \quad \forall \quad r \in [r_3, r_4] \quad (5.2)$$

The upper bound on the extent of cure can be specified as,

$$\alpha_U(r,t) = \alpha^R(r,t) \quad \forall \quad r \in [r_3, r_4] \quad (5.3)$$

where $\alpha^R(r,t)$, is the required degree of cure in the composite.

Thus, the extent of the cure reaction can be controlled at any instant of the process to lie within the decision space identified by the limits as follows.

$$\alpha_L(r,t) \leq \alpha(r,t) \leq \alpha_U(r,t) \quad (5.4)$$

As an example if the initial resin is uncured then $\alpha_L(r,t)$ is zero and if complete cure is desired then $\alpha_U(r,t)$ approaches unity.

3. STOPPING CONDITION

The degree of cure at every point in the composite $r \in [r_3, r_4]$ must be uniform. This uniformity can be ensured if the thermal gradients at each instant of the process are minimized. If the temperature distribution in the composite can be controlled in such a manner that uniformity is maintained at all instants of the process, then a uniform cure can be achieved at all times.

The constraint specification that every point within the composite must be cured to a prespecified degree of cure ($\alpha^R(r,t)$) and the cure must be uniform can be used as a criterion to terminate the curing process. An objective function $J_1(r,t)$ to implement this criterion can be formulated as a spatial integral of the difference between the desired degree of cure distribution and the degree of cure at final time ($t = t_f$)

$$J_1(r,t) = \frac{1}{2} \int_{r_3}^{r_4} [\alpha(r,t_f) - \alpha^R(r,t_f)]^2 dr \quad (5.5)$$

The degree of cure gives an estimate of the extent of the reaction in the composite. This knowledge, along with the bounds on the degree of cure, can be utilized to recognize the particular instant ($t = t_f$) when sufficient polymerization has been attained and the reaction (or cure) can be terminated. This is the stopping condition for the curing process and is defined as the time t at which the composite reaches the required degree of cure. Mathematically the stopping condition is

$$\alpha(r,t_f) = \alpha^R(r,t_f) \quad (5.6)$$

where t_f is the final time.

4. UNIFORMITY OF TEMPERATURE

Since it has been recognized that the temperature plays a predominant role in the control of the curing process, it is necessary that the temperature distribution in the FWC assembly remain uniform at all instants of time. The condition of an uniform temperature distribution can be imposed through a dynamic objective function $J_2(r,t)$ as follows

$$J_2(r,t) = \frac{1}{2} \int_{t_i}^{t_f} \int_{r_1}^{r_5} [T(r,t) - T^D(r,t)]^2 dr dt \quad (5.7)$$

where t_i is the initial time of the process, (usually $t = 0$), t_f is the final time, and $T^D(r,t)$ is the average temperature distribution in the FWC assembly at any particular instant of time t .

5. CONSTRAINTS ON THE TEMPERATURE DISTRIBUTION

The objective $J_2(r,t)$ identified in Eq.(5.7) represents the least squares error between the actual temperature $T(r,t)$ and the average temperature $T^D(r,t)$. For a distributed system, the average temperature $T^D(r,t)$ at any instant of time t can be calculated as follows.

$$T^D(r,t) = \frac{1}{(r_5 - r_1)} \int_{r_1}^{r_5} T(r,t) dr \quad \forall r \in [r_1, r_5] \quad (5.8)$$

In order to determine the constraints on the internal temperature distribution two very important aspects of the curing process have to be recognized. Namely the presence of an exotherm (i.e., heat generation due to the chemical reactions) and a lag in the temperature response of the system. It is noted that both the exotherm and the thermal lag are thickness (i.e., geometry) and time dependent.

a. CONSTRAINT IDENTIFICATION FOR THE EXOTHERM REGION

As the oven heats up and the curing process in the FWC assembly is initiated, the time at which the exotherm begins can be estimated as the time at which any point within the composite case has a temperature $T(r,t)$ greater than the cure cycle temperature at that instant. This instant of time will be denoted t_e^* , and called the exotherm initiation time.

After identifying the exotherm initiation time, it is necessary to estimate the extent of the peak exotherm for the reaction. This can be done by tracking the difference between the temperature of the composite and the cure cycle temperature at every point within the composite at each instant of time. The peak exotherm temperature is specified as $T_p^e(r,t)$ at the maximum difference point.

Beyond the peak exotherm, temperature decreases and approaches the cure cycle temperature $T_\infty(r,t)$ (Figure 29). The time t_f^e is defined as the time beyond which there are no exothermic reactions occurring inside the composite.

Once the exothermic region is recognized, the temperature distribution in this region can be constrained to lie within feasible bounds enabling us to minimize the least squares error between the actual temperature and the average temperature. An estimate of the average temperature distribution can be written as

$$T_e^D(r,t) = \frac{1}{(r_5 - r_1)} \int_{r_1}^{r_5} T(r,t) dr - \frac{T_p^e(r,t) - T_\infty(t)}{2} \quad (5.9)$$

where $T_e^D(r,t)$ is the modified average temperature distribution valid for all times $t \in [t_i^e, t_f^e]$ in the exotherm region. In Eq.(5.9) the first term on the right hand side corresponds to the average temperature (Eq.(5.8)) and the second term is used to correct the average temperature when exotherms are present. It is to be noted that the second term is a correction factor which approaches zero as the exotherm of the system decreases. Thus, as the system

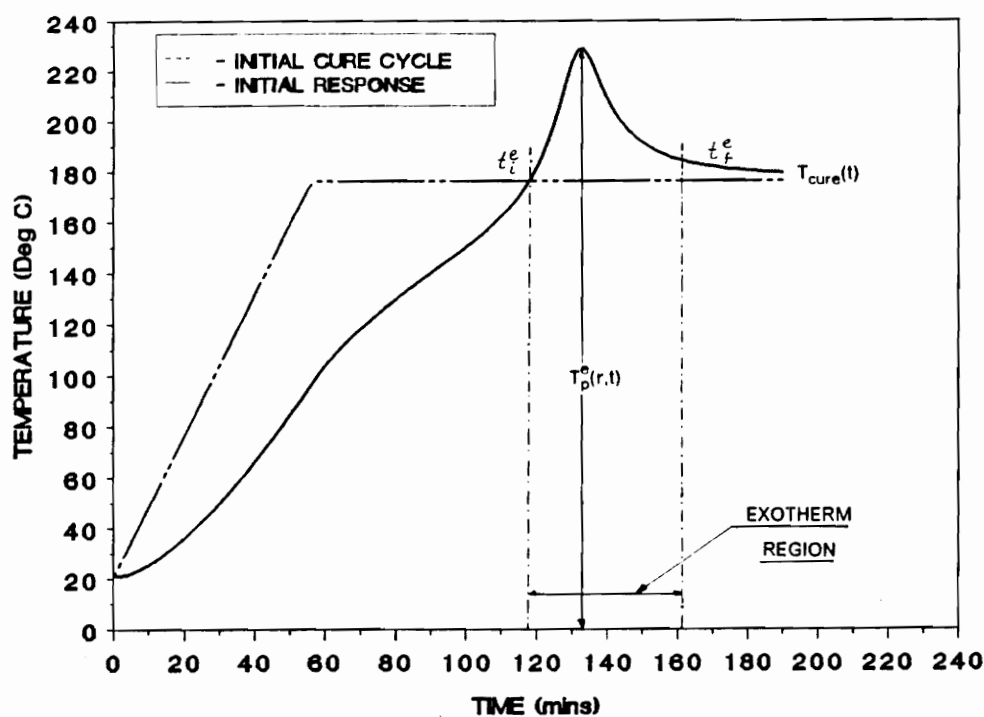


Figure 29. EXOTHERM REGION - Temperature Vs Time:

The inception of the exotherm region is at a time $t = t_i^e$ and reaches a peak overshoot temperature of $T_p^o(r,t)$. The exotherm then converges to the cure temperature of $T_\infty(r,t)$ at a time $t = t_f^e$. The exotherm region lies in the time domain $t \in [t_i^e, t_f^e]$

exotherm is minimized the modified average approaches the actual average temperature distribution.

b. CONSTRAINT IDENTIFICATION FOR THE LAG REGION

As the exothermic region was recognized, a similar approach can be adopted to recognize the lag region (Figure 30). The time t_l^b , at which the lag begins, and the time t_l^e , where the lag ends can be recognized as the temporal bounds of the region. The maximum difference between the actual temperature and the cure cycle temperature $T_\infty(t)$ is the peak lag temperature which is denoted by $T_p^L(r,t)$. The modified average temperature for the lag region is denoted as $T_L^D(r,t)$ and expressed as follows

$$T_L^D(r,t) = \frac{1}{(r_5 - r_1)} \int_{r_1}^{r_5} T(r,t) dr + \frac{T_\infty(t) - T_p^L(r,t)}{2} \quad (5.10)$$

where the first term on the right hand side represents the average temperature distribution defined in Eq.(5.8) and the second term is used to correct the average temperature in the lag region. It is to be noted that the second term on the right hand side of Eq.(5.10) is a correction factor which approaches zero as the lag of the system decreases. Thus, as the system lag decreases the modified average approaches the actual average temperature distribution.

The objective functions $J_1(r,t)$ and $J_2(r,t)$ described earlier in this section are combined to form a single scalar valued overall performance index $J(r,t)$ [49].

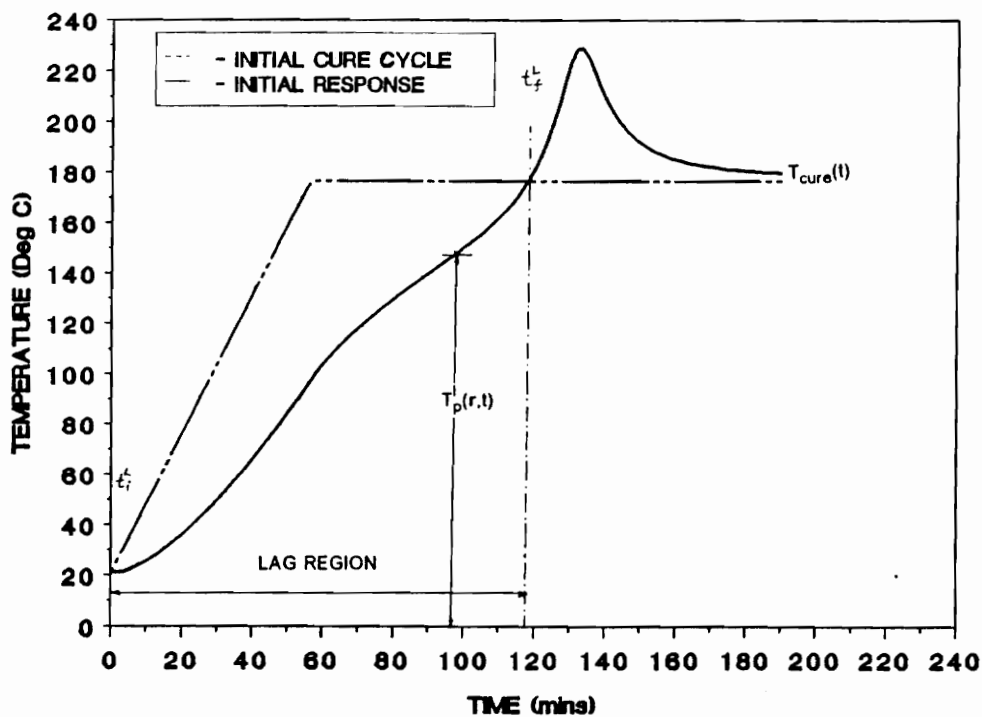


Figure 30. LAG REGION - Temperature vs Time:

The inception of the lag region is at a time $t = t_i^L$ and reaches a peak lag temperature of $T_p(r,t)$. The lag then converges to the cure temperature of $T_{\infty}(r,t)$ at a time $t = t_f^L$. The lag region lies in the time domain $t \in [t_i^L, t_f^L]$

$$J(r,t) = \frac{1}{2} \int_{r_3}^{r_4} [\alpha(r,t) - \alpha^R(r,t)]^2 dr + \frac{1}{2} \int_{t_i}^{t_f} \int_{r_1}^{r_5} [T(r,t) - T^D(r,t)]^2 dr dt \quad (5.11)$$

The primary aim of the optimal control problem is to minimize the performance index $J(r,t)$ by suitably altering the cure cycle temperature $T_\infty(r,t)$ applied at the boundaries of the system.

CHAPTER 6

OPTIMAL CURE CYCLE IDENTIFICATION

The curing process control problem is governed by a performance index $J(r,t)$ (see Section 5.4) that needs to be minimized subject to constraints on the temperature distribution in the FWC assembly, degree of cure distribution in the composite, and the cure temperature $T_{\infty}(r,t)$. The performance index can be written as

$$J(r,t) = \frac{1}{2} \int_{r_3}^{r_4} [\alpha(r,t_f) - \alpha^R(r,t_f)]^2 dr + \frac{1}{2} \int_{t_1}^{t_f} \int_{r_1}^{r_5} [T(r,t) - T^D(r,t)]^2 dr dt \quad (6.1)$$

and describes the individual objectives of uniformity of cure (Eq.(5.5)) at final time ($t = t_f$) and the uniformity of temperature (Eq.(5.7)) simultaneously.

6.1 Equation Of State For Control

It is observed from the definition of the objectives functions $J_1(r,t)$ and $J_2(r,t)$ in Section 5.4 that both objectives have to be minimized in order to minimize the performance index $J(r,t)$ (Eq.(6.1)). This is rather difficult if both objectives $J_1(r,t)$ and $J_2(r,t)$ are independent. From the definition of $J_2(r,t)$, that the least squares error between the actual temperature distribution $T(r,t)$ and the average temperature distribution $T^D(r,t)$ be minimized simultaneously in the time domain as well as the spatial domain, allows us to treat $J_2(r,t)$ as an additional state variable and treat the least squares error as a stochastic disturbance input to the system.

Consider the one-dimensional unsteady heat conduction equation in radial coordinates with heat generation,

$$\frac{\partial(\rho_j C_j T_j)}{\partial t} = \frac{1}{r} \frac{\partial}{\partial r} (K_j r \frac{\partial T_j}{\partial r}) + \rho_j \dot{H} \quad \forall \quad r \in [r_1, r_5] \quad (6.2)$$

where ρ_j , C_j , and, K_j are the density, specific heat capacity, and the thermal conductivity, respectively of the region described by the specific domain, $r \in [r_1, r_5]$. $T_j(r,t)$ and \dot{H} are the temperature and the rate of heat generation over the domain modeled.

The generalized heat flux boundary conditions for the domain can be written as

$$K_j \frac{\partial T_j}{\partial r} \eta_1 + h_r(T_j(r,t) - T_\infty(t)) = 0 \quad \text{at } r = r_1 \quad (6.3)$$

and

$$K_j \frac{\partial T_j}{\partial r} \eta_5 + h_5(T_j(r,t) - T_\infty(t)) = 0 \quad \text{at } r = r_5 \quad (6.4)$$

where η_1 and η_5 are the outward pointing normals at r_1 and r_5 , respectively. The heat transfer coefficients at r_1 and r_5 are denoted by h_1 and h_5 . $T_\infty(t)$ is the cure cycle temperature.

If the state of the system (i.e., temperature) in the domain $r \in [r_1, r_5]$ can be described completely by 'M' discrete equations of the type Eq.(6.2) then the space described by these 'M' equations is said to be 'M' dimensional. Thus, if the discretized state of the system has a dimension 'M' and if $J_2(r,t)$ is treated as an additional state variable then it can be written as

$$T^{M+1}(r,t) = J_2(r,t) \quad \forall \quad t \geq 0 \quad (6.5)$$

Eq.(6.5) implies that the state of the system instead of being of dimension 'M' as in the process modeling problem would be of dimension 'M + 1' for the control problem where $T^{M+1}(r,t)$ is the added state. Substituting Eq.(5.7) for $J_2(r,t)$ in Eq.(6.5) we get

$$T^{M+1}(r,t) = \frac{1}{2} \int_{t_i}^{t_f} \int_{r_1}^{r_5} [T(r,t) - T^D(r,t)]^2 dr \, dt \quad (6.6)$$

Differentiating Eq.(6.6) with respect to time t, gives

$$\frac{\partial T^{M+1}}{\partial t} = \frac{1}{2} \int_{r_1}^{r_5} [T(r,t) - T^D(r,t)]^2 dr \quad (6.7)$$

subject to the initial condition

$$T^{M+1}(r,0) = 0 \quad \text{at } t = 0 \quad (6.8)$$

and the final time condition

$$T^{M+1}(r, t_f) = J_2(r, t) \quad \text{at} \quad t = t_f \quad (6.9)$$

Following the work of Tzafestas and Nightingale [23], if the objective function $J_2(r, t)$ is treated as an additional state variable $T^{M+1}(r, t)$ Substituting Eq.(2.3) for $H(t)$ into Eq.(6.2) the equation of state for the control problem can be written as

$$\frac{\partial T}{\partial t} = \left\{ \frac{K_j}{C_j \rho_j} \frac{\partial^2 T}{\partial r^2} + \frac{K_j}{C_j \rho_j r} \frac{\partial T}{\partial r} + \frac{\rho_r H_r v_r}{\rho_j C_j} f_1(T, \alpha) \right\} + B(r, t) W(r, t) \quad (6.10)$$

where ρ_j , C_j , and K_j are assumed constant in the domain. $B(r, t)$ is a known matrix operator acting on the stochastic disturbance input $W(r, t)$.

Treating $J_2(r, t)$ as an additional state variable allows us to treat the least squares error between the temperature $T(r, t)$ and the average temperature $T^D(r, t)$ distributions Eq.(6.7) as a stochastic disturbance input $W(r, t)$. Hence for the optimal process control problem the stochastic disturbance input $W(r, t)$ can be written as

$$W(r, t) = \frac{1}{2} \int_{r_1}^{r_5} [T(r, t) - T^D(r, t)]^2 dr \quad (6.11)$$

Substituting Eqs.(6.2) and (6.11) into Eq.(6.10) gives the equation of state for the curing process optimal control problem

$$\frac{\partial T}{\partial t} = \left\{ \frac{K_j}{C_j \rho_j} \frac{\partial^2 T}{\partial r^2} + \frac{K_j}{C_j \rho_j r} \frac{\partial T}{\partial r} + \frac{\rho_r H_r v_r}{\rho_j C_j} f_1(T, \alpha) \right\} + \frac{1}{2} \int_{r_1}^{r_5} [T(r, t) - T^D(r, t)]^2 dr \quad (6.12)$$

It is to be noted from Eq.(6.12) that the operator $B(r, t)$ is taken to be unity. Eq.(6.12) is the generalized equation of state for the control problem valid for all discretized

points in the domain of the FWC assembly ($r \in [r_1, r_5]$). However, heat generation is present only in the subdomain ($r \in [r_3, r_4]$) representing the composite case. For the mandrel, insulator, and outer layer Eq.(6.12) is valid without the heat generation term.

6.2 Co-state Equation

In addition to the equation of state (Eq.(6.12)), the continuum is governed by the co-state equation (Eq.(2.4)) which is the expression specifying the cure or the reaction rate of the resin system being used as the matrix material. The co-state equation was written in Chapter 2 as

$$\frac{d\alpha(t)}{dt} = f_1(T, \alpha) \quad (6.13)$$

6.3 Initial Conditions

The generalized equations governing the state (temperature) and the co-state (degree of cure) of the system Eq.(6.12) and Eq.(6.13), respectively are governed by initial conditions at $t=0$. The initial conditions governing the system are

$$T(r,0) = T_o^*(r) \quad \forall \quad r \in [r_1, r_5] \quad (6.14)$$

$$\alpha(r,0) = \alpha^*(r) \quad \forall \quad r \in [r_3, r_4] \quad (6.15)$$

where, $T_0^*(r)$ and $\alpha^*(r)$ are the initial temperature and degree of cure distributions. The initial condition on the added state Eq.(6.8) also needs to be satisfied in addition to Eq.(6.14) and Eq.(6.15).

6.4 Hamiltonian Functions

The system performance index $J(r,t)$ (Eq.(6.1)), the generalized equation of state (Eq.(6.2)), the generalized boundary conditions (Eq.(6.3) and Eq.(6.4)) and the generalized co-state equation (Eq.(6.13)) are used to define the system Lagrangian (modified performance index) $\tilde{J}(r,t)$ by adjoining Eq.(6.2) - Eq.(6.4) and Eq.(6.13) using Lagrange multipliers

$$\begin{aligned}
 \tilde{J}(r,t) = & \frac{1}{2} \int_{r_3}^{r_4} [\alpha(r,t) - \alpha^R(r,t)]^2 dr \\
 & + \int_{t_1}^{t_f} \int_{r_1}^{r_5} \lambda_3(r,t) [f_1(T, \alpha) - \frac{\partial \alpha}{\partial t}] dr dt \\
 & + \int_{t_1}^{t_f} \int_{r_1}^{r_5} \frac{1}{2} [T(r,t) - T^D(r,t)]^2 + \lambda_1(r,t) \left[\frac{K_j}{C_j \rho_j} \frac{\partial^2 T}{\partial r^2} + \frac{K_j}{C_j \rho_j r} \frac{\partial T}{\partial r} + \frac{\rho_r H_r v_r}{\rho_j C_j} f_1(T, \alpha) - \frac{\partial T}{\partial t} \right] dr dt \\
 & + \int_{t_1}^{t_f} \lambda_2(r,t) \left[K_j \frac{\partial T}{\partial r} \eta_r + h_r (T(r,t) - T_\infty(t)) \right] \Big|_{r_1}^{r_5} dt
 \end{aligned} \tag{6.16}$$

where, $\lambda_1(r,t)$ is the Lagrange multiplier associated with the state equation, $\lambda_2(r,t)$ is the Lagrange multiplier associated with boundary conditions and $\lambda_3(r,t)$ is the Lagrange multiplier associated with the co-state equation.

Holliday and Storey [52] developed a simple yet effective method to derive the necessary conditions for optimality for a distributed parameter system. They identified the individual sub Hamiltonians for the system and applied the calculus of variations technique to minimize the system Lagrangian. The system Lagrangian or modified performance index $\tilde{J}(r,t)$ for the curing process is defined in Eq.(6.16). The individual Hamiltonian functions can be recognized from Eq.(6.16). The state Hamiltonian function H_1 can be written as

$$H_1 = \left\{ \frac{1}{2} [T - T^D]^2 \right\} + \left\{ \lambda_1(r,t) \left[\frac{K_j}{C_j \rho_j} \frac{\partial^2 T}{\partial r^2} + \frac{K_j}{C_j \rho_j r} \frac{\partial T}{\partial r} + \frac{\rho_r H_r v_r}{\rho_j C_j} f_1(T, \alpha) \right] \right\} \quad (6.17)$$

where the first term on the right hand side of Eq.(6.17) comes from the objective function $J_2(r,t)$ being considered as an additional state variable. The second term on the right hand side comes from adjoining the state equation Eq.(6.2) with the Lagrange multiplier $\lambda_1(r,t)$.

The boundary condition Hamiltonian H_2 valid only at the boundaries of the domain $r \in [r_1, r_5]$ is formed by adjoining the boundary condition Lagrange multiplier $\lambda_2(r,t)$ to the generalized boundary conditions Eq.(6.3) and Eq.(6.4) and can be written as

$$H_2 \Big|_{r_1}^{r_5} = \lambda_2(r,t) \left[K_j \frac{\partial T}{\partial r} \eta_r + h_r [T(r,t) - T_\infty(t)] \right] \Big|_{r_1}^{r_5} \quad (6.18)$$

The co-state Hamiltonian is formed by adjoining the Lagrange multiplier $\lambda_3(r,t)$ to the co-state Equation (Eq.(6.13)) and can be written as

$$H_3 = \lambda_3(r,t) f_1(T, \alpha) \quad (6.19)$$

Eq.(6.17) - Eq.(6.19) are the generalized expressions for the Hamiltonians associated with specific Lagrange multipliers. The total Hamiltonian describing the system can be written as

$$\tilde{H} = H_1 + H_2 \big|_{r_1}^{r_s} + H_3 \quad (6.20)$$

6.5 Transversality Conditions

The transversality conditions are based on the fact that the system Hamiltonian \tilde{H} (Eq.(6.20)) is a constant along the optimal path [52]. The equation relating the adjoint variable of state $\lambda_1(r,t)$ to the state (temperature) and the co-state (degree of cure) is derived from the system Hamiltonian (Eq.(6.20)) and the modified performance index $\tilde{J}(r,t)$ (Eq.(6.16)). The derivation is based on the idea that the first variation of the modified performance index $\tilde{J}(r,t)$ (Eq.(6.16)) should vanish for arbitrary variations in the state ($T(r,t)$), co-state ($\alpha(r,t)$), and the control variable $T_\infty(r,t)$. This idea leads to the transversality conditions or the adjoint equations for the Lagrange multipliers $\lambda_1(r,t)$, $\lambda_2(r,t)$, and $\lambda_3(r,t)$, as well as, the boundary conditions that need to be satisfied, both in the spatial domain $r \in [r_1, r_s]$ and in the time domain $t \in [t_i, t_f]$. The calculus of variations approach leads to the fact that the optimum for the system lies on canonical paths. Applying the canonical relationship between the adjoint variable $\lambda_1(r,t)$ and the system Hamiltonian \tilde{H} (Eq.(6.20)), the transversality conditions on the state adjoint variable $\lambda_1(r,t)$ can be derived as

$$\frac{\partial \lambda_1(r,t)}{\partial t} = - \left\{ \frac{\partial \tilde{H}}{\partial T} \right\} + \frac{\partial}{\partial r} \left\{ \frac{\partial \tilde{H}}{\partial T_r} \right\} - \frac{\partial^2}{\partial^2 r} \left\{ \frac{\partial \tilde{H}}{\partial T_{rr}} \right\} \quad (6.21)$$

where, $\lambda_1(r,t)$ has been previously defined as the Lagrange multiplier associated with the state of the system $T(r,t)$, $T_r(r,t)$ is the first partial derivative of the state of the system $T(r,t)$ with respect to the spatial parameter 'r', and $T_{rr}(r,t)$ is the second partial derivative of the state of the system with respect to the spatial parameter 'r'.

Substituting Eqs.(6.17) - (6.19) into Eq.(6.20), differentiating Eq.(6.20) and substituting into Eq.(6.21) gives the adjoint state equation in the domain $r \in [r_1, r_5]$ becomes

$$\frac{\partial \lambda_1(r,t)}{\partial t} = - \{ (T - T^D) + \frac{\rho_r H_r v_r}{\rho_j C_j} \lambda_1 \frac{\partial f_1}{\partial T} + \lambda_3 \frac{\partial f_1}{\partial T} + \frac{\partial^2}{\partial r^2} \left[\frac{\lambda_1 K_j}{\rho_j C_j} \right] - \frac{\partial}{\partial r} \left[\frac{\lambda_1 K_j}{\rho_j C_j r} \right] \} \quad (6.22)$$

The domain of the FWC assembly $r \in [r_1, r_5]$ can be divided into discrete subdomains representing the mandrel, insulator, composite case, and the outer layer. Eq.(6.22) can be written for each subdomain by considering appropriate material properties and by neglecting the heat generation term in the mandrel, insulator and outer layer. The set of adjoint state equations for the individual domains of the FWC assembly (Figure 2) can be written as

$$\begin{aligned} \frac{\partial \lambda_1}{\partial t} &= - \frac{K_m}{\rho_m C_m} \frac{\partial^2 \lambda_1}{\partial r^2} + \frac{K_m}{\rho_m C_m} \frac{\partial}{\partial r} \left[\frac{\lambda_1}{r} \right] - (T - T^D) \quad \forall r \in [r_1, r_2] \\ \frac{\partial \lambda_1}{\partial t} &= - \frac{K_i}{\rho_i C_i} \frac{\partial^2 \lambda_1}{\partial r^2} + \frac{K_i}{\rho_i C_i} \frac{\partial}{\partial r} \left[\frac{\lambda_1}{r} \right] - (T - T^D) \quad \forall r \in [r_2, r_3] \\ \frac{\partial \lambda_1}{\partial t} &= - \frac{K_c}{\rho_c C_c} \frac{\partial^2 \lambda_1}{\partial r^2} + \frac{K_c}{\rho_c C_c} \frac{\partial}{\partial r} \left[\frac{\lambda_1}{r} \right] - \rho_r H_r v_r \frac{\lambda_1}{\rho_c C_c} \frac{\partial f_1}{\partial T} \\ &\quad - \lambda_3 \frac{\partial f_1}{\partial T} - (T - T^D) \quad \forall r \in [r_3, r_4] \\ \frac{\partial \lambda_1}{\partial t} &= - \frac{K_o}{\rho_o C_o} \frac{\partial^2 \lambda_1}{\partial r^2} + \frac{K_o}{\rho_o C_o} \frac{\partial}{\partial r} \left[\frac{\lambda_1}{r} \right] - (T - T^D) \quad \forall r \in [r_4, r_5] \end{aligned} \quad (6.23)$$

where, K_m , ρ_m , and C_m are the thermal conductivity, density and the specific heat of the mandrel, K_i , ρ_i , and C_i are the thermal conductivity, density and the specific heat of the insulator, K_c , ρ_c , and C_c are the thermal conductivity, density and the specific heat of the composite case, and K_o , ρ_o , and C_o are the thermal conductivity, density and the specific heat of the outer layer respectively. ρ_r , H_r , and v_r are the density, heat of reaction and the volume fraction of the resin system used as the matrix material.

The adjoint co-state variable $\lambda_3(r,t)$ can be related to the co-state variable $\alpha(r,t)$ through the canonical relationship

$$\frac{\partial \lambda_3(r,t)}{\partial t} = - \left\{ \frac{\partial \tilde{H}}{\partial \alpha} \right\} \quad (6.24)$$

The adjoint co-state equation can be derived from Eq.(6.24) and the system Hamiltonian \tilde{H} (Eq.(6.20)) as follows

$$\frac{\partial \lambda_3(r,t)}{\partial t} = - \left\{ \frac{\rho_r H_r v_r}{\rho_i C_i} \lambda_1 \frac{\partial f_1}{\partial \alpha} + \lambda_3 \frac{\partial f_1}{\partial \alpha} \right\} \quad (6.25)$$

For the composite case Eq.(6.25) can be written as

$$\frac{\partial \lambda_3(r,t)}{\partial t} = - \left\{ \frac{\rho_r H_r v_r}{\rho_c C_c} \lambda_1 \frac{\partial f_1}{\partial \alpha} + \lambda_3 \frac{\partial f_1}{\partial \alpha} \right\} \quad (6.26)$$

The temperature of the system (state variable) alone influences the boundary conditions through the boundary condition Hamiltonian H_2 which is defined only at the domain boundaries r_1 and r_5 . The adjoint operator $\lambda_2(r,t)$ acting on the generalized boundary conditions Eq.(6.3) and Eq.(6.4), shown in Eq.(6.18), can be eliminated from the set of equations by $\lambda_1(r,t)$. Holliday and Storey [52] showed that the adjoint

boundary conditions can be calculated from the following expressions of the state Hamiltonian H_1 and the boundary condition Hamiltonian H_2 . From the first variation of the modified performance index $\tilde{J}(r,t)$ we get

$$\frac{\partial[H_2]}{\partial T} + \frac{\partial[H_1]}{\partial T_r} - \frac{\partial}{\partial r} \frac{\partial[H_1]}{\partial T_{rr}} = 0 \quad (6.27)$$

$$\frac{\partial[H_2]}{\partial T_r} + \frac{\partial[H_1]}{\partial T_{rr}} = 0 \quad (6.28)$$

$$\frac{\partial[H_2]}{\partial \lambda_2} = 0 \quad (6.29)$$

Substituting Eq.(6.17) for H_1 and Eq.(6.18) for H_2 into Eqs.(6.27) - (6.29) and simplifying we get, the adjoint boundary conditions at $r = r_1$ and $r = r_5$ as

$$K_j \frac{\partial \lambda_1}{\partial r} \eta_r + \lambda_1 [h_r - K_j \frac{\eta_r}{r}] = 0 \quad (6.30)$$

where K_j is the thermal conductivity of the domain, h_r is the heat transfer coefficient, and η_r is the outward drawn normal at the radial position 'r'.

For the FWC assembly the adjoint state boundary condition at the inner surface of the mandrel ($r = r_1$) can be written as

$$K_m \frac{\partial \lambda_1}{\partial r} \eta_{mr} + \lambda_1 [h_l - K_m \frac{\eta_{mr}}{r}] = 0 \quad (6.31)$$

at the inner surface $r = r_1$ of the hollow mandrel.

At the interfacial points of the FWC assembly, the continuity of the heat flux is specified as :

$$\begin{aligned}
 (K_m \frac{\partial \lambda_1}{\partial r} - \frac{\lambda_1 K_m}{r}) \eta_{mr} + (K_l \frac{\partial \lambda_1}{\partial r} - \frac{\lambda_1 K_l}{r}) \eta_{lr} &= 0 \quad \text{at } r = r_2 \\
 (K_l \frac{\partial \lambda_1}{\partial r} - \frac{\lambda_1 K_l}{r}) \eta_{lr} + (K_c \frac{\partial \lambda_1}{\partial r} - \frac{\lambda_1 K_c}{r}) \eta_{cr} &= 0 \quad \text{at } r = r_3 \quad (6.32) \\
 (K_c \frac{\partial \lambda_1}{\partial r} - \frac{\lambda_1 K_c}{r}) \eta_{cr} + (K_o \frac{\partial \lambda_1}{\partial r} - \frac{\lambda_1 K_o}{r}) \eta_{or} &= 0 \quad \text{at } r = r_4
 \end{aligned}$$

For the outer most point of the outer layer in contact with the oven fluid, the flux boundary condition is,

$$K_o \frac{\partial \lambda_1}{\partial r} \eta_{or} + \lambda_1 [h_o - K_o \frac{\eta_{or}}{r}] = 0 \quad \text{at } r = r_5 \quad (6.33)$$

where η_{mr} , η_{lr} , η_{cr} , and η_{or} are the outerward pointing normals at the boundary points of the mandrel, insulator, composite case and the outer layer respectively.

In addition to the spatial boundary conditions the adjoint variables $\lambda_1(r,t)$ and $\lambda_3(r,t)$ need to satisfy final time conditions which arise from the first variation of the system Lagrangian or the modified performance index $\tilde{J}(r,t)$. The final time condition on the state variable is defined as

$$\lambda_1(r, t_f) = \frac{\partial J_2(r, t_f)}{\partial T} \quad (6.34)$$

where $J_2(r,t)$ is the objective function described in Section 5.4. Since $J_2(r,t)$ is treated as an additional state variable and is considered as part of the state equation for the

optimal control problem (see Section 6.3), then $J_2(r,t)$ can be treated as a constant at final time $t = t_f$. Hence the final time condition on the adjoint state becomes

$$\lambda_1(r, t_f) = 0 \quad (6.35)$$

Considering the uniformity of cure objective $J_1(r,t)$ defined in Eq.(5.5) as

$$J_1(r,t) = \frac{1}{2} \int_{r_3}^{r_4} [\alpha(r,t) - \alpha^R(r,t)]^2 dr$$

at any spatial location $r \in [r_3, r_4]$ a terminal error function $E(r,t)$ can be defined as

$$E(r,t) = \frac{1}{2} [\alpha(r,t) - \alpha^R(r,t)]^2 \quad \text{at } t = t_f \quad (6.36)$$

where $\alpha^R(r,t)$ is the required degree of cure in the composite at final time t_f . The final time condition on the co-state Lagrange multiplier $\lambda_3(r,t)$ becomes

$$\lambda_3(r, t_f) = \frac{\partial E(r, t_f)}{\partial \alpha} \quad (6.37)$$

Differentiating Eq.(6.36) with respect to $\alpha(r,t)$ gives the following result at final time $t = t_f$

$$\lambda_3(r, t_f) = \alpha(r, t_f) - \alpha^R(r, t_f) \quad \forall r \in [r_3, r_4] \quad (6.38)$$

If the final time ($t = t_f$) is an unknown, then it can be derived as the time at which the Hamilton - Jacobi Equation [26] is zero.

$$\frac{\partial \tilde{J}(r, t_f)}{\partial t_f} = 0 \quad (6.39)$$

subject to the additional final time conditions on the state and co-state.

It is noted that in Eq.(6.39), $\tilde{J}(r,t)$ is the modified performance index evaluated for the optimal cure cycle $T_\infty(t)$. Eq.(6.1) - Eq.(6.39) complete the identification of the conditions needed for the curing process to be optimized. The calculus of variations approach adopted has lead to a two point boundary value problem (TPBVP) that needs to be solved subject to constraints.

6.3 Minimum Principle

The heating cycle $T_\infty(r,t)$ which minimizes the modified performance index $\tilde{J}(r,t)$ (Eq.(6.16)) can be said to be optimal if the system Hamiltonian \tilde{H} Eq.(6.20) is a minimum when all the constraints are satisfied [19,26,53]. An arbitrary change in the cure cycle temperature $\delta T_\infty(t)$ leads to a corresponding change in the temperature $\delta T(r,t)$ and the degree of cure $\delta \alpha(r,t)$ which leads to changes in the adjoint variables. The first variation in the modified performance index $\tilde{J}(r,t)$ due to a variation in the cure cycle temperature $\delta T_\infty(t)$, can be written as

$$\delta \tilde{J}(r,t) = \int_{t=0}^{t=t_f} \delta T_\infty(t) \left[\frac{\partial H_2}{\partial T_\infty(t)} \right] dt \quad \text{at } r = r_1 \text{ and } r = r_5 \quad (6.40)$$

Differentiating Eq.(6.18) with respect to $T_\infty(t)$, gives

$$\frac{\partial H_2}{\partial T_\infty} = - \lambda_2(r,t) h_r \quad \text{at } r = r_1 \text{ and } r = r_5 \quad (6.41a)$$

Eliminating $\lambda_2(r,t)$ using Eq.(6.28), and substituting the result into Eq.(6.41a) gives

$$\delta\tilde{J}(r,t) = \int_{t=0}^{t=t_f} \delta T_{\infty}(t) \left(- \frac{\lambda_1(r,t)}{C_j \rho_j \eta_r} \right) h_r dt \quad \text{at } r = r_1 \text{ and } r = r_5 \quad (6.41b)$$

where C_j , ρ_j are the specific heat and density, respectively of the material at the boundaries, h_r is the heat transfer coefficient at the boundary point of interest, and η_r is the outward pointing normal at the boundary points.

The variation in the cure cycle $\delta T_{\infty}(t)$ cannot be arbitrarily chosen if the cure cycle temperature $T_{\infty}(t)$ is restricted to lie within a decision space $U_L(t) \leq T_{\infty}(t) \leq U_U(t)$. The optimal cure cycle may end up hitting either the upper bound $U_U(t)$ or the lower bound $U_L(t)$ of the decision space. This is called the bang-bang phenomena and the cure cycle is said to be bang-bang [53,54].

6.4 First Order Gradient Method

The calculus of variations approach leads to a descent type of algorithm to seek the optimal point in the decision space. The perturbation in the cure cycle temperature $\delta T_{\infty}(t)$ (Eq.(6.40)) should be appropriately chosen so that changes in the performance index $\delta\tilde{J}(r,t)$ will make $\tilde{J}(r,t)$ the performance index move towards a minimum point. It is observed from Eq.(6.40) that an appropriate perturbation in the cure cycle should be of the form

$$\delta T_{\infty}(t) = - W_1(t) \left(\frac{\partial H_2}{\partial T_{\infty}(t)} \right) \quad \text{at } r = r_1 \text{ and } r = r_5 \quad (6.42)$$

where $W_1(t)$ is a positive weighing function chosen such that the cure cycle $T_\infty(t)$ lies within the restricted decision space $U_L(t) \leq T_\infty(t) \leq U_U(t)$. Using Eq.(6.41a) for the partial of the boundary condition Hamiltonian H_2 with respect to $T_\infty(t)$ gives

$$\delta T_\infty(t) = - W_1(t) \left(- \frac{\lambda_1(r,t)}{C_j \rho_j \eta_r} h_r \right) \text{ at } r = r_1 \text{ and } r = r_5 \quad (6.43)$$

The first order gradient method gives the magnitude of the change in the cure cycle as well as, the direction for the performance index to change towards a minimum.

6.5 Computational Algorithm

It is observed from the methods adopted to convert the minimization problem with constraints on the state and co-state variables to an unconstrained minimization problem, that the objective function, the constraints, and the stopping conditions are all implicit functions of the state and co-state variables and time. From Pontryagin's minimum principle [16,26,48] derivatives of the modified performance index $\tilde{J}(r,t)$ are required to predict the direction of minimization in order to converge to an optimum point [55].

The optimal control problem can be divided into two primarily independent problems with regard to the final time :

1. The fixed final time problem, where the final process time is fixed and the constraints are satisfied at the specified final time t_f . This can be called as the optimal filtering problem
2. The final time is unrestricted making the optimal control problem a final time prediction problem where
 - a. if t_f is greater than the final time of the initial problem, it is an extrapolation problem.
 - b. if t_f is less than the final time of the initial problem, it is treated as an interpolation problem in the time domain.

Both cases of the unrestricted final time problem can be treated as a series of fixed time problems. If the objective function is not minimum or if any of the constraints are violated then the final time can be adjusted to arrive at an improved cure cycle. This procedure is repeated until the true optimal cure cycle can be identified which satisfies all constraints and minimizes the performance index.

Step by Step Computation Procedure

The calculus of variations approach naturally leads to a steepest descent type of algorithm. An outline of the solution procedure is given as follows

1. Assume an initial heating cycle $T_{\infty}^i(t)$

2. The cure model with the assumed heating cycle is then used to calculate the temperature distribution in the FWC assembly and the degree of cure and viscosity in the composite case. The final time condition is used as the initial final time estimate for the optimal control problem.
3. Solve the state and co-state estimation problem for the assumed heating cycle $T_i^\infty(t)$, (where i denotes the i th iteration) by integrating forward in time from $t = 0$ to a time $t = t_f^i$, where either the stopping condition terminates the process or the final time conditions are satisfied.
4. Calculate the derivative functions $\frac{\partial \dot{\alpha}}{\partial \alpha} \Big|_\tau$ and $\frac{\partial \dot{\alpha}}{\partial T} \Big|_\alpha$ at all instants of time.
5. Solve the adjoint state and co-state equations (6.23 - 6.26), by integrating backwards in time from $t = t_f^i$ to $t = 0$. This is necessary as the resultant two point boundary value problem needs final time conditions to be satisfied as described earlier. The principle of duality in distributed parameter systems, as stated by Tzafestas and Nightingale [23] and Hermes and Lasalle [50], is utilized to convert the final time boundary condition problem to an initial value problem by making a time transformation of the form

$$\tau = t_f^i - t \quad (6.44)$$

where t_f^i is the final time of the i th iteration. Using the principle of duality, integration is performed on the dual variable $\lambda_i(r, \tau)$ and the solution to the adjoint equations $\lambda_i(r, t)$ can be recovered using Eq.(6.44).

6. On arriving at the solution to the dual problem, the direction of descent is estimated by the application of the minimum principle. The resulting variation in the objective function is estimated as indicated in Eq.(6.41b).
7. The variation in the cure cycle is then calculated from the first order gradient described in Section 6.4. The resultant perturbation Eq.(6.43) is a function of the weighting function $W_i(t)$ and can be chosen so as to prevent any violation of the constraints on the cure cycle.
8. The variation in the control can be applied to the heating cycle of the present iteration $T_\infty^i(t)$, to calculate a new heating cycle

$$T_\infty^{i+1}(t) = T_\infty^i(t) + \delta T_\infty(t) \quad (6.45)$$

can be calculated from Eq.(6.43)

$$T_\infty^{i+1}(t) = T_\infty^i(t) + W_i(t)\delta T_\infty^i(t) \quad (6.46)$$

where $W_i(t)$ acts as the control on the step size and thus permits the cure cycle to lie within the specified decision space.

9. The performance index is calculated at each iteration and compared with the performance index obtained from the previous iterate. The steepest descent method is stopped when the performance index is a minimum. This can be checked by evaluation of a prespecified criterion on the performance index

$$\left| \frac{J^{i+1} - J^i}{J^i} \right| \leq \varepsilon \quad (6.47)$$

where ϵ is a chosen tolerance TOL1.

Unrestricted Final Time

All steps outlined above in the solution procedure are common to the case of a specified final time, as well as, to the case of unrestricted final time. However, one additional condition needs to be satisfied for the case of unrestricted final time as outlined by Denn et al.[18], Bryson and Ho [47], and Leondes and Niemann [56]. This condition specifies the magnitude of the change in the time step needed to extrapolate the time domain. The extrapolation in the time step is calculated using the stationarity of the system Hamiltonian as the necessary condition to be satisfied. The time estimate for the next iteration is calculated as

$$t_f^{l+1} = t_f^l + \delta t_f^l \quad (6.48)$$

and δt_f^l is defined as

$$\delta t_f^l = W_l(t) \frac{\partial E(r, t_f)}{\partial t_f} \quad (6.49)$$

where $E(r, t)$ the error function in Eq.(6.36) specified at final time t_f and defined at any prespecified spatial location ' r '.

Method For Estimating Final Time Increments

Since it is the primary objective to achieve a prespecified degree of cure in the composite at the final time, the objective function $J_1(r,t)$ is used to define a terminal error function $E(r,t)$ (see Section 6.5)

Consider the objective function $J_1(r,t)$ defined by

$$J_1(r,t) = \frac{1}{2} \int_{r_3}^{r_4} [\alpha(r,t) - \alpha^R(r,t)]^2 dr \quad \text{at } t = t_f$$

At any spatial location $r \in [r_3, r_4]$, the terminal error function $E(r,t)$ has been previously defined in Eq.(6.36) as

$$E(r,t) = \frac{1}{2} [\alpha(r,t) - \alpha^R(r,t)]^2 \quad \text{at } t = t_f \quad (6.36)$$

where $\alpha^R(r,t)$ is the required degree of cure in the composite at final time t_f . From Eq.(6.36) it is clear that the minimum value of $E(r,t)$ is zero. Thus, the problem of determining an optimal t_f can be considered as a problem of minimizing the error function $E(r,t)$.

Consider a small change in final time t_f , say δt_f , the corresponding change in the error $E(r,t)$ is then equal to

$$\frac{\Delta E(r,t_f)}{\Delta t_f} = \frac{E(r,t_f + \delta t_f) - E(r,t_f)}{\delta t_f} \quad (6.50)$$

Neglecting the higher order terms in δt_f , Eq.(6.50) can be written as

$$\Delta E(r, t_f) = \frac{\partial E(r, t_f)}{\partial t_f} \Delta t_f \quad (6.51)$$

In order to make $E(r, t_f)$ a minimum, we can choose δt_f such that

$$\delta t_f = W_i(t) \frac{\partial E(r, t_f)}{\partial t_f} \quad (6.52)$$

where $W_i(t)$ is a scalar constant. Differentiating Eq.(6.36) with respect to the final time t_f Eq.(6.52) can be written as

$$\delta t_f = W_i(t) [\alpha(r, t_f) - \alpha^R(r, t_f)] \frac{\partial \alpha(r, t_f)}{\partial t_f} \quad (6.53)$$

Eq.(6.53) can be discretized using the values for the degree of cure $\alpha(r, t_f)$ at the final time for the previous iteration ($i-1$) and the degree of cure at the final time at the present iteration (i) to estimate δt_f^i as follows

$$\delta t_f^i = W_i(t) [\alpha(r, t_f^i) - \alpha^R(r, t_f)] \left\{ \frac{[\alpha(r, t_f^i) - \alpha(r, t_f^{i-1})]}{[t_f^i - t_f^{i-1}]} \right\} \quad (6.54)$$

Thus, the final time for the $i+1$ iteration can be estimated using Eq.(6.54) and Eq.(6.48)

$$t_f^{i+1} = t_f^i + \delta t_f^i \quad (6.55)$$

where

$$\delta t_f^i = W_i(t) [\alpha(r, t_f^i) - \alpha^R(r, t_f)] \left\{ \frac{[\alpha(r, t_f^i) - \alpha(r, t_f^{i-1})]}{[t_f^i - t_f^{i-1}]} \right\}$$

Hence, the change in the next time iteration can be determined from the estimated final time. The algorithm iterates on the final time t_f . In order to use this approach an initial guess of the final time is needed. The final time is determined by solving the process modeling problem as an initial value problem and calculating the final time at which the the process is stopped and at least one of the points in the composite will have reached the required degree of cure. The significance of each event in the optimal control of the curing process is illustrated in the flow chart presented in Figure 31.

The value of the scalar weight function $W_i(t)$ in Eq.(6.48) and Eq.(6.49) can be chosen for an axisymmetric system [26] as

$$W_i(t) = \frac{TOL2}{\int_0^{t_f} \lambda_1(r,t) dt} \quad \text{at } r = r_1 \text{ and } r_5 \quad (6.56)$$

where TOL2 is an arbitrary constant chosen such that any perturbation on the control or the time increment lie within the allowed decision space. The extension of the fixed time problem to the unrestricted final time case requires solution of the Hamilton - Jacobi equation (Eq.(6.39)).

$$\frac{\partial \tilde{J}(r,t)}{\partial t_f} = 0 \quad (6.39)$$

where, $\tilde{J}(r,t)$ is the modified performance index evaluated for the optimal cure cycle $T_\infty(t)$.

The step by step solution procedure outlined above is contained in a FORTRAN computer program "CUREOPT". The input parameters describing the variables needed for the program "CUREOPT", are briefly outlined in Table 5.

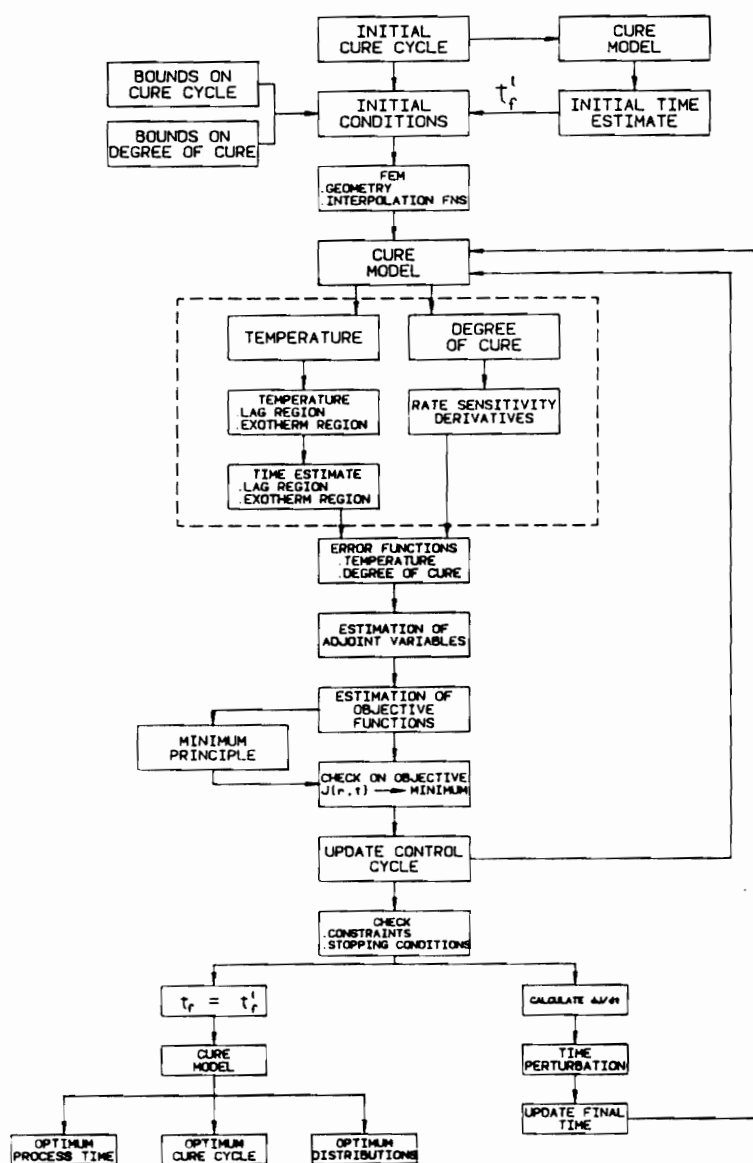


Figure 31. OPTIMAL CURE - Flow Chart:

The flow chart illustrates the hierarchy of events for the optimal control strategy developed in optimal cure program "CUREOPT".

Table 5. INPUT PARAMETERS FOR PROGRAM "CUREOPT".

- | | |
|---|--|
| <ol style="list-style-type: none"> 1. CONTROL PARAMETERS AND TOLERANCES <ol style="list-style-type: none"> a. Initial estimate of the final time of cure. b. Initial time estimates for lag and overshoot regions. c. Lower and upper bounds of the degree of cure. d. Required degree of cure at all points of the composite. e. Lower and upper bounds of the cure cycle. f. Initial operational weight on the cure cycle perturbations. g. Initial operational weight on the time perturbations. h. Required tolerance on the objective error function. i. Required tolerance on the time weight parameter. 2. GEOMETRY <ol style="list-style-type: none"> a. Shape of the structure. b. Number of layers. c. Thickness of individual layers. 3. MANDREL PROPERTIES <ol style="list-style-type: none"> a. Density. b. Specific Heat Capacity. c. Thermal Conductivity. 4. INSULATOR PROPERTIES <ol style="list-style-type: none"> a. Density. b. Specific Heat Capacity. c. Thermal Conductivity. 5. PREPREG PROPERTIES <ol style="list-style-type: none"> a. Initial resin mass fraction. b. Type of fiber being used. c. Type of resin being used in the composite. | <ol style="list-style-type: none"> 6. RESIN PROPERTIES <ol style="list-style-type: none"> a. Density. b. Specific Heat Capacity. c. Thermal Conductivity. d. Heat of Reaction. e. Relationship between cure rate, temperature and degree of cure. f. Relationship between viscosity, temperature and degree of cure. 7. FIBER PROPERTIES <ol style="list-style-type: none"> a. Density. b. Specific Heat Capacity. c. Thermal Conductivity. 8. OUTER LAYER PROPERTIES <ol style="list-style-type: none"> a. Density. b. Specific Heat Capacity. c. Thermal Conductivity. 9. FINITE ELEMENT MESH PARAMETERS <ol style="list-style-type: none"> a. Type of element being used. b. Type of mesh - symmetric or unsymmetric. c. Number of elements in the mesh. d. Number of nodes in the mesh. e. Number of elements modeling each subdomain. f. Time step parameter θ g. Time step h. Boundary nodes for convective heat transfer. 10. INITIAL AND BOUNDARY CONDITIONS <ol style="list-style-type: none"> a. Initial temperature distribution in the composite. b. Initial degree of cure distribution in the composite. c. Cure cycle temperature as a function of time. |
|---|--|

CHAPTER 7

OPTIMUM CURE CONTROL CYCLE

The axisymmetric cure model for a filament wound composite has been proposed and validated thus far. The optimal control of the curing process and a computational strategy have been proposed in Chapter 6. The method of tailoring the composite to have a property that can be controlled through a process control variable has been described in Figure 31. The computational strategy adopted here, is initially verified for a linear heat transfer problem popularly called the Butkovskii - Sakawa boundary control problem and then extended to the nonlinear heat transfer problem with heat generation describing the curing process in composites.

7.1 Optimal Control : Linear Diffusion Problem

The optimization technique developed for the FWC assembly in Chapters 5 and 6 was used to solve the Butkovskii - Sakawa boundary control problem. The temperature distribution in a homogeneous flat plate can be steered to a desired temperature distribution at the end of the heating process by suitably altering the temperatures of the heating cycle applied at the boundary of the flat plate. This was initially proposed by Butkovskii [16] and solved by Sakawa [17]. This problem came to be known as the Butkovskii - Sakawa boundary control problem. The state equation and boundary conditions for the Butkovskii - Sakawa boundary control problem are stated below

$$\frac{\partial \Theta}{\partial \tau} = \frac{\partial^2 \Theta}{\partial \xi^2} \quad \forall \quad \xi \in [0,1] \quad (7.1)$$

where $\Theta(r,t)$ is the dimensionless temperature, τ is the dimensionless time, and ξ is the dimensionless position. The boundary and initial conditions can be written as

$$\frac{\partial \Theta}{\partial \xi} = 0 \quad \text{at} \quad \xi = 1 \quad \forall \quad \tau \quad (7.2)$$

$$\frac{\partial \Theta}{\partial \xi} = h (\Theta - U(\tau)) \quad \text{at} \quad \xi = 0 \quad \forall \quad \tau \quad (7.3)$$

$$\Theta(\xi,0) = 0 \quad \text{at} \quad \tau = 0 \quad \forall \quad \xi \quad (7.4)$$

where h is a constant coefficient of the surface in contact with the convective environment. $U(\tau)$ is the heating cycle temperature.

Since the objective is to achieve a nondimensional temperature of 0.2 at a specified time τ_f the performance index for the linear diffusion problem can be written as

$$J(\xi, \tau_f) = \int_0^1 [0.2 - \Theta(\xi, \tau_f)]^2 d\xi \quad (7.5)$$

where 0.2 is the desired temperature distribution inside the flat plate and $\Theta(\xi, \tau_f)$ is the temperature inside the flat plate at final time τ_f . The performance index $J(\xi, \tau_f)$ measures the error between desired temperature and existing temperature in the flat plate due to a particular heating environment.

Comparison Studies

The one dimensional heat transfer problem stated above is solved using quadratic finite elements and compared with the solutions obtained for the temperature behavior from reference [18].

The spatial domain and the time domain were both equally divided into 20 divisions giving 21 discretized nodal points. The coefficient h is taken as 10.0, and the desired temperature in the flat plate is 0.2 with a constant initial heating of $U(\tau) = 1.0$. The weight $W_i(\tau)$ in Eq.(6.46) was arbitrarily set at 10. It was chosen such that it would carry the heating cycle temperature to a boundary of the admissible region of the decision space defined by $0.0 \leq U(\tau) \leq 1.0$ and halved whenever a decrease in the objective Eq.(7.5) was not obtained.

Figure 32, shows a comparison between the predicted temperature distribution from the program and the measured temperature data obtained from reference 18, for an

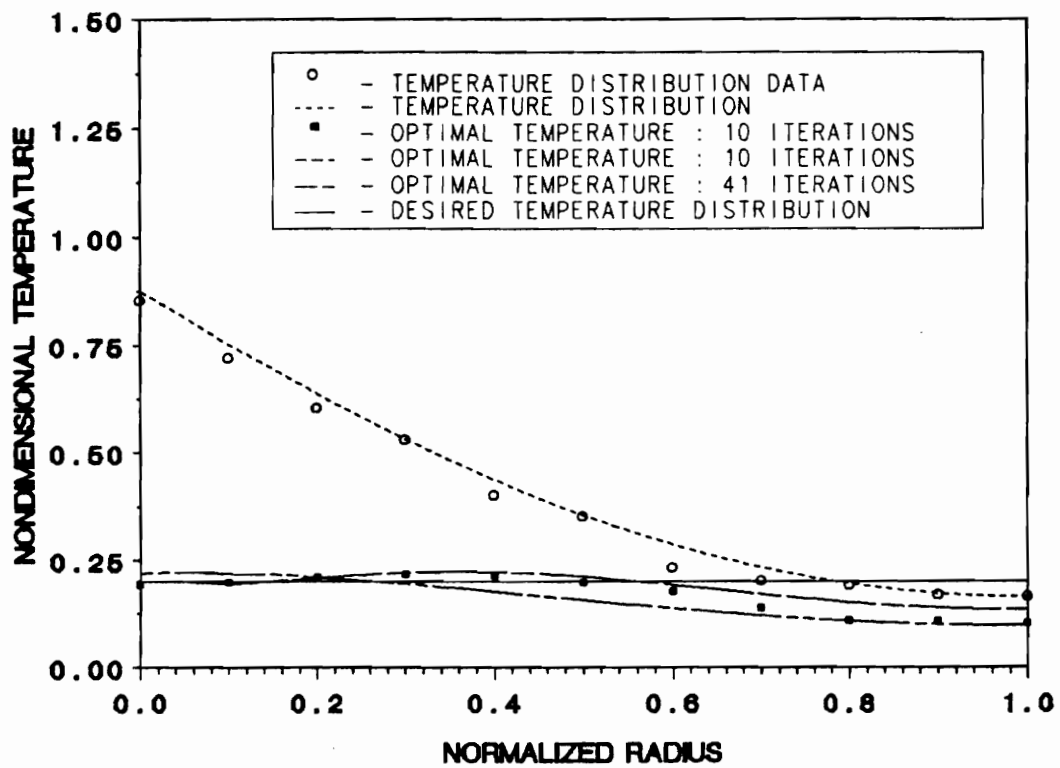


Figure 32. LINEAR DIFFUSION PROBLEM - Temperature vs Normalized Radius:

Temperature profiles at $t = 0.2$ using an initial heating cycle $U(\tau) = 1.0$. The symbols represent data from reference 18.

initial heating cycle $U(\tau) = 1.0$. The desired temperature distribution of 0.2 is achieved within 10 iterations. The data obtained from reference 18, was measured assuming the transportation lag (time needed by the heating cycle to attain a specified hold temperature from the initial temperature) of the heating cycle was 0.04. Since the transportation lag was small it was neglected for our study. The optimal heating cycles plotted in Figure 33 as a function of the nondimensional time, indicate that the heating cycle appears to approach the boundaries of the decision space. Thus, the optimal heating cycle for the flat plate problem shows a tendency to approach a bang - bang behavior.

Figure 34 shows the reduction in the objective for the steepest descent calculations starting from the constant heating cycles of $U(\tau) = 0.5$ and 1.0. It is observed that the objective Eq.(7.5) approaches the minimum fairly rapidly within the first 10 iterations and does not indicate a large change after that.

7.2 Cure Cycle Optimization

It has been observed during cure of thermoset composites that exothermic chemical reactions occur which may lead to runaway reactions and nonuniformity of cure. It is characteristic of thick section composites that as the thickness increases, thermal gradients develop due to differential temperature drop across the composite thickness. Munjal [2] made a qualitative assessment of the effect of thickness variations and processing of large thick section rocket motor components. It was concluded that there is a 20 - 30 % degradation of Kevlar reinforced pressure vessel strength as the

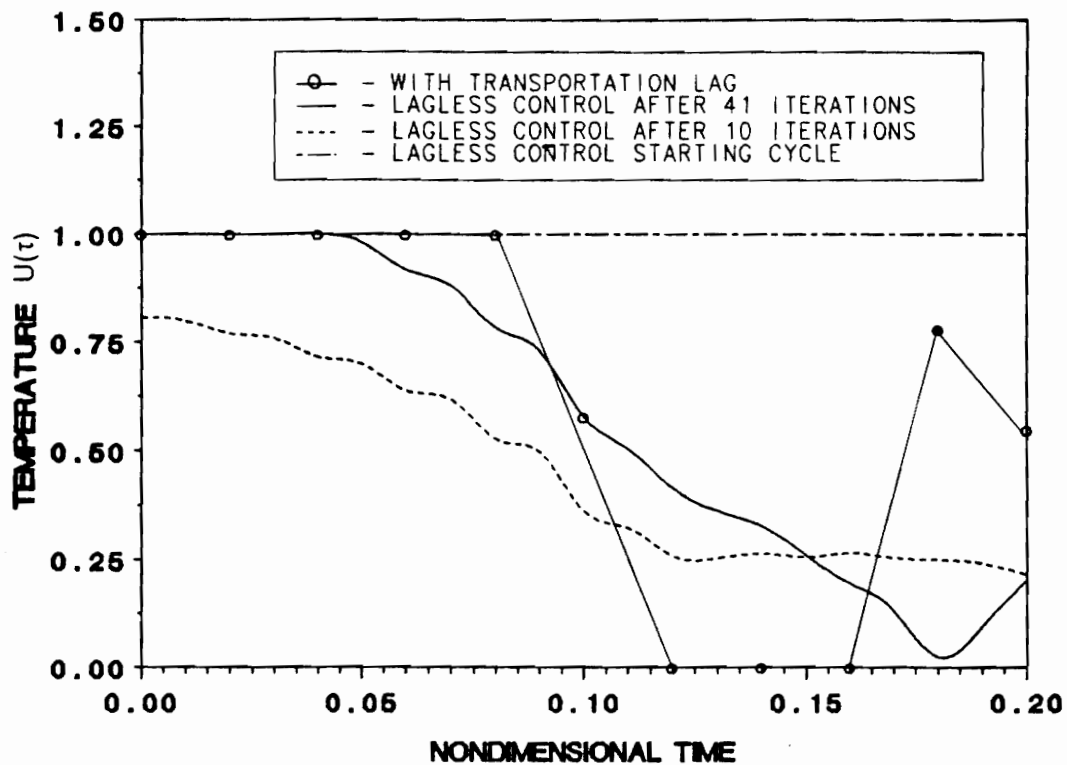


Figure 33. LINEAR DIFFUSION PROBLEM - Control Cycle vs Time:

Successive approximations to the optimal heating cycle using initial heating cycle as $U(\tau) = 1.0$. The symbols represent data from reference 18.

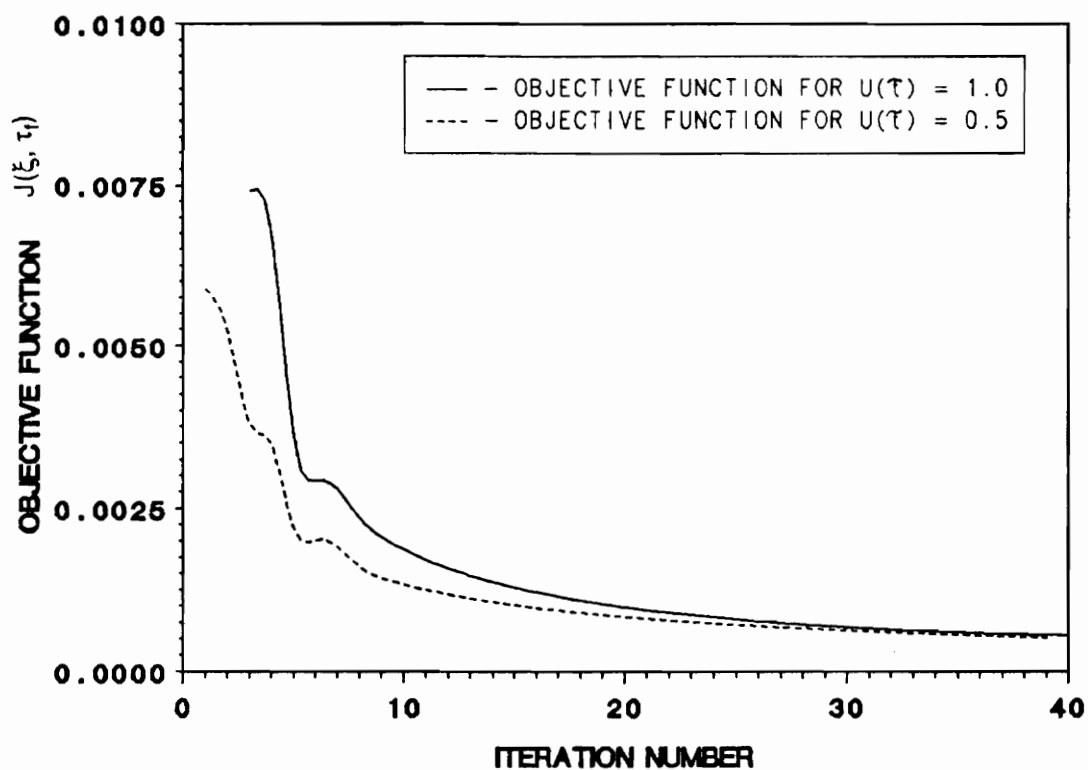


Figure 34. LINEAR DIFFUSION PROBLEM - Objective $J(\xi, \tau)$ vs Iterations:

The variation of the objective as the function of the number of needed to reach the minimum.

geometry is changed from a 5.75 inch diameter pressure vessels with a case thickness of 0.05 inch, to a 90.0 inch diameter vessel with a 1 inch thick case. A similar study for identical cases fabricated with graphite fibers indicated a degradation of 10 %.

A Fortran computer code "CUREOPT" was developed to optimize the curing process of the FWC assembly using the techniques described in Chapters 5 and 6. Results of the cure simulations for the 18 inch test bottle with a 0.0254 m thick graphite - epoxy case showed (a). a very large thermal lag in the FWC assembly during heat up and (b). a large temperature overshoot inside the composite (see Section 4.5). The optimization program was used to determine a modified cure cycle which would reduce the thermal lag and at the same time eliminate the temperature overshoot. Specifically, the optimization program was used to determine the optimal cure cycle for the following problems :

1. Exotherm minimization subject to process time being minimum.
2. Simultaneous lag and exotherm minimization subject to process time being minimum.
3. Effect of changes on the initial cure cycle on the optimum process time.
4. Effect of changes in mandrel material on the optimum process time.

The temperature and temperature dependent property tailoring (i.e., tailoring of the degree of cure to achieve an uniform distribution and a desired prespecified degree across the thickness of the composite), for all the above cases was carried out ac-

according to a common design cure window which facilitated a common basis for the comparison studies.

7.3 Design Cure Window

The design cure window defines :

1. The decision space within which the optimal control cycle should lie.
2. Describes the constraints on the state and co-state variables.

The design cure window used for the curing process optimal control problem can be identified by :

1. BOUNDS ON THE PROCESS CONTROL VARIABLE

The cure cycle temperature $T_{\infty}(t)$, is restricted to lie within bounds specified by a lower and an upper limit. The lower bound $U_L(t) = 21.11^{\circ}\text{C}$ and the upper bound is taken to be $U_U(t) = 180.0^{\circ}\text{C}$ for all the four cases considered.

2. BOUNDS ON THE EXTENT OF REACTION

The initial degree of cure was used as the lower bound $\alpha_L(r,t) = 0.0$. The upper bound of the degree of cure was taken to be the desired degree of cure of the composite. For the optimal process control problem it was taken to be $\alpha_U(r,t) = 0.99$.

3. STOPPING CONDITION

The stopping condition can be described as the time at which all the points in the composite achieved the desired degree of cure.

4. PROCESS PARAMETERS

The geometry used for the case study was the FWC assembly shown in Figure 2. The outer diameter of the mandrel was 18 inches (referred to as an 18 inch test bottle) and the properties of each layer in the in the assembly are given in Table 6. The mandrel properties were changed for the final case when aluminum was used instead of PVA SAND. The resin system used in all the four cases was Fiberite 976, along with T-300 graphite fibers. The composite was 1 inch thick. The inner insulator was EPDM rubber while the outer layer was a layer of polyester film. The heat transfer coefficients at the inner surface of the mandrel and outer surface outer layer were taken to be $100 \text{ W/m}^2\text{K}$.

5. CURE CYCLE

The initial cure cycle used for all the cases (except Case 3) was a cycle where the cure temperature was increased at a constant heating rate of 2.8°C/min (5°F/min) from room temperature of 21.1°C to the maximum cure temperature of 177°C (350°F). The temperature was held at 177°C until cure was complete. It is termed as a single step cycle. The cure cycle used for Case 3 will be described later.

6. INITIAL ESTIMATE OF THE FINAL TIME

The initial estimate for the final time of the process was calculated from the cure model using the single step cure cycle described in the preceding paragraph. This was used as an initial prediction of the final time for the optimal process control problem. The minimum degree of cure in the composite case at the estimated final time was used as a first estimate for the degree of cure at final time. Both the initial estimate of the final time as well as the minimum degree of cure achieved in the composite at this time were used as input variables for the optimal control problem.

A nonuniform finite element mesh made up of axisymmetric finite elements is used to model the spatial domain. The mesh used for the optimal control problem in the spatial domain is similar to that used earlier for the cure simulation of the 5.75 inch bottle. The time domain is allowed to change at a time step of $\Delta t = 100$ secs. The spatial domain is divided into 15 quadratic finite elements. Due to the varying geometric thickness of each individual layer the domain is modeled by an unsymmetric mesh. The weight $W_i(t)$ on the cure cycle $\delta T_\infty(t)$ in Eq.(6.46), as well as, that on the time δt_i in Eq.(6.55) was taken to be a positive scalar value not greater than 10. The tolerance TOL1 and TOL2 (see Section 6.5) were both taken to be 0.0001.

7.4 Optimal Cure Simulation : Case - 1

Exotherm Minimization

The cure cycle optimization program was used to determine a cure cycle which minimizes the exothermic chemical reactions in the composite case.

1. OPTIMIZED - 1 : FIXED FINAL TIME PROBLEM

In this case, the initial time estimate of the curing process t_i is taken as the final process time of the optimal control problem and no changes in the time domain is permitted. (i.e., the final process time is fixed). The temperature vs time profiles for the center of the case are shown in Figure 35. The temperature versus time curve for the initial single step cure cycle (initial response, Figure 35) indicates that the reaction exotherm begins around $t = 110.0$ mins and reaches a maximum of 228.9°C at 133.3 mins into the process.

At this stage the initial time estimate for the optimal curing process control problem is taken as 158.3 mins. The average distributed temperature $T^D(r,t)$ is calculated according to Eq.(5.8) and corrected using the cure cycle temperature and the peak exotherm temperature as per Eq.(5.9). The objective functions $J_1(r,t)$ and $J_2(r,t)$ are calculated using Eq.(5.6) and Eq.(5.7), respectively. The cumulative error due to both the objectives is estimated and the overall performance index $J(r,t)$ is calculated using Eq.(5.11). Both the objective functions $J_1(r,t)$ and $J_2(r,t)$ are objective functions which are quadratic in nature.

The perturbation in the control is then calculated from the solution of the minimization problem posed by the optimality conditions and the minimum principle. The perturbation on the control can then be evaluated as a function of time using Eq.(6.24). It is observed that the optimum cure cycle indicated as OPTIMIZED - 1 in Figure 36, has an identical heating rate as that of the initial cure cycle of

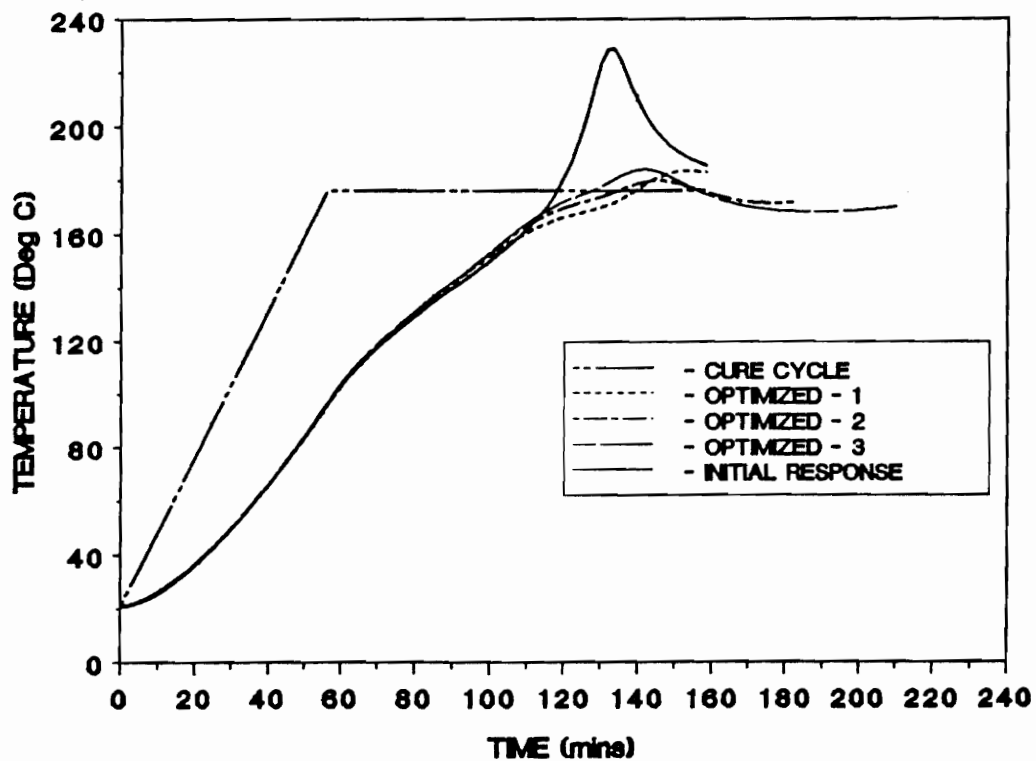


Figure 35. EXOTHERM MINIMIZATION - Temperature vs Time:

Temperature vs Time profiles at the case center for the initial case and three optimized cases :- (a). OPTIMIZED - 1 = Fixed final time case, (b). OPTIMIZED - 2 = Variable process time, (c). OPTIMIZED - 3 = Actual final time.

2.8°C/min. However, in the hold region of the initial cure cycle, a distinct departure from the final cure temperature is observed. The fixed time optimal control cycle approaches the upper temperature bound $U_u(t)$ in a small region at the beginning of the hold region. In the exotherm region (see Figure 35), the optimal cure cycle dips down and shows a maximum departure of about 27°C below the initial cure cycle hold temperature of 176.6°C.

The OPTIMIZED - 1 response (Figure 35) to the new cure cycle indicates a significant reduction in the peak exotherm temperature. It is observed that the fixed time exotherm minimization cure cycle causes composite to reach a degree of cure of 0.99 at the center of the case. The number of iterations taken to approach the minimum performance index in this case was 10 (this depends to a certain extent on the value of the weight taken in Eq.(6.46)). This indicates that if the entire composite is to reach an uniform degree of cure of 0.99 the process control time will have to be extended.

2. OPTIMIZED - 2 : VARIABLE PROCESS TIME

The extension of the process time from the final time of the fixed time problem is carried out by calculating the extrapolation in the final time using Eq.(6.55) where δt_f is calculated using Eq.(6.54) and the error function $E(r,t)$.

OPTIMIZED - 2 curves are the intermediate times between the initial final time estimate of 158.3 mins and the actual final time estimate. The Optimized - 2 search is stopped when more than half of the discretized points across the thickness of the composite attain a degree of cure of 0.99. The temperature vs time profile shown in Figure 35 indicates the time domain has been extended to

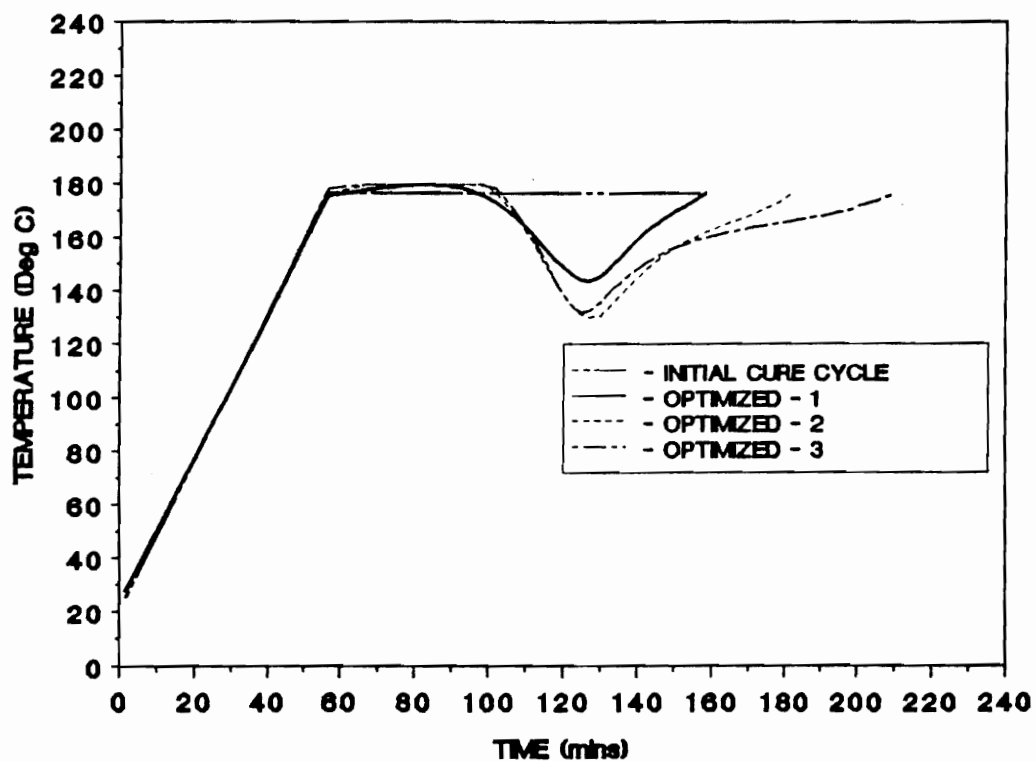


Figure 36. EXOTHERM MINIMIZATION - Cure Cycles:

Control policy profiles for the initial case and three optimized cases :- (a). OPTIMIZED - 1 = Fixed final time case. (b). OPTIMIZED - 2 = Variable process time. (c). OPTIMIZED - 3 = Actual final time.

$t = 181.7$ mins. In this case the number of iterations needed to reach the minimum by the performance index were 11. A further decrease in the peak temperature overshoot is observed and more than one point inside the composite have reached a degree of cure of 0.99. The cure cycle temperature for this case, denoted OPTIMIZED - 2 in Figure 36 follows a similar trend as indicated by the fixed time cure cycle (OPTIMIZED - 1), but shows a greater departure from the initial cure cycle. The maximum departure is estimated to be about 42°C .

3. OPTIMIZED - 3 : ACTUAL FINAL PROCESS TIME

In order for all the points across the thickness of the composite case to achieve an uniform degree of cure of 0.99, further extrapolation of the final time was required. The final time was estimated by the stopping condition Eq.(5.5) which satisfies the Hamilton - Jacobi equation, Eq.(6.39). The total number of iterations to converge to the minimum were 10. For the curing process under consideration it came out to be 210.0 mins. The temperature vs time response and the OPTIMIZED - 3 cure cycle are shown in Figure 35, and Figure 36, respectively. The cure cycle converges to the maximum cure temperature at a longer time than observed for the fixed time case or the intermediate time case. The additional time allows all points inside the composite to achieve an uniform temperature and reach the specified degree of cure.

The degree of cure vs time profiles are shown in Figure 37. The initial cure cycle results in rapid curing due to the presence of large reaction exotherms leading to a greater amount of non-uniformity in the state of cure through the thickness of the

composite. As the cure cycle is modified the degree of cure shows a response more like the degree of cure of an uniformly cured composite case (Figure 18). As the time domain is extended, the degree of cure at the center of the composite approaches the required value of 0.99 as the final time is reached.

The temperature distribution across the cross section of the FWC assembly is shown in Figure 38. The solid line represents the temperature distribution at 133 minutes (time of maximum temperature overshoot, Figure 35) for the initial cure while the dashed line represents the temperature distribution for the OPTIMIZED - 3 cure at the same time. It is to be noted that the temperature distribution for the FWC assembly using the OPTIMIZED - 3 cure cycle is much more uniform than the temperature distribution for the initial case.

The degree of cure vs normalized radius profiles are plotted for a time of 133 minutes (time of maximum temperature overshoot) in Figure 39. It is obvious from the curves that the presence of reaction exotherms in the initial response leads to non-uniformity of cure across the case thickness. Minimizing the cure exotherms provides a more uniform cure distribution across the case thickness.

The minimum degree of cure and the degree of cure at the composite center for the initial cure and the optimized cure are plotted as a function of time in Figure 40. It is observed that the cure rate is slower and more uniform for the optimized cure as compared to the initial cure with the presence of reaction exotherms. This can be observed at 120.0 minutes into the process where the rate of cure for the optimum cure is slower than the initial cure. One of the primary reasons for this behavior can be attributed to the reduction of thermal gradients across the thickness of the com-

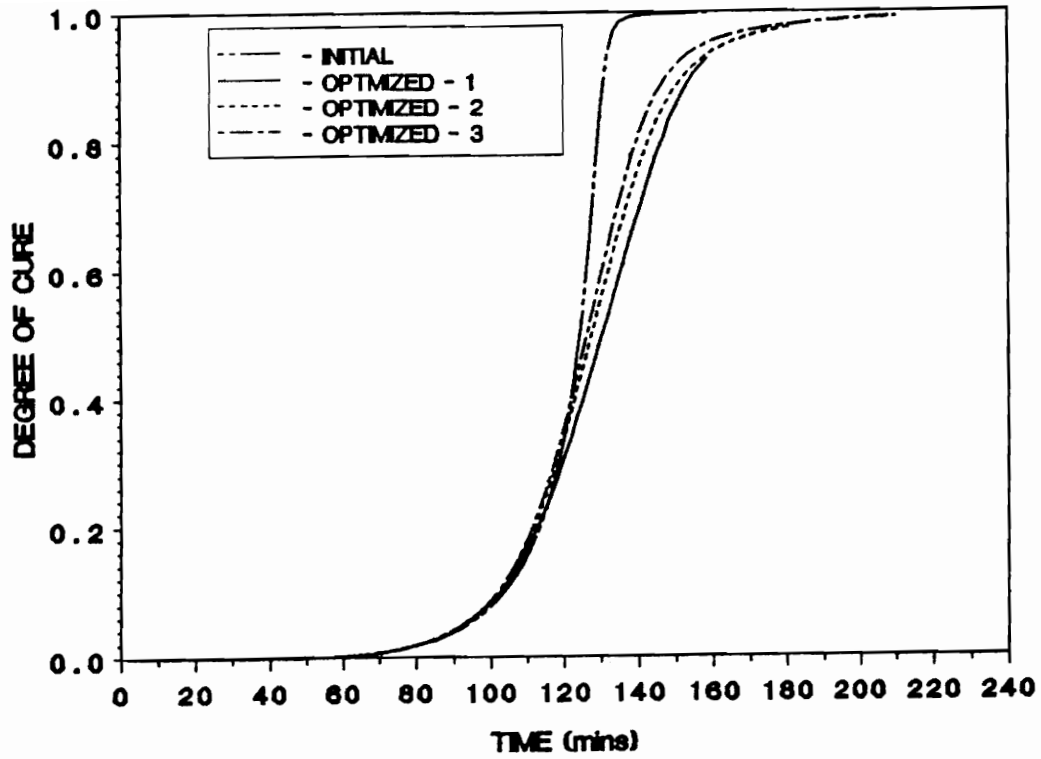


Figure 37. EXOTHERM MINIMIZATION - Degree of Cure vs Time.:

Degree of Cure vs Time at the center of the composite for the initial cure and three optimized cures :- (a). OPTIMIZED - 1 = Fixed final time case. (b). OPTIMIZED - 2 = Variable process time. (c). OPTIMIZED - 3 = Actual final time.

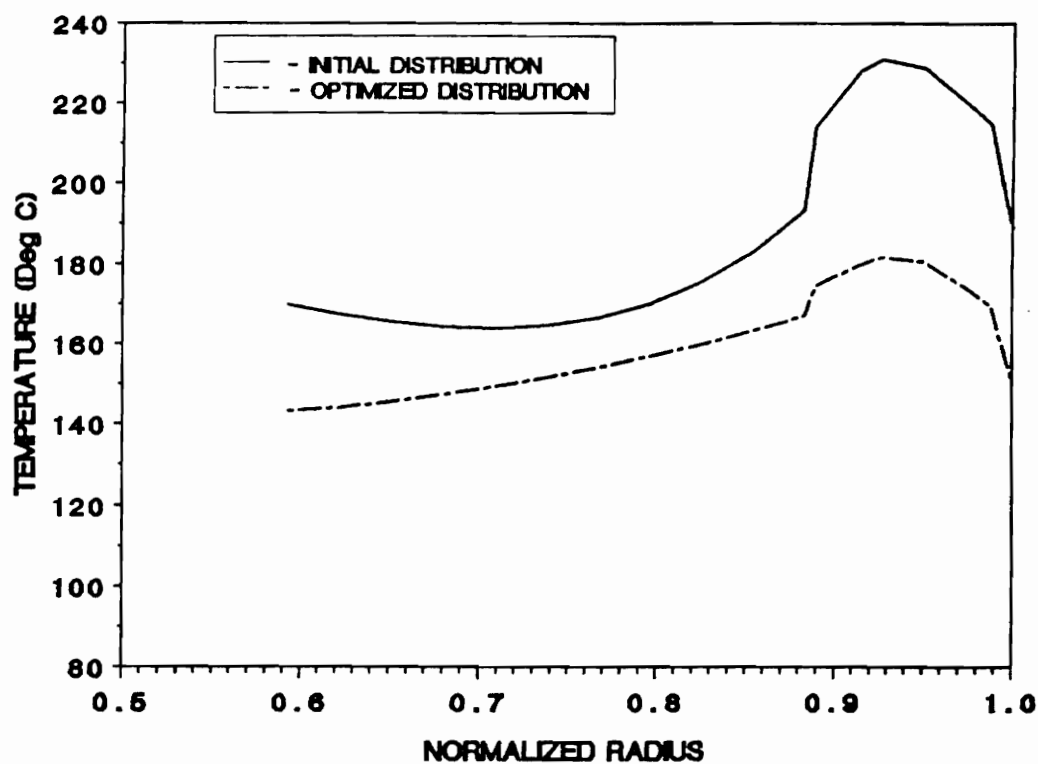


Figure 38. EXOTHERM MINIMIZATION - Temperature vs Normalized Radius.:

Temperature vs Normalized Radius profiles at :- (a). INITIAL OVERSHOOT = temperature distribution across the thickness at time $t = 133.33$ mins for the initial cure cycle. (b). OPTIMIZED OVERSHOOT = temperature distribution across the thickness at time $t = 133.33$ mins for the optimized - 3 cure cycle.

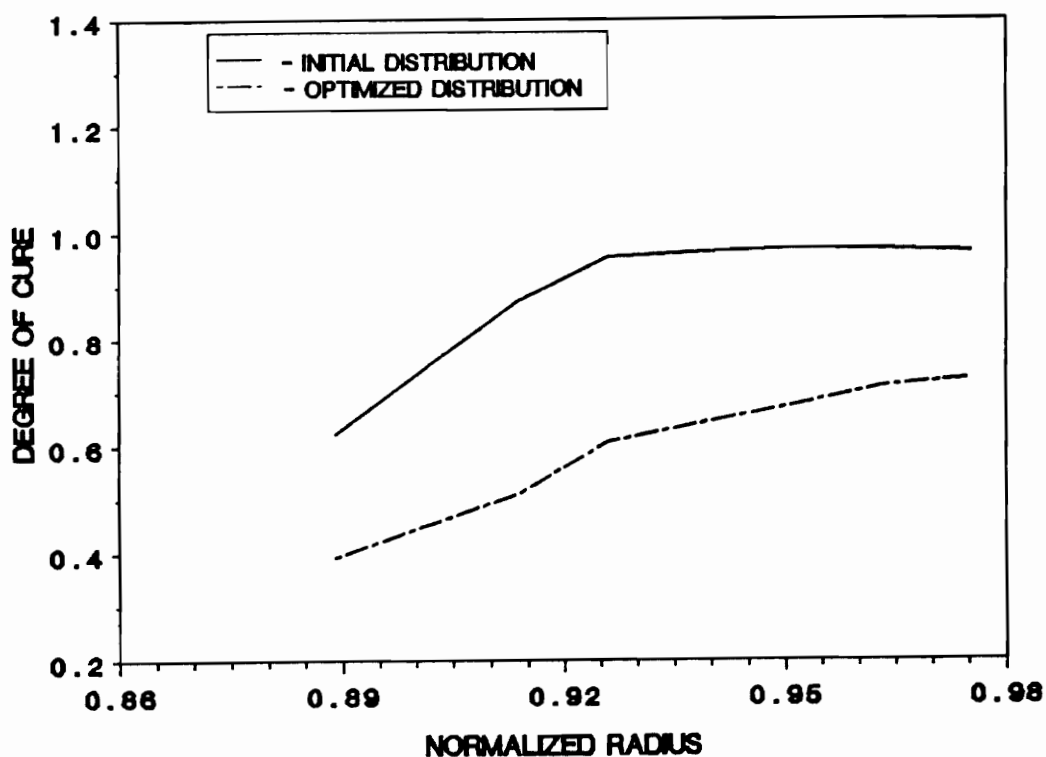


Figure 39. EXOTHERM MINIMIZATION - Degree of Cure vs Normalized Radius.:

Degree of Cure vs Normalized Radius profiles at :- (a). INITIAL DISTRIBUTION = Degree of Cure distribution across the case thickness at time $t = 133.33$ mins for the initial cure cycle. (b). OPTIMIZED DISTRIBUTION = Degree of Cure distribution at time $t = 133.33$ mins for the optimized - 3 case.

posite, as well as, the minimization of reaction exotherms, thus reducing the differential drop in the temperature across the case thickness.

The maximum viscosity and the viscosity at the center of the case are plotted as a function of time in Figure 41. The optimized cure cycle leads increases the resin gel time compared to the resin gel time for the initial cure cycle. The increased gel time may lead to a larger amount of resin flow and better compaction in thick section composites.

The cure rate sensitivity derivative $\frac{\partial \dot{\alpha}}{\partial \alpha} \Big|_T$ characterizing the change in the cure rate with respect to the changes in the degree of cure at the center of the case is shown in Figure 42. The sensitivity is very low initially, but in the exotherm region the sensitivity suddenly drops and reaches a minimum value at the same time as the peak reaction overshoot occurs for the initial cure cycle. The sensitivity derivative for the Optimized - 3 cure cycle becomes more uniform as the temperature gradients, as well as, the cure rate are reduced.

The cure rate sensitivity derivative $\frac{\partial \dot{\alpha}}{\partial T} \Big|_{\alpha}$ characterizes the change in the cure rate due to changes in temperature with the degree of cure remaining a constant. The sensitivity plots for the initial and optimized behavior at the center of the case are shown in Figure 43. It is observed that the sensitivity derivative reaches a maximum value at the time of the peak overshoot temperature for the initial cure. The cure rate sensitivity derivative rises rapidly in the exotherm region for the initial cure cycle but changes gradually for the optimized cure. The uniformity of temperature ensures a more uniform cure rate behavior as indicated by the optimized sensitivity curve.

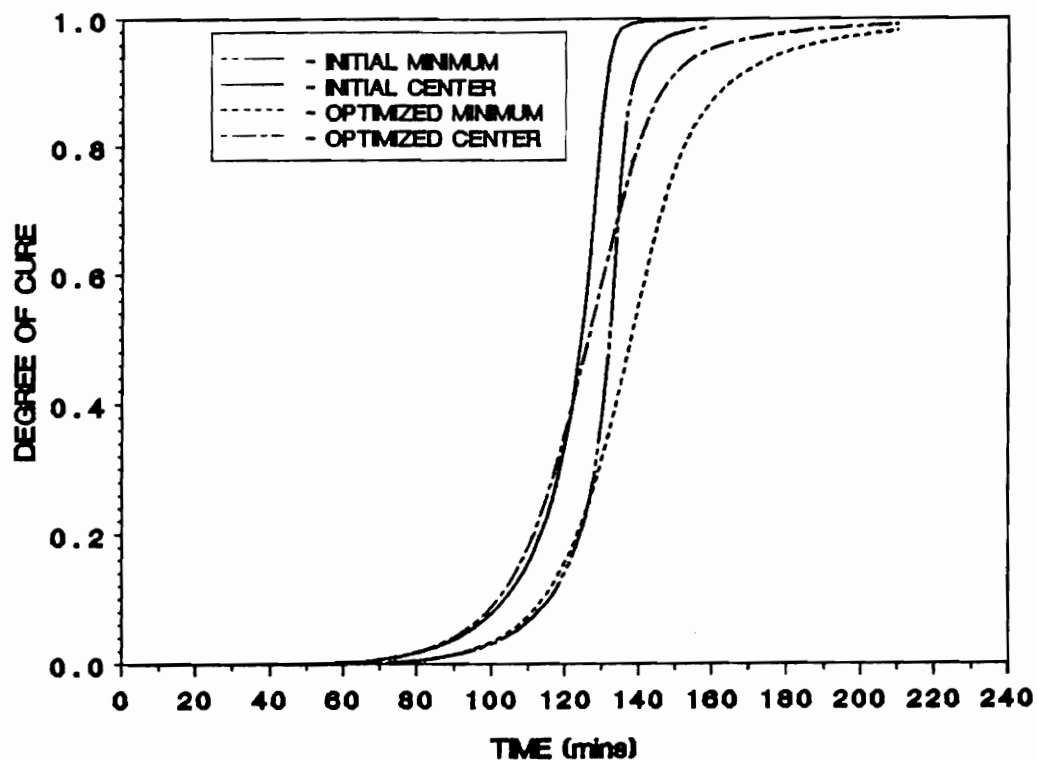


Figure 40. EXOTHERM MINIMIZATION - Degree of Cure vs Time:

Degree of Cure vs Time profiles at :- (a). INITIAL MINIMUM = the minimum degree of cure as a function of time for the initial cure cycle. (b). INITIAL CENTER = the degree of cure at the center of the case for the initial cure cycle. (c). OPTIMIZED MINIMUM = the minimum degree of cure as a function of time for the optimized - 3 case. (d). OPTIMIZED CENTER = the degree of cure at the center of the case for the optimized - 3 case.

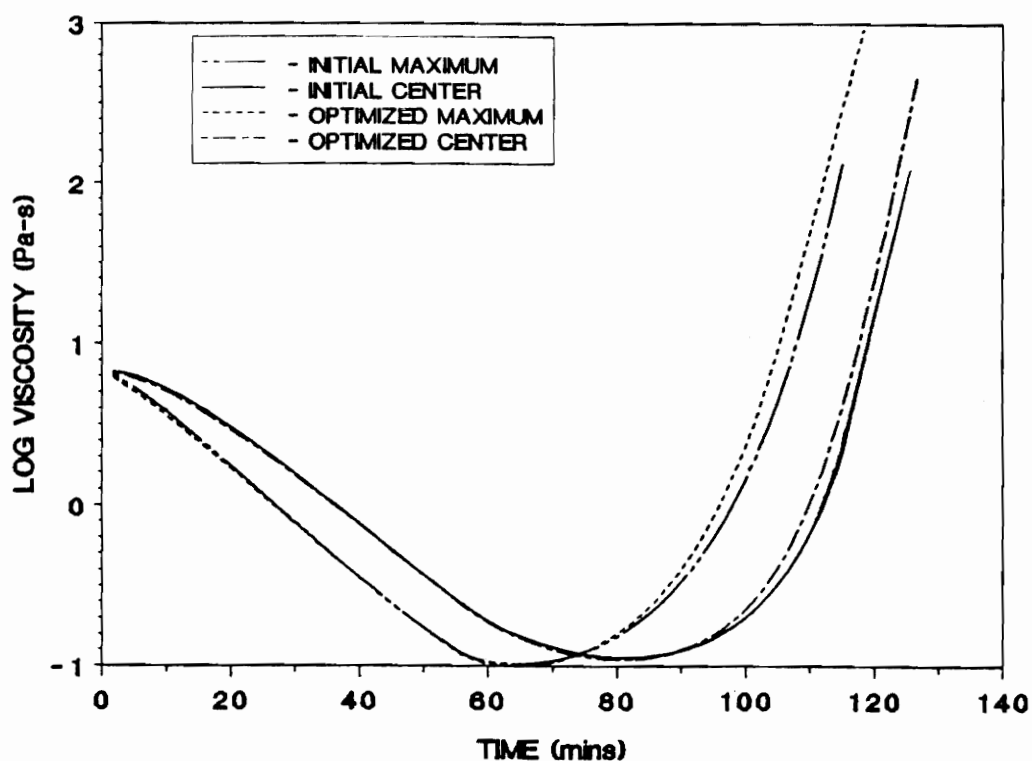


Figure 41. EXOTHERM MINIMIZATION - Log Viscosity vs Time:

Log Viscosity vs Time profiles at :- (a). INITIAL MAXIMUM = the maximum log viscosity as a function of time for the initial cure cycle. (b). INITIAL CENTER = the log viscosity at the center of the case for the initial cure cycle. (c). OPTIMIZED MAXIMUM = the maximum log viscosity as a function of time for the optimized - 3 case. (d). OPTIMIZED CENTER = the log viscosity at the center of the case for the optimized - 3 case.

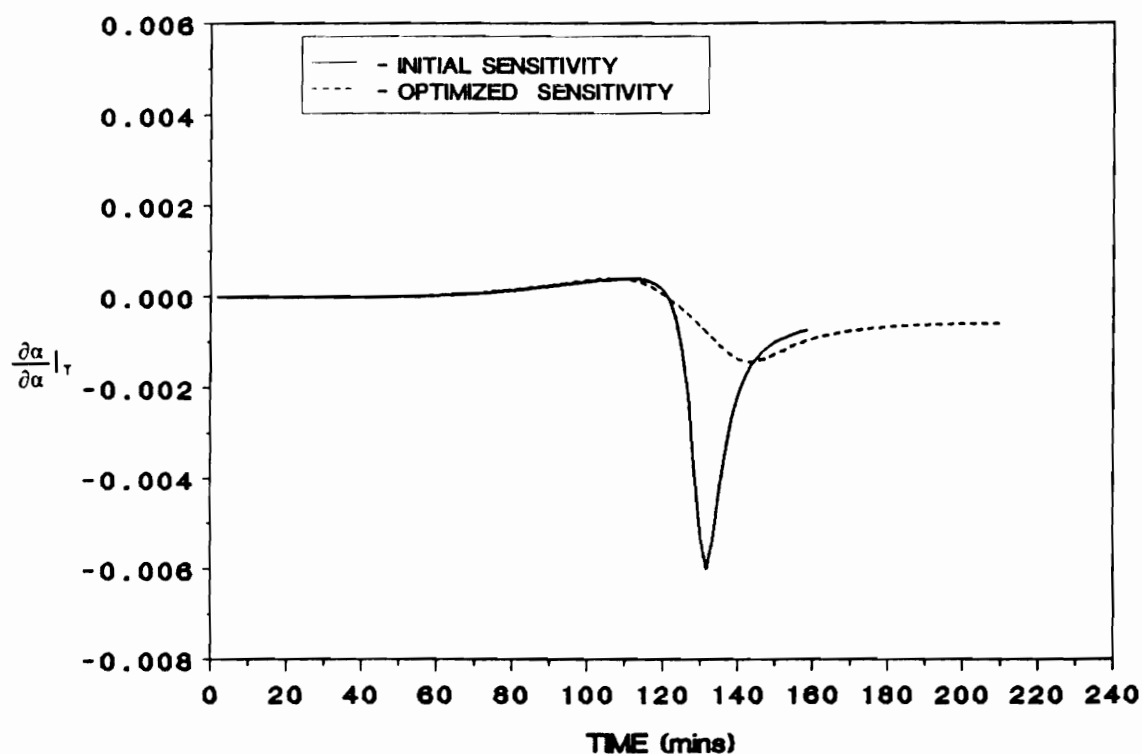


Figure 42. EXOTHERM MINIMIZATION - Cure Rate Sensitivity Derivative vs Time:

Cure rate sensitivity derivative at constant temperature vs time (a). INITIAL SENSITIVITY = Cure rate sensitivity derivative for the initial cure cycle. (b). OPTIMIZED SENSITIVITY = Cure rate sensitivity derivative for the optimized - 3 case.

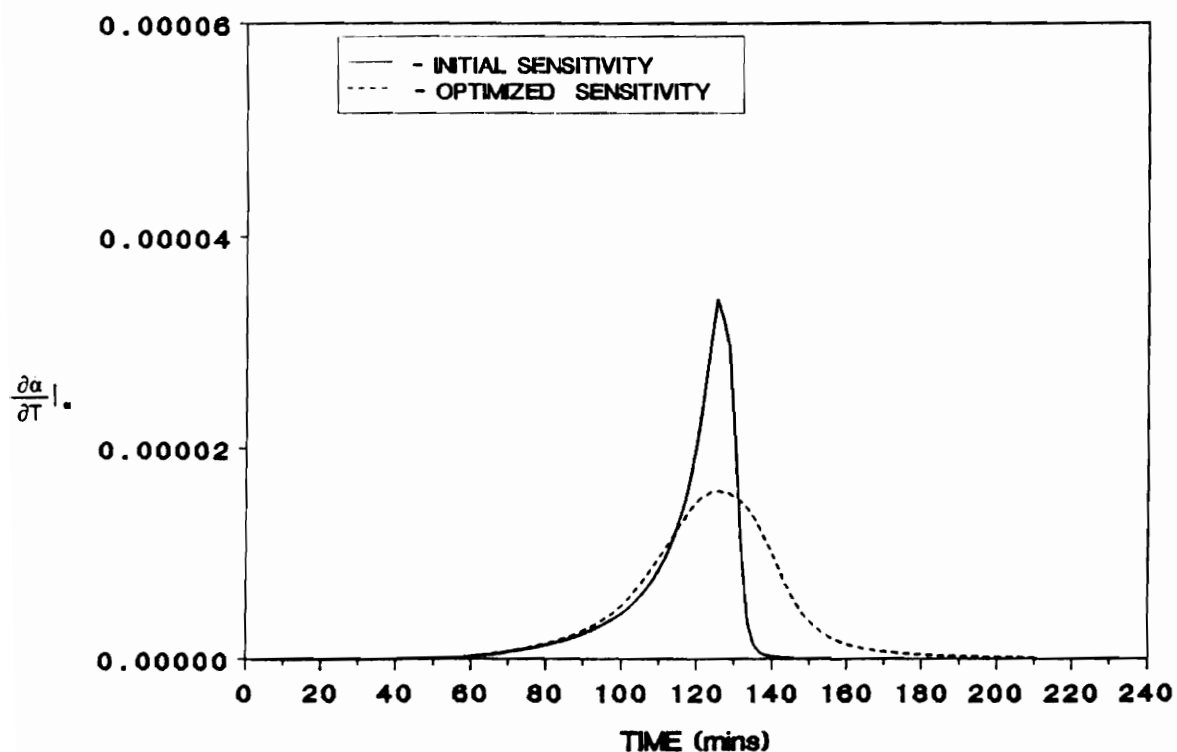


Figure 43. EXOTHERM MINIMIZATION - Cure Rate Sensitivity Derivative vs Time:

Cure rate sensitivity derivative at constant degree of cure vs time :- (a). INITIAL SENSITIVITY = Cure rate sensitivity derivative for the initial cure cycle. (b). OPTIMIZED SENSITIVITY = Cure rate sensitivity derivative for the optimized - 3 case.

The steepest descent of the objective function $J(r,t)$ as it approaches the minimum is shown for the three optimized cure cycles in Figure 44.

The cure cycle optimization procedure clearly indicates that the method adopted can lead to minimization of the peak exotherms occurring during cure of thick section composites. It also enables the tailoring of temperature dependent properties like the degree of cure within a composite by ensuring the minimization of temperature gradients during the process. This procedure is now extended to a problem where the thermal lag, as well as, the exotherm are minimized simultaneously.

7.5 Optimal Cure Simulation : Case - 2

Exotherm and Lag Minimization

The simultaneous minimization of the exotherm, as well as, the thermal lag is again divided into three suboptimal time domain problems. The approach adopted for the exotherm minimization procedure is extended to include the thermal lag by tailoring the temperature in the lag region to satisfy additional constraint.

1. OPTIMIZED - 1 : FIXED FINAL TIME PROBLEM

The cure simulation is repeated for the initial cure cycle used in Case 1 (see Section 7.4 and Figure 35). The final time is fixed and the lag as well as the

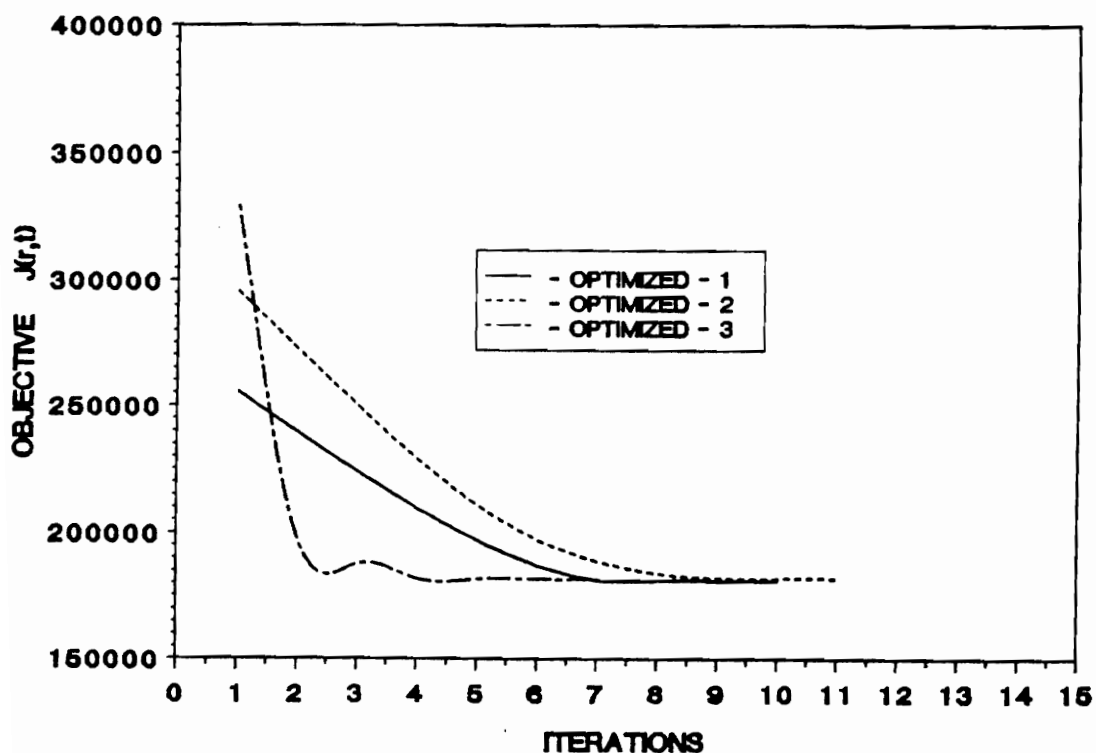


Figure 44. EXOTHERM MINIMIZATION - Objective $J(r,t)$ vs Iterations:

Steepest descent behavior as a function of iterations taken to reach a minimum :- (a). OPTIMIZED - 1 = Steepest descent behavior of the objective for the fixed time problem. (b). OPTIMIZED - 2 = Steepest descent behavior of the objective for the variable time problem with intermediate final time $t = 181.7$ mins. (c). OPTIMIZED - 3 = Steepest descent behavior of the objective for the variable time problem with actual final process control time $t = 210.0$ mins.

exotherm have to be minimized for this fixed final time. The temperature vs time profiles for the center of the case are shown in Figure 45.

Again the initial time estimate for the optimal curing process control problem is taken as 158.3 mins. The average distributed temperature $T^0(r,t)$ is calculated using Eq.(5.9) in the exotherm region, as well as, Eq.(5.10) in the lag region. The rest of the procedure for the simultaneous minimization is similar to the exotherm minimization case. It is observed that the optimum cure cycle indicated as OPTIMIZED - 1 in Figure 46, shows a distinct bang-bang behavior hitting the upper bound temperature of 180.0°C. However, around 70 mins into the process a distinct departure from the upper boundary temperature is observed for the optimal cure cycle.

The OPTIMIZED - 1 response (Figure 45) to the new cure cycle indicates a shift in the peak temperature. The peak temperature is reduced along with a reduction in the temperature lag. It should be noted that the fixed time minimization problem resulted in the center of the case to achieving a degree of cure of 0.99. The performance index reaches a minimum in 6 iterations.

2. OPTIMIZED - 2 : VARIABLE PROCESS TIME

The extension of the process time from the final time of the fixed time problem is carried out by calculating the extrapolation in the final time using Eq.(6.55) where δt_f is calculated using Eq.(6.54) and the error function $E(r,t)$.

OPTIMIZED - 2 curves are at times between the initial final time estimate of 158.3 mins and the actual final time estimate. The temperature vs time profile shown

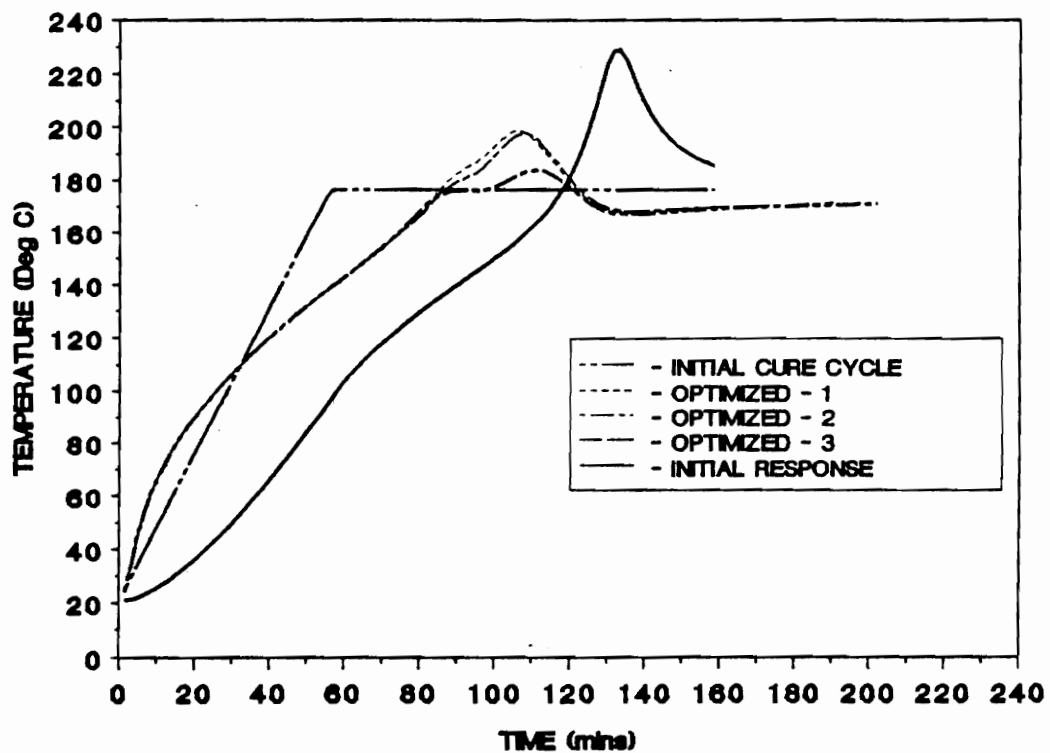


Figure 45. EXOTHERM & LAG MINIMIZATION - Temperature vs Time:

Temperature vs Time profiles at the case center for the initial case and three optimized cases : (a). OPTIMIZED - 1 = Fixed final time case. (b). OPTIMIZED - 2 = Variable process time. (c). OPTIMIZED - 3 = Actual final time.

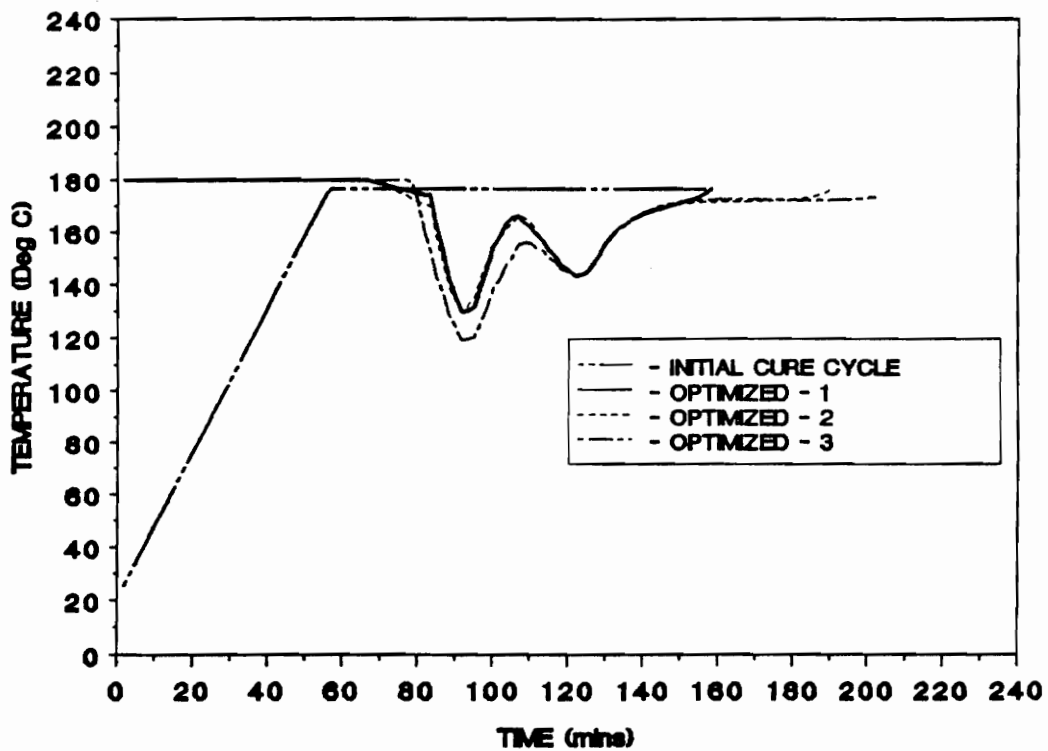


Figure 46. EXOTHERM & LAG MINIMIZATION - Cure Cycles:

Control policy profiles for the initial case and three optimized cases : (a). OPTIMIZED - 1 = Fixed final time case. (b). OPTIMIZED - 2 = Variable process time. (c). OPTIMIZED - 3 = Actual final time.

in Figure 45 shows the temperature response to the OPTIMIZED - 2 cure cycle. The extrapolated final time is $t = 190.0$ mins. A further decrease in the peak overshoot temperature is observed. The additional process time allows more than one point in the composite to reach a degree of cure of 0.99. The performance index reaches a minimum in 6 iterations. The OPTIMIZED cure cycle temperature shown in Figure 46 is similar to the OPTIMIZED - 1 cure cycle except for the additional process time.

3. OPTIMIZED - 3 : ACTUAL FINAL PROCESS TIME

In order for all the points inside the composite to achieve a uniform degree of cure of 0.99 the final time was extended. The final time was estimated by the stopping condition Eq.(5.5) and by satisfying of the Hamilton - Jacobi equation Eq.(6.21). For the curing process under consideration the final time was estimated to be 201.0 mins. The temperature vs time response and the OPTIMIZED - 3 cure cycle are shown in Figure 45 and Figure 46, respectively. The cure cycle converges towards the final initial cure temperature and the longer cure time allows all the points inside the composite to achieve a uniform temperature and a degree of cure of 0.99.

The degree of cure vs time curves for the initial cure and the optimized cure are shown in Figure 47. Reducing the peak exotherm temperature decreases the cure rate resulting in a more uniformly cured composite. The viscosity vs time for the initial and the optimized cures are compared in Figure 48. Minimizing the temperature lag during heat up shifts the viscosity curves to the left reducing the gel time.

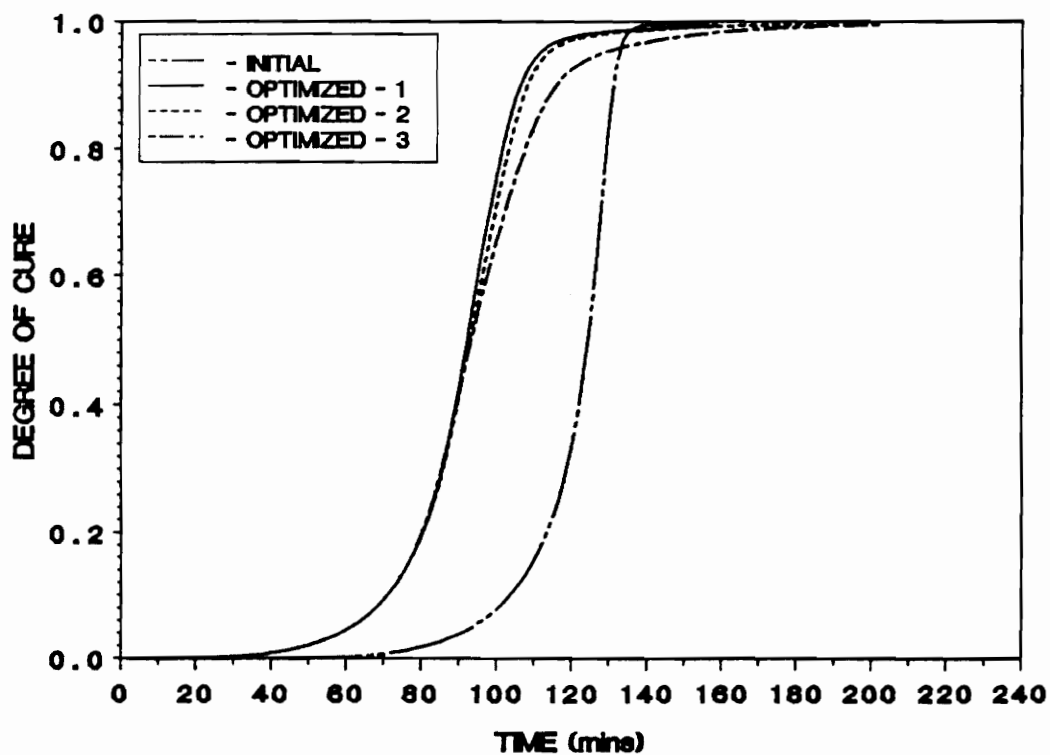


Figure 47. EXOTHERM & LAG MINIMIZATION - Degree of Cure vs Time.:

Degree of Cure vs Time at the center of the composite for the initial cure and three optimized cures :- (a). OPTIMIZED - 1 = Fixed final time case. (b). OPTIMIZED - 2 = Variable process time. (c). OPTIMIZED - 3 = Actual final time.

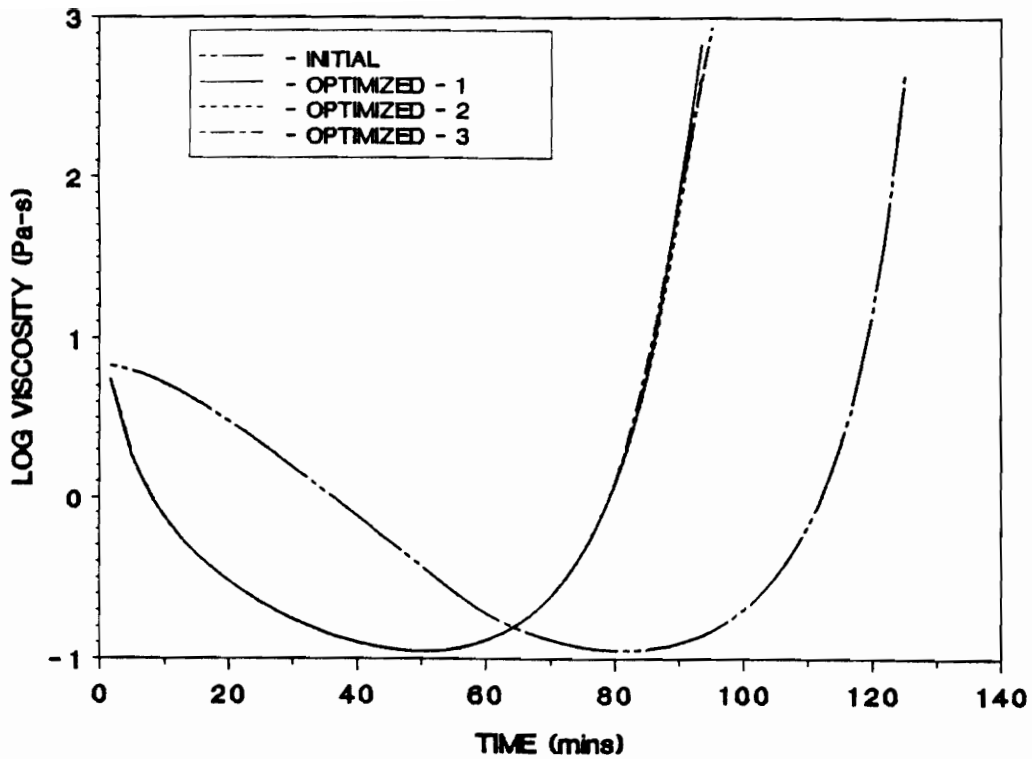


Figure 48. EXOTHERM & LAG MINIMIZATION - Log Viscosity vs Time.:

Log Viscosity vs Time at the center of the composite for the initial cure and three optimized cures :- (a). OPTIMIZED - 1 = Fixed final time case. (b). OPTIMIZED - 2 = Variable process time. (c). OPTIMIZED - 3 = Actual final time.

The temperature distribution across the cross section of the FWC assembly is shown in Figure 49. The temperature distribution due to the initial cure cycle and the optimized cure cycle are compared at 133 minutes.

The degree of cure vs normalized radius is plotted at time $t = 133$ mins for the initial and the optimized cure cycles in Figure 50. It is observed from Figure 50 that the optimized cure cycle results in uniform cure of the composite case.

The minimum degree of cure and the degree of cure at the center of the composite case for the initial cure cycle and the optimized cure cycle are plotted as a function of time in Figure 51. It is observed that the rate of curing is slower and more uniform for the optimized cure when compared to the initial cure with reaction exotherms being present.

The maximum viscosity and the viscosity at the center of the composite case are plotted as a function of time in Figure 52 for the initial cure cycle and the optimized cure cycle.

The cure rate sensitivity derivative $\frac{\partial \dot{\alpha}}{\partial \alpha} \big|_T$ characterizing the change in the cure rate with respect to the changes in the degree of cure at the center of the case is shown in Figure 53. The sensitivity derivative for the initial cure cycle suddenly drops and reaches a minimum around the same time as the peak temperature overshoot occurs in the composite. As expected the cure rate sensitivity derivative is more uniform for the optimized cure cycle.

The cure rate sensitivity derivative $\frac{\partial \dot{\alpha}}{\partial T} \big|_{\alpha}$ characterizes the change in the cure rate due to changes in the temperature with degree of cure remaining constant. The sen-

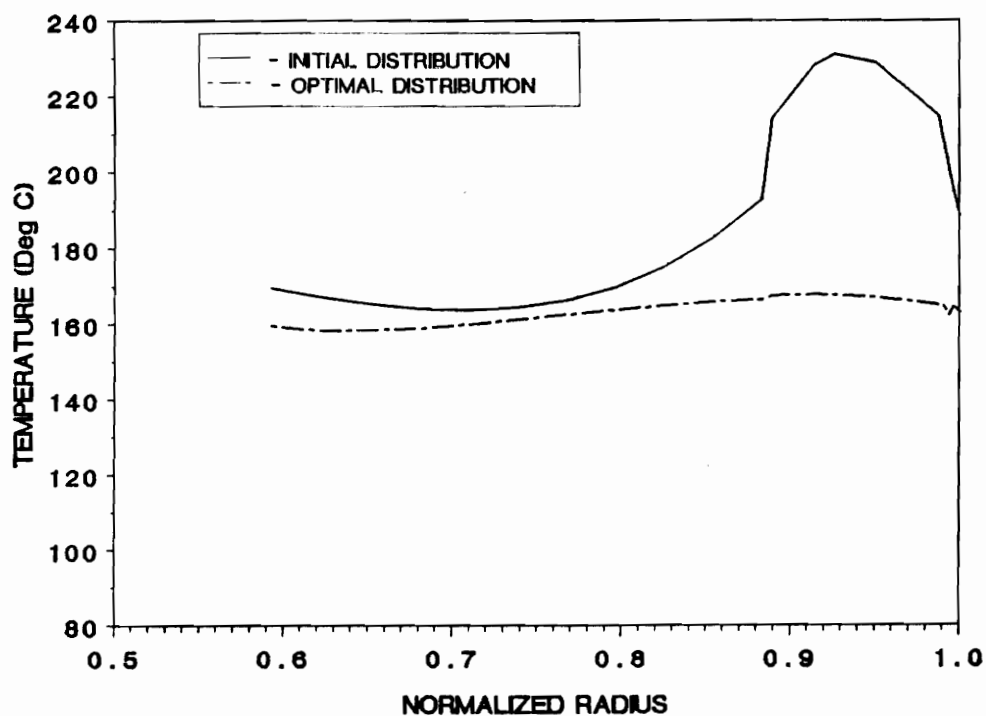


Figure 49. EXOTHERM & LAG MINIMIZATION - Temperature vs Normalized Radius.:

Temperature vs Normalized Radius profiles at :- (a). INITIAL DISTRIBUTION = temperature distribution across the thickness at time $t = 133.33$ mins for the initial case. (b). OPTIMIZED DISTRIBUTION = temperature distribution across the thickness at time $t = 133.33$ mins for optimized - 3 case.

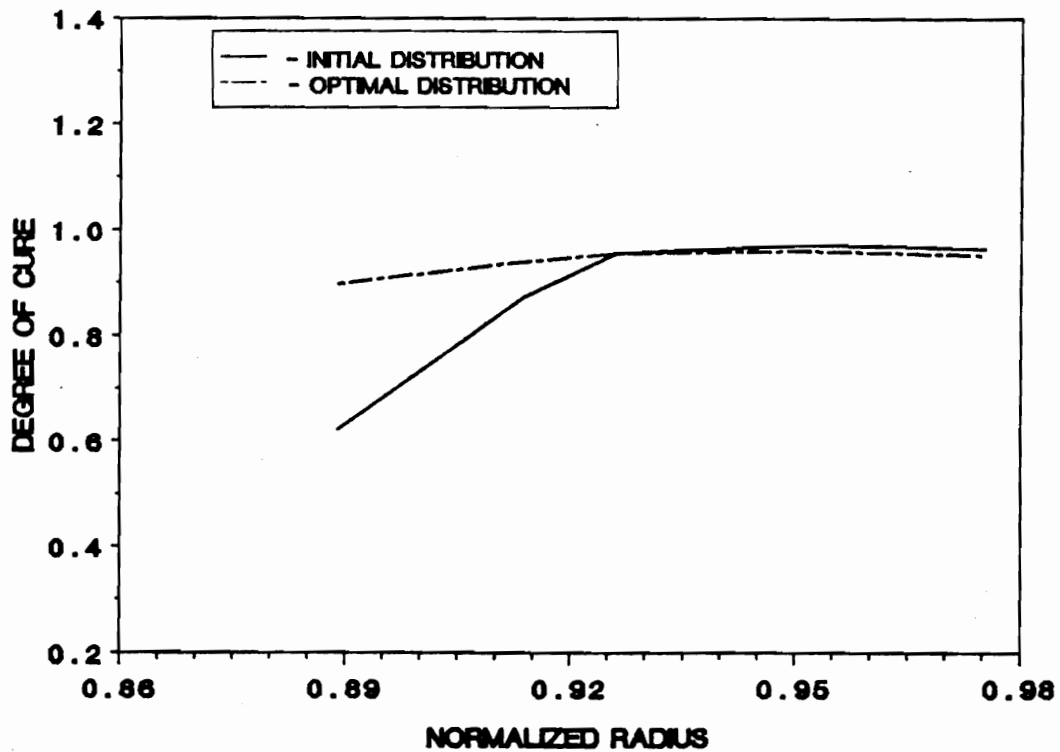


Figure 50. EXOTHERM & LAG MINIMIZATION - Degree of Cure vs Normalized Radius.:

Degree of Cure vs Normalized Radius profiles at :- (a). INITIAL DISTRIBUTION = Degree of Cure distribution for the composite case at time $t = 133.33$ mins for the initial cure cycle. (b). OPTIMIZED DISTRIBUTION = Degree of Cure distribution at time $t = 133.33$ mins for the optimized - 3 case.

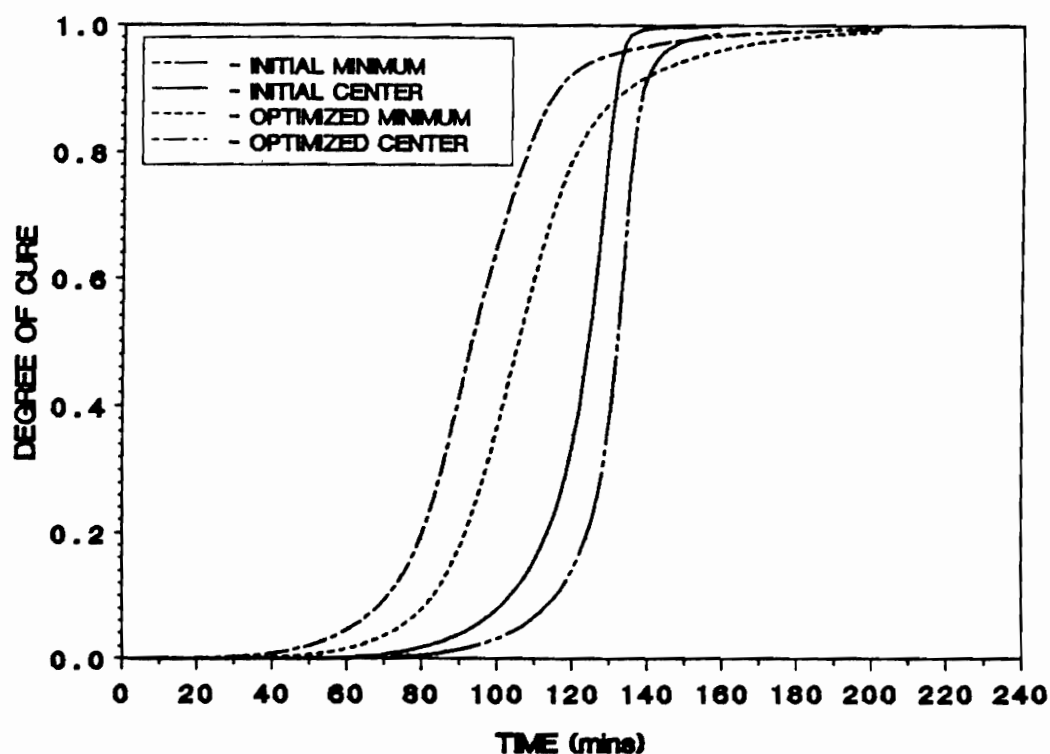


Figure 51. EXOTHERM & LAG MINIMIZATION - Degree of Cure vs Time:

Degree of Cure vs Time profiles at :- (a). INITIAL MINIMUM = the minimum degree of cure as a function of time for the initial cure cycle. (b). INITIAL CENTER = the degree of cure at the center of the composite case for the initial cure cycle. (c). OPTIMIZED MINIMUM = the minimum degree of cure as a function of time for the optimized - 3 case. (d). OPTIMIZED CENTER = the degree of cure at the center of the composite case for the optimized - 3 case.

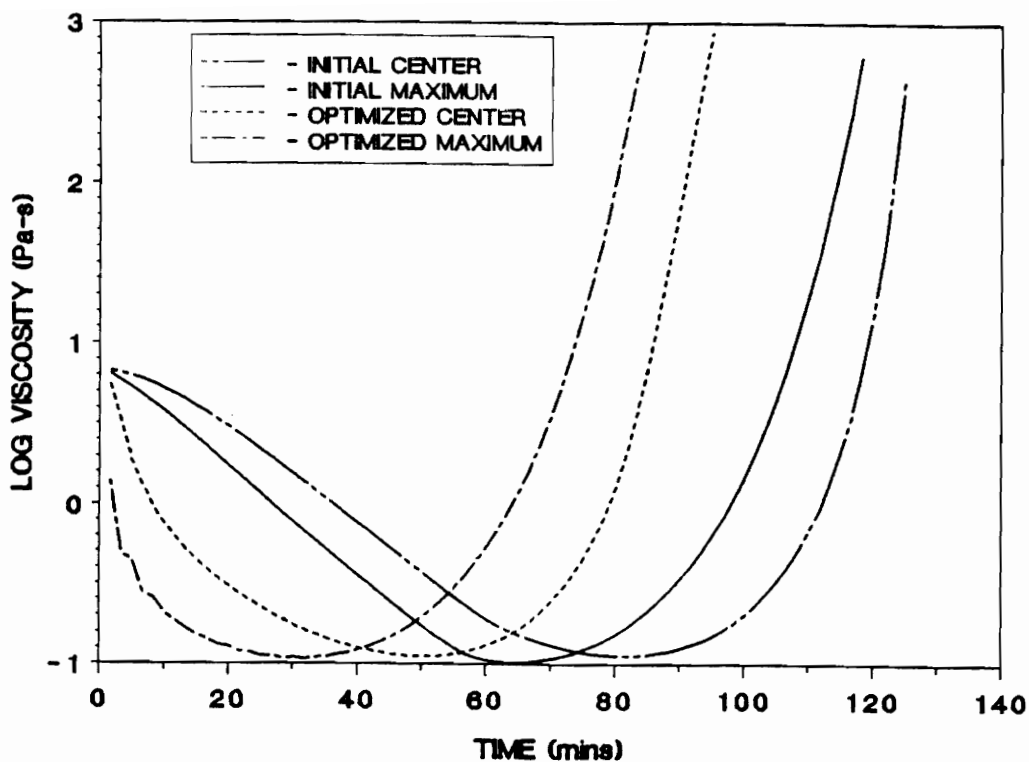


Figure 52. EXOTHERM & LAG MINIMIZATION - Log Viscosity vs Time:

Log Viscosity vs Time profiles at :- (a). INITIAL MAXIMUM = the maximum log viscosity as a function of time for the initial cure cycle. (b). INITIAL CENTER = the log viscosity at the center of the composite case for the initial cure cycle. (c). OPTIMIZED MAXIMUM = the maximum degree of cure as a function of time for the optimized - 3 case. (d). OPTIMIZED CENTER = the log viscosity at the center of the composite case for the optimized - 3 case.

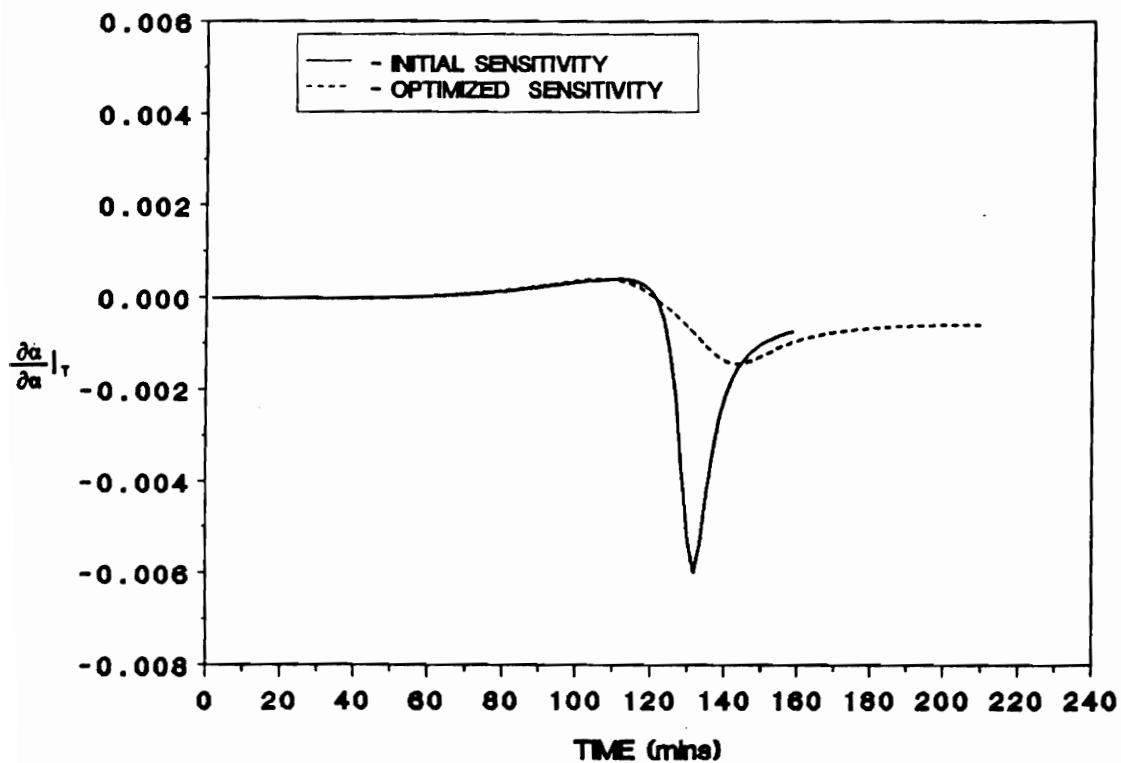


Figure 53. EXOTHERM & LAG MINIMIZATION - Cure Rate Sensitivity Derivative vs Time:

Cure rate sensitivity derivative at constant temperature vs time (a). INITIAL SENSITIVITY = Cure rate sensitivity derivative for the initial cure cycle. (b). OPTIMIZED SENSITIVITY = Cure rate sensitivity derivative for the optimized - 3 case.

sitivity plots for the initial and optimized behavior at the center of the case are shown in Figure 54. It is observed that the sensitivity peaks at the time of the peak overshoot temperature for the initial cure. The sensitivity derivative increases rapidly in the exotherm region for the initial cure but changes gradually for the optimized behavior. The uniformity of temperature ensures a more uniform cure rate as indicated by the optimized sensitivity curve.

The steepest descent of the performance index $J(r,t)$ (Eq.(6.1)) approaches the minimum is shown for the three optimized cure cycles in Figure 55.

7.6 Optimal Cure Simulation : Case - 3

Effect of Cure Cycle

The effect of changing the initial assumption for the cure cycle was studied in Case 3. The design window is identical to that specified for the two previously considered cases and the constraints, as well as, the program control parameters are similar. Again, the only change is in the cure cycle considered as the initial assumption.

The cure cycle considered is a cycle starting at 21.11°C and rising at a steady rate of 2.77°C/ min to an intermediate hold temperature of 115.5°C. The cycle is then held at this temperature for the next 22 minutes. Temperature is then raised at a rate of 2.77°C/ min to the final hold temperature of 176.6°C and held at this temperature until the composite cures. This is referred to as a double step cycle.

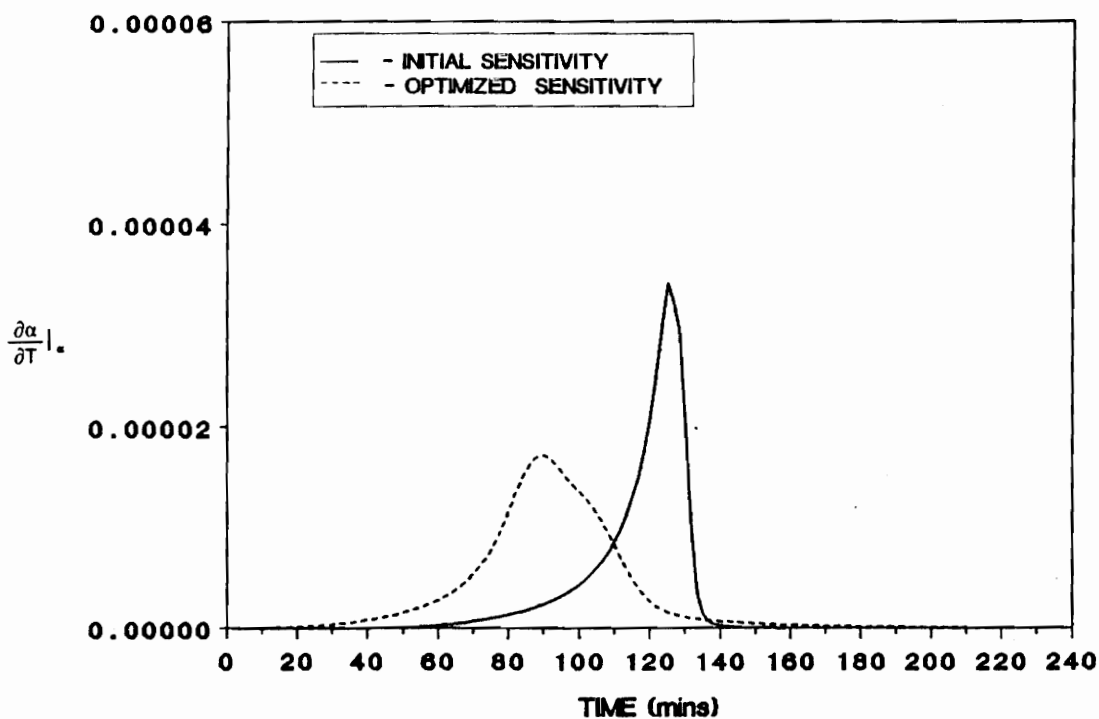


Figure 54. EXOTHERM & LAG MINIMIZATION - Cure Rate Sensitivity Derivative vs Time:

Cure rate sensitivity derivative at constant degree of cure vs time :- (a). INITIAL SENSITIVITY = Cure rate sensitivity derivative for the initial cure cycle. (b). OPTIMIZED SENSITIVITY = Cure rate sensitivity derivative for the optimized - 3 case.

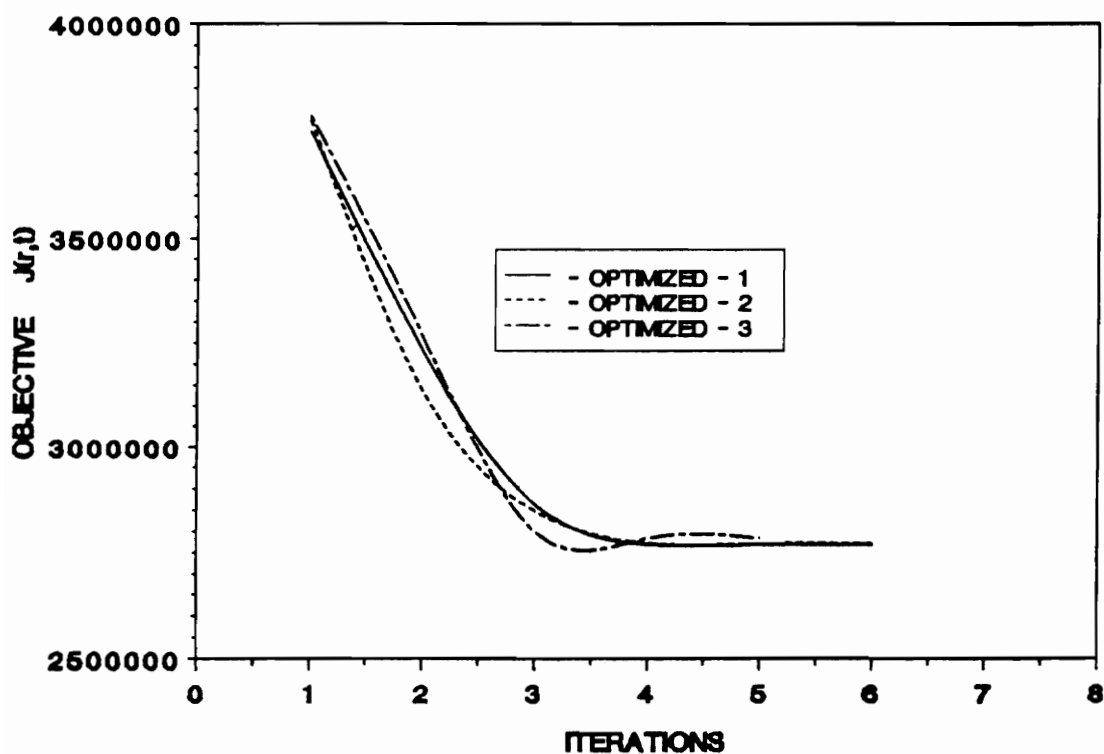


Figure 55. EXOTHERM & LAG MINIMIZATION - Objective $J(r,t)$ vs Iterations:

Steepest descent behavior as a function of number of iterations taken to reach a minimum :- (a). OPTIMIZED - 1 = Steepest descent behavior of the objective for the fixed time problem. (b). OPTIMIZED - 2 = Steepest descent behavior of the objective for the variable time problem with intermediate final time $t = 190.0$ mins. (c). OPTIMIZED - 3 = Steepest descent behavior of the objective for the variable time problem with actual final process control time $t = 201.0$ mins.

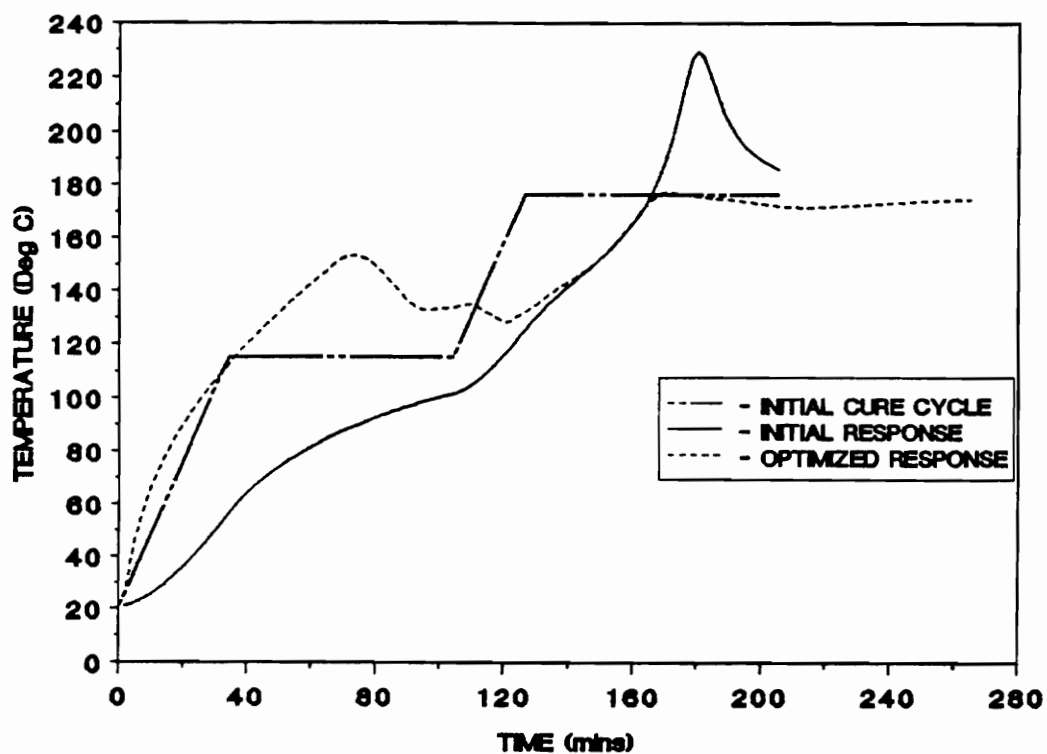


Figure 56. DOUBLE STEP CURE CYCLE - Temperature vs Time:

The temperature behavior at the center of the composite case are plotted as a function of time for the initial double step cure cycle and the optimized cure cycle.

The search for the optimum cure cycle is carried out in a similar manner as the optimization procedure outlined for the exotherm and lag minimization. The temperature vs time curves are shown in Figure 56. The composite requires 205 minutes to reach a degree of cure of 0.99 at the center when cured using the initial cure cycle. The optimal cure cycle, shown in Figure 57, indicates that the uniform cure is achieved at a final time of 265 minutes. It is to be observed that the optimal cure cycle also shows a bang-bang behavior particularly at the beginning of the process.

The minimum degree of cure and the degree of cure at the composite center for the initial cure and the optimized cure are plotted as a function of time in Figure 58. It is observed that for the optimized cycle the rate of curing is initially faster for the initial cure due to the higher cure temperature. However, as the cure progresses the cure reactions become slower and more uniform for the optimized case compared with the initial case with high reaction exotherms present. This can be observed around 160.0 minutes into the process where the cure rate for the optimum case is slower than the initial cure.

The maximum viscosity and the viscosity at the center of the composite are plotted as a function of time in Figure 59. The optimized cure cycle leads to an earlier gel time as compared to the gel time for the initial cure cycle. The viscosity is actually more nonuniform for the optimized case due to the higher initial cure temperature required to minimize the thermal lag.

The cure rate sensitivity derivatives $\frac{\partial \dot{\alpha}}{\partial \alpha}|_T$ and $\frac{\partial \dot{\alpha}}{\partial T}|_{\alpha}$, and the temperature and degree of cure distributions show a similar trends reported in Cases 1 and 2.

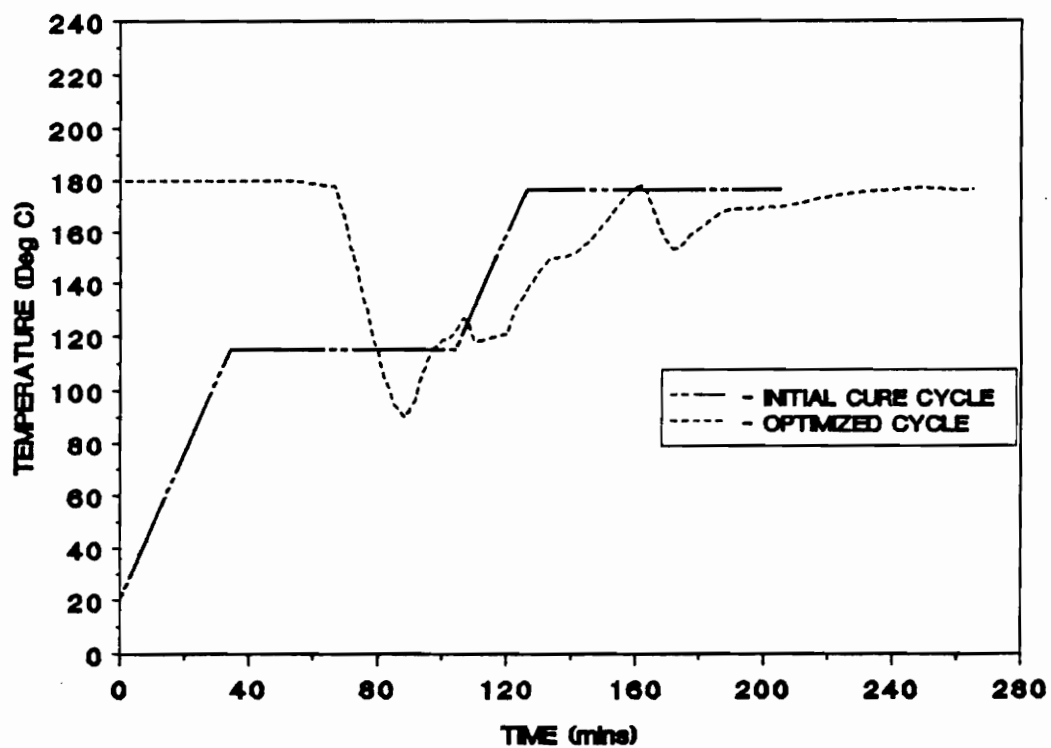


Figure 57. DOUBLE STEP CURE CYCLE - Cure Cycle:

Cure cycle profiles for the initial cure and the optimal curing cycle plotted as a function of time.

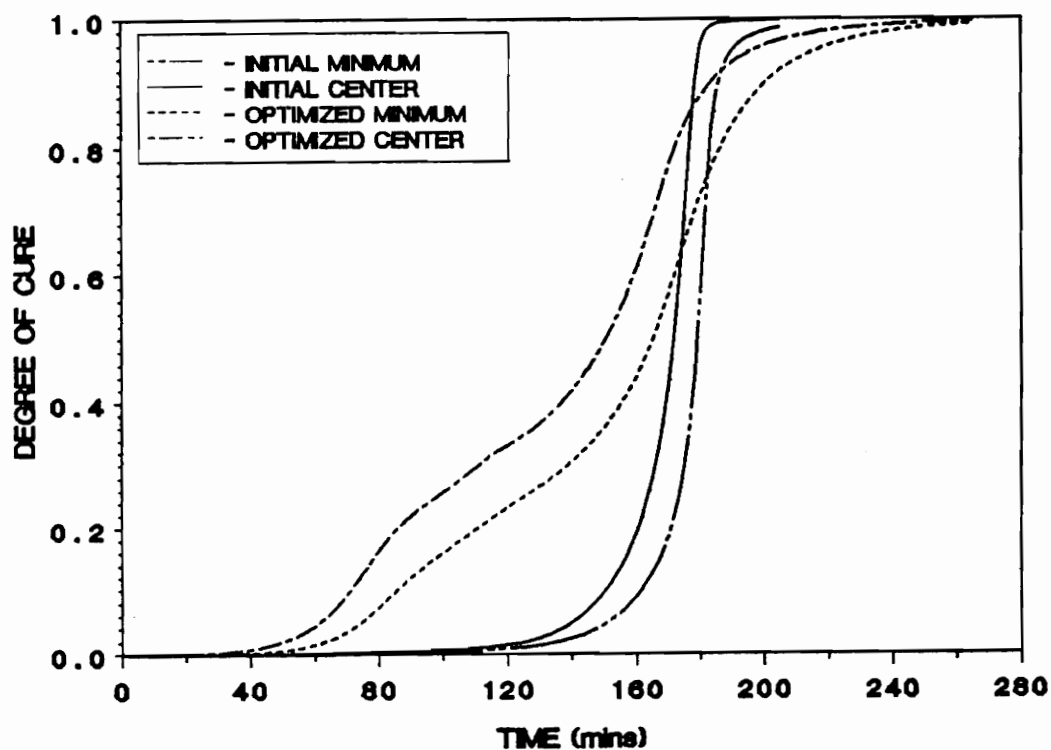


Figure 58. DOUBLE STEP CURE CYCLE - Degree of Cure vs Time:

Degree of Cure vs Time profiles at :- (a). INITIAL MINIMUM = the minimum degree of cure as a function of time for the initial cure cycle. (b). INITIAL CENTER = the degree of cure at the center of the composite case for the initial cure cycle. (c). OPTIMIZED MINIMUM = the minimum degree of cure as a function of time for the optimized cure cycle. (d).OPTIMIZED CENTER = the degree of cure at the center of the composite case for the optimized cure cycle.

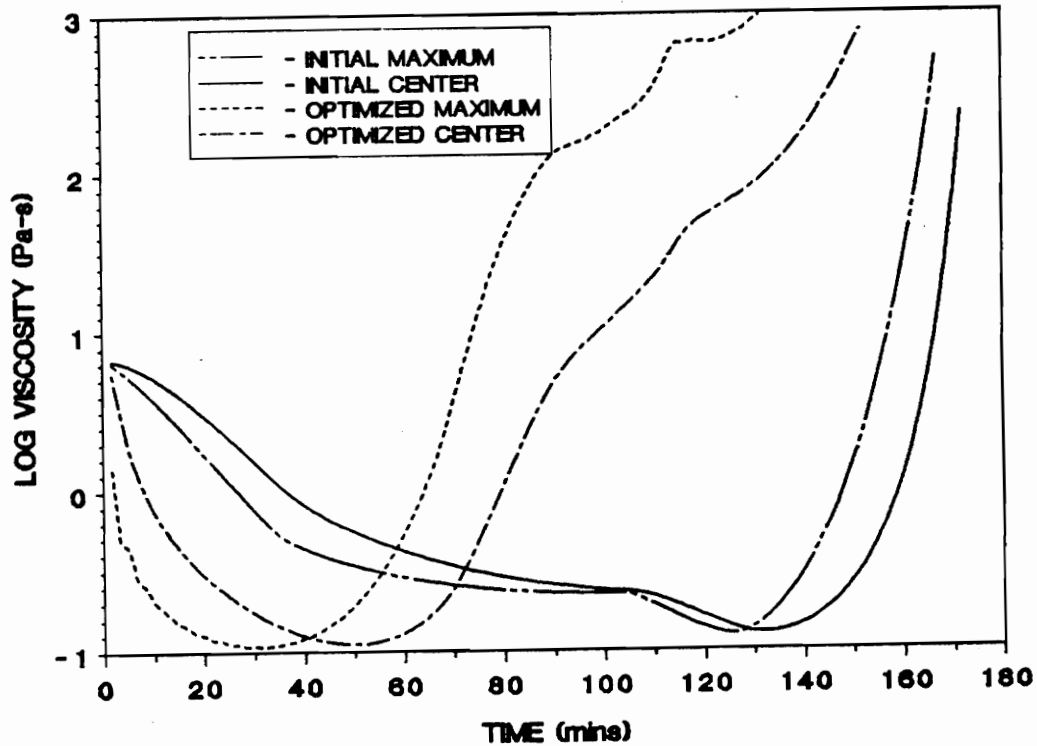


Figure 59. DOUBLE STEP CURE CYCLE - Log Viscosity vs Time:

Log Viscosity vs Time profiles at :- (a). INITIAL MAXIMUM = the maximum log viscosity as a function of time for the initial cure cycle. (b). INITIAL CENTER = the log viscosity at the center of the composite case for the initial cure cycle. (c). OPTIMIZED MAXIMUM = the maximum log viscosity as a function of time for the optimized cure cycle. (d). OPTIMIZED CENTER = the log viscosity at the center of the composite case for the optimized cure cycle.

7.7 Optimal Cure Simulation : Case - 4

Effect of Mandrel Material

The effect of changes in mandrel material on the curing of thick section composites can be studied using an aluminum Al 6061 mandrel instead of the PVA Sand mandrel. The higher conductivity of aluminium as compared to sand can influence the cure characteristics, as well as, the optimal curing time. Using the single step cure cycle, it is observed that the center of the case reaches a degree of cure of 0.96 in 141.0 mins as compared to 158.3 mins with the PVA Sand mandrel. Figure 60, shows the temperature vs time profiles at the center of the composite case. The optimized response shows initial lag correction but as the process progresses the lag correction does not occur to a very great extent. The exotherm is minimized and a uniform temperature is achieved. A final time of 208.3 mins is required to minimize the performance index and to obtain a degree of cure distribution in the composite of 0.99. The cure cycle temperature is plotted as a function of time in Figure 61. The optimal cure cycle is observed to increase at a finite rate and then shows a clear bang - bang behavior as it hits both the lower and upper bounds of the design window. This clearly indicates that if the thermal lag is be minimized a different upper bound temperature will have to be chosen. The optimal cure cycle behaves exactly like the other cases in the exotherm region, as well as, towards the end of the curing process ensuring an exotherm minimization and achieving uniform temperature distribution.

The minimum degree of cure and the degree of cure at the composite center for the initial cure and the optimized cure are plotted as a function of time in Figure 62. It is

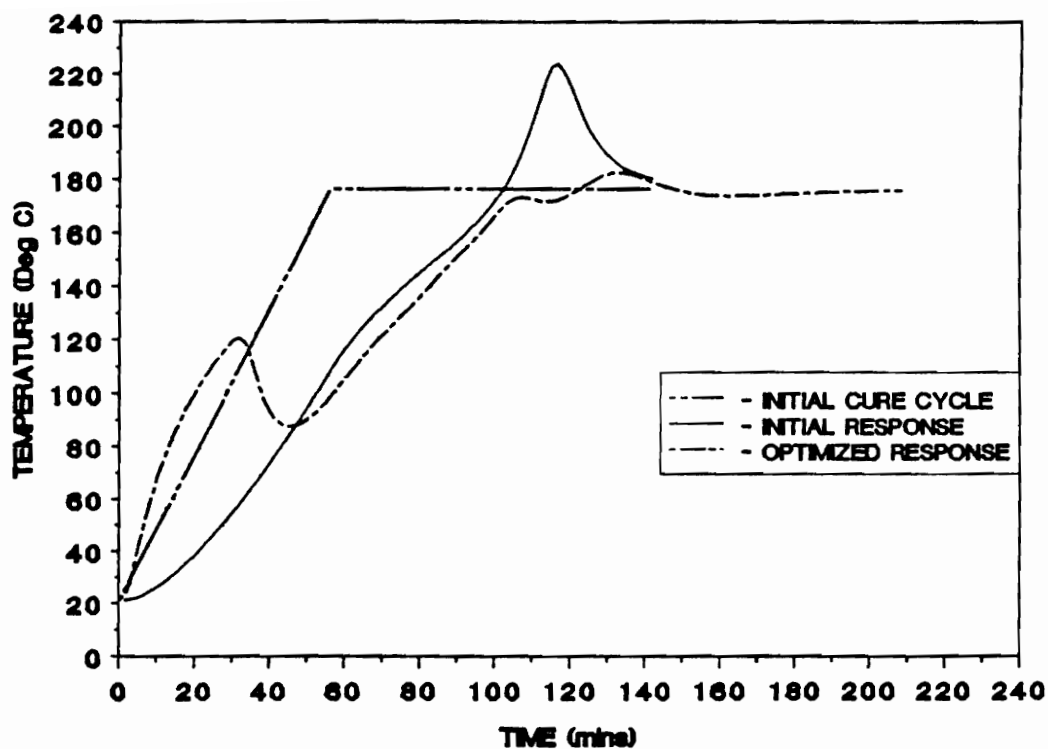


Figure 60. Al 6061 MANDREL - Temperature vs Time:

The temperature behavior at the center of the composite case are plotted as a function of time for the initial single step cure cycle and the optimized cure cycle.

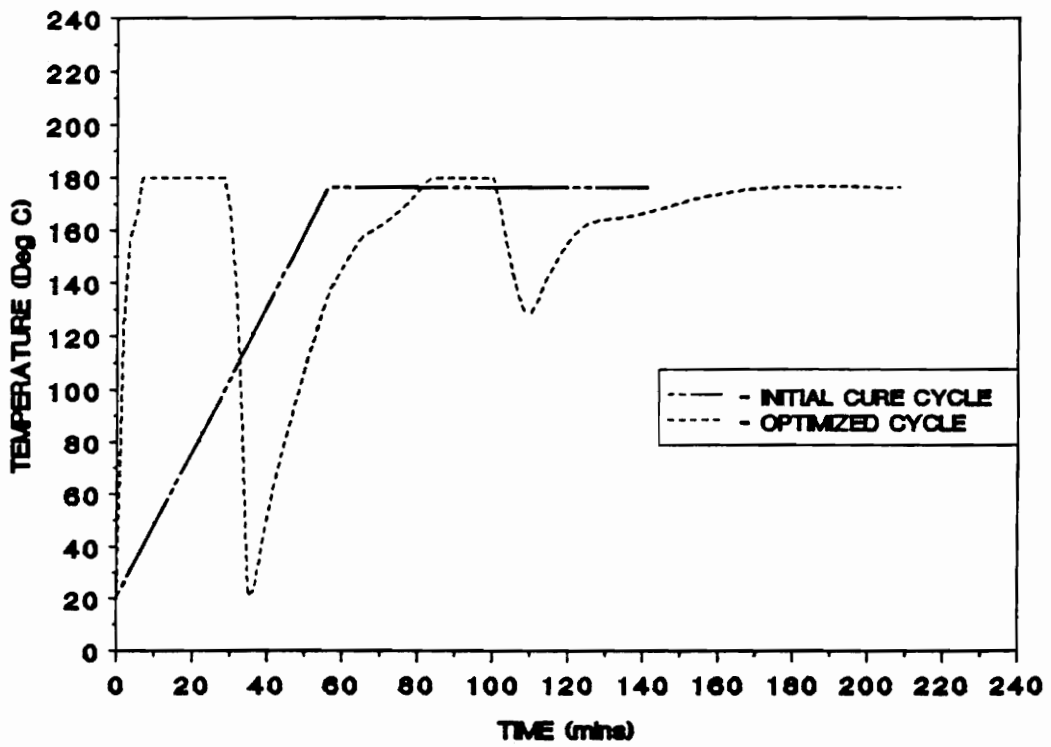


Figure 61. AL 6061 MANDREL - Cure Cycle:

Cure cycle profiles for the initial cure and the optimal curing cycle are plotted as a function of time.

observed that for the optimized cure the rate of curing is initially faster due to increased heating from the surroundings. However, as the reaction progresses the cure rate becomes slower and more uniform compared to the initial cure with reaction exotherms being present.

The maximum viscosity and the viscosity at the center of the case are plotted as a function of time in Figure 63. The optimized cure cycle leads to a delayed gel time as compared to the gel time for the initial cure cycle.

The cure rate sensitivity derivatives, $\frac{\partial \dot{\alpha}}{\partial \alpha}|_T$ and $\frac{\partial \dot{\alpha}}{\partial T}|_{\alpha}$, described earlier and the temperature and degree of cure distributions show a similar type of trend as seen in CASE 2.

The minimization procedure clearly indicates that the method adopted can lead to the minimization of the peak exotherms occurring during the curing of thick section composites subject to different types of cure cycles. However, in order to facilitate exact temperature tailoring additional temperature constraints would have to be specified during the process. The effects of changes in material properties of the individual layers of the FWC assembly can influence the behavior of the cure cycle, as well as, the tailoring of temperature dependent properties inside the composite.

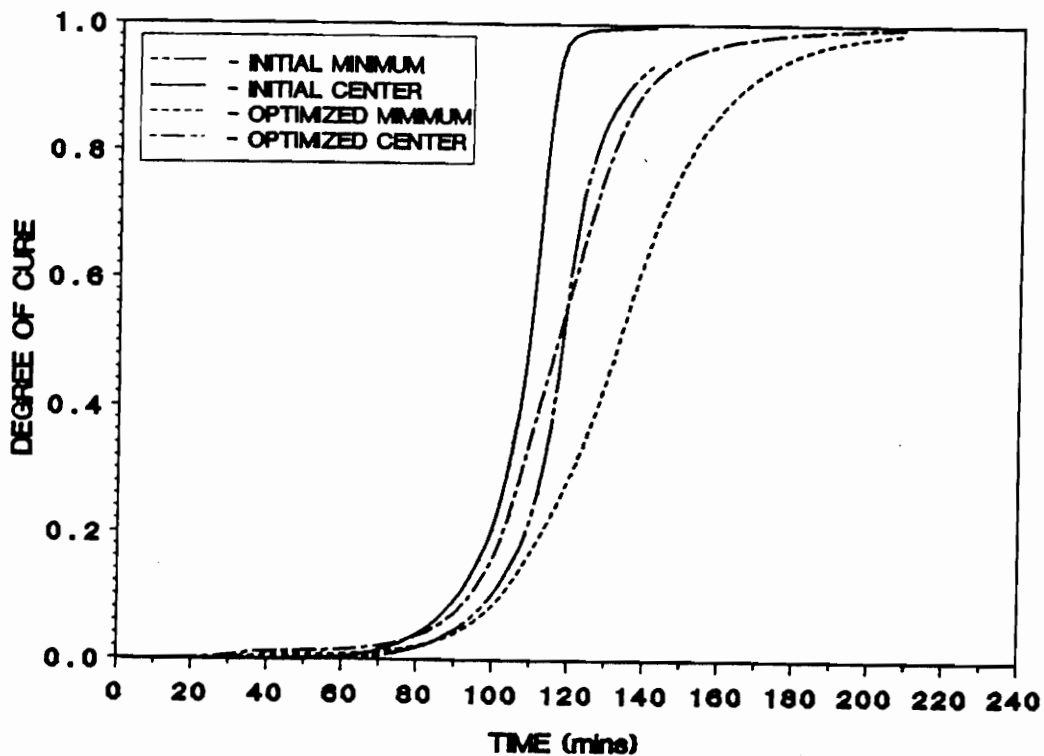


Figure 62. Al 6061 MANDREL - Degree of Cure vs Time:

Degree of Cure vs Time profiles at :- (a). INITIAL MINIMUM = the minimum degree of cure as a function of time for the initial cure cycle. (b). INITIAL CENTER = the degree of cure at the center of the composite case for the initial cure cycle. (c). OPTIMIZED MINIMUM = the minimum degree of cure as a function of time for the optimized cure cycle. (d). OPTIMIZED CENTER = the degree of cure at the center of the composite case for the optimized cure cycle.

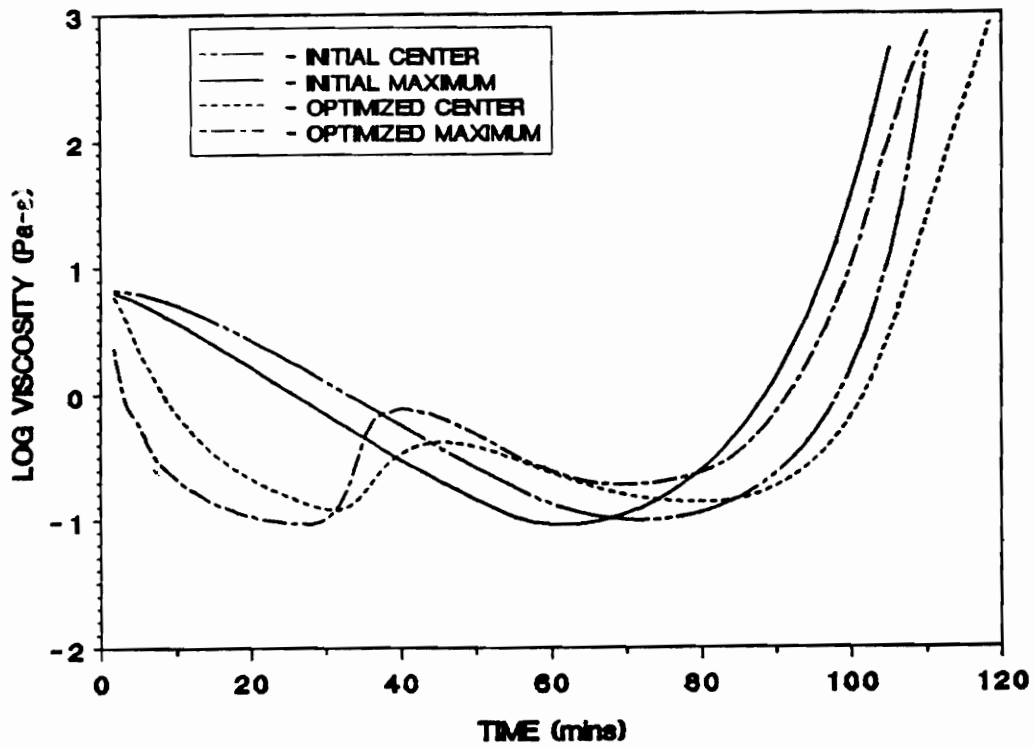


Figure 63. AL 6061 MANDREL - Log Viscosity vs Time:

Log Viscosity vs Time profiles at :- (a). INITIAL MAXIMUM = the maximum log viscosity as a function of time for the initial cure cycle. (b). INITIAL CENTER = the log viscosity at the center of the composite case for the initial cure cycle. (c). OPTIMIZED MAXIMUM = the maximum degree of cure as a function of time for the optimized cure cycle. (d). OPTIMIZED CENTER = the log viscosity at the center of the composite case for the optimized cure cycle.

CHAPTER 8

IN CONCLUSION

8.1 Curing Process in Filament Wound Composites

1. Models were developed which can be used to simulate the curing process of an axisymmetric filament wound composite case. The models relate the cure cycle to the thermal, chemical and physical processes occurring in the FWC assembly during cure.
2. The axisymmetric heat transfer model can be extended to an axisymmetric cure model by taking into account the resin cure kinetics and the resin viscosity behavior.
3. On the basis of the model, a finite element computer code "FEMCURE" was developed which can be used to determine the following information was developed

used to determine the following information for filament wound composites cured by a specified cure cycle :-

- a. The temperature inside the mandrel, insulator, composite, and outer layer as a function of position and time.
 - b. The degree of cure of the resin as a function of position and time.
 - c. The resin viscosity as a function of position and time.
 - d. The effects of geometry, material properties and cure cycle on the curing of filament wound composites.
4. The input parameters required in the computer code for the solution of the models were specified.
 5. Experimental data measuring the temperature distribution in a 0.14605 m (5.75 in.) diameter bottle with a graphite - epoxy composite case were obtained and used to validate the axisymmetric cure model.
 6. Cure simulations were carried out on an 18 diameter graphite - epoxy case to illustrate the type of information that can be generated by the model and to determine the effects of various processing parameters on the curing process.

8.2 Curing Process Optimal Control

The composite cure problem was extended to an optimal process control problem. It has been demonstrated that the cure cycle significantly influences the final mechanical properties of the composite. Curing of thick section composites using cure cycles developed for thin laminates often results in large thermal gradients due to the presence of exothermic chemical reactions resulting in a nonuniformly cured composite. Thus, it is necessary to tailor the cure cycle such that reaction exotherms would be minimized, the composite temperature distribution is uniform (uniform cure), and the composite achieves the desired degree of cure at the end of the process.

The process control problem was looked upon as a free time optimal control problem with end point constraints, a stopping condition, as well as, a uniformity constraint on the state and co-state variables. The state and co-state variables were related to the constraints through adjoint variables. The individual Hamiltonians were recognized and the control variable was identified. The calculus of variations approach adopted to formulate the optimal control problem lead to the calculation of transversality conditions, system of adjoint equations, and final time conditions needed to be satisfied by the adjoint variables.

The solution of the state estimation problem and the adjoint problem was recognized as a classical two point boundary value problem posed by the calculus of variations approach to distributed parameter systems. The curing process was modeled as a nonlinear, time optimal control problem with the cure cycle temperature entering through the flux boundary of the state equations.

A Fortran computer code "CUREOPT" was developed to solve the time optimal control problem. The program had the capability to solve both the fixed time and variable time problems in order to satisfy the design criteria identified by the design window. The program was initially verified using the classical Butkovskii - Sakawa boundary control problem for optimal control of the heat transfer process in flat plates. The program was then extended to solve the nonlinear, variable time, unsteady heat transfer process in filament wound composites.

In summary the following major conclusions could be arrived at for the optimal process control problem :-

1. The exotherms caused by runaway reactions in thick section thermoset composites could be minimized.
2. In all the cases studied it was observed that the optimal cure cycle showed tendencies of approaching a bang - bang nature.
3. The method adopted gave an estimate of the cure rate design sensitivities. The cure rate sensitivities give an indication of how the rate of cure of the system changes with changes in the state (temperature) and co-state (degree of cure) variables during the optimal curing of composites.
4. The final optimal process time could be logically derived and identified, from the degree of cure and the stopping condition.
5. The optimal process control of the curing process gave a logical and effective method to arrive at an optimal cure cycle.

8.3 Future Research

The program "CUREOPT" can be used as an operational base to set up an expert control system for the optimal control and temperature related property tailoring of composites. It can be utilized to extend the existing knowledge base in the quality assurance, and design of composite structures. Real time optimal control of composite curing has not yet been implemented and is an area where optimal control techniques can be applied.

BIBLIOGRAPHY

1. Munjal, A.K., "Optimization of Design Allowables for Composite Structures", **SAMPE Quarterly**, Vol 18, No 2, pp. 18-27, (1987)
2. Munjal, A.K., "Use of Fiber Reinforced Composites in Rocket Motor Industry", **SAMPE Quarterly**, Vol 17, No 2, pp. 1-11, Jan, (1986)
3. Munjal, A.K., Kulkarni, S.B., and Starett, H.S., "Characterization of Filament wound Kevlar & Glass Composites for Rocket Motor Applications", **9th National SAMPE Symposium**, pp. 324-337,(1984)
4. Springer, G.S., "A Model of the Curing Process of Epoxy Matrix Composites", in **Progress of Science and Engineering of Composites** , (T.Hayashi and K.Kawaka, eds), Japan Society of Composite Materials, pp. 23 - 35, (1982)
5. Springer, G.S., "Resin Flow During the Cure of Fiber Reinforced Composites", **Journal of Composite Materials**, Vol.16, pp. 400 - 410, (1982)
6. Loos, A.C., and Springer, G.S., "Calculation of Cure Process Variables of Graphite - Epoxy Composites", in **Composite Materials Quality, Assurance and Processing** (C.E. Browning, ed.), ASTM STP 797, pp. 110 - 118, (1983)
7. Loos, A.C., and Springer, G.S., "Curing of Graphite / Epoxy Composites", **Air Force Materials Laboratory Report AFWAL-TR-83-4040** , Wright Aeronautical Laboratories, Wright Patterson Airforce Base, Dayton, Ohio, (1983)
8. Loos, A.C., and Springer, G.S., "Curing of Epoxy Matrix Composites", **Journal of Composite Materials**, Vol.17, pp. 135 - 169 (1983)
9. Lee, W.I., Loos, A.C., and Springer, G.S., "Heat of Reaction, Degree of Cure and Viscosity of Hercules 3501 - 6 Resin", **Journal of Composite Materials**, Vol.16, pp. 510 - 520, (1982)
10. Dusi, M.R., Lee, W.I., Ciriscioli, P.R., and Springer, G.S., "Cure Kinetics and Viscosity of Fiberite 976 Resin", **Journal of Composite Materials**, Vol.21, March (1987)

11. Blankenship, L.D., "Thermal Behaviour of Graphite/Epoxy Composite in a Sub-cured State", **Composite Materials Testing and Design (Sixth Conference)**, (I.M. Daniel, ed.), ASTM-STP-787, pp. 65 - 72, (1982)
12. Johnson, J.B., and Owston, C.N., "The Effect of Cure Cycle on the Mechanical Properties of Carbon Fibre / Epoxide Resin", **Composite**, pp. 111 - 117, May, (1973)
13. Hayes, B., "Polymer selection and Matrix Aspects of Processing and Manufacture of Fibre Composites", **Composite**, Vol 14, No 2, pp. 93-99, April, (1973)
14. Aylward, L., Douglas, C., and Roylance, D. "Analysis of Cure in Composites Processing", **16th National SAMPE Technical Conference**, pp. 148-158, (1984)
15. Young, M.H., and Lloyd, B.A., "Rocket Case Performance Optimization", **17th National SAMPE Technical Conference**, pp. 482-494, (1985)
16. Butkovskii, A.G., "A Generalized Maximum Principle for Problems in Optimal Control", **Automation and Remote Control**, Vol.24., No.3, pp. 292 - 304, (1963)
17. Sakawa, Y., "Solution of an Optimal Control Problem in a Distributed Parameter System", **IEEE Transactions on Automatic Control**, AC-9, pp. 420 - 426, (1964)
18. Denn, M.M., Gray, R.D., Jr., and Ferron, J.R., "Optimization in a Class of Distributed Parameter Systems", **Industrial Engineering and Chemistry Fundamentals**, Vol.5, pp. 59 - 66, (1966)
19. Denn, M.M., "Optimal Boundary Control for a Non-Linear Distributed System", **International Journal of Control**, Vol.4., No.2., pp. 167 - 178, (1966)
20. Meric, R.A., "Finite Element Methods for an Optimal Steady State Control Problem", **International Journal for Numerical Methods in Engineering**, Vol.12., pp. 1375 - 1382. (1978)
21. Chen, W.H., and Seinfeld, J.H., "Estimation of Spatially Varying Parameters in Partial Differential Equations", **International Journal of Control**, Vol. 15, No. 3, pp. 487 - 485, March (1972)
22. Seinfeld, J.H., "Nonlinear Estimation for Partial Differential Equations", **Chemical Engineering Science**, Vol.26, pp. 355 - 383 (1969)
23. Tzafestas, S.G. and Nightingale, J.M., "Optimal Control of a Class of Linear Stochastic Distributed Parameter Systems", **Proc. Instn Electrical Engineers**, Vol.15., No.8., pp. 1213 - 1220, (1968)
24. Nakamichi, J., and Washizu, K., "Application of the Finite Element Method to an Optimal Control Problem", **International Journal for Numerical Methods in Engineering**, Vol.12., pp. 1559 - 1574. (1978)
25. Ray, A.K., and Gupta, S.K., "Optimization of Nonvaporizing Nylon 6 Reactors with Stopping Conditions and End Point Constraints", **Polymer Engineering and Science**, Vol. 26, No. 15, pp. 1033 - 1040, August (1986)
26. Denn, M.M., **"Optimization by Variational Methods"**, McGraw Hill, New York (1969)

27. Shibley, A.M., "Filament Winding", **Handbook of Composites**, (G.Lubin .ed), Van Nostrand Reinhold Co., pp. 448 - 478,(1982)
28. Schwartz, M.M., "**Composite Materials Handbook** ", McGraw-Hill, New York (1983)
29. Arpaci, V.S., "**Conduction Heat Transfer**", Addison-Wesley Publishing Co., Reading, MA (1966)
30. White, F.M., "**Heat Transfer**", Addison - Wesley Publishing Co., Reading, MA (1984)
31. Lindt, J.T., "Curvature Effects in Reaction Injection Molding", in **Proceedings of the 37th Annual Technical Conference** Society of Plastic Engineers, Inc, New Orleans, LA (May 7-10), pp. 448 - 481, (1979)
32. Springer, G.S., and Tsai, S.W., "Thermal Conductivities of Unidirectional Materials", **Journal of Composite Materials**, Vol.16, pp. 166 - 173, (1967)
33. Jones, R.M., "**Mechanics of Composite Materials**", McGraw-Hill, New York (1980)
34. Chamis, C.C., "Simplified Composite Micromechanics Equations for Hygral, Thermal and Mechanical Properties", **Proceedings of the 38th Annual Conference**, Reinforced Plastics / Composites Institute, pp. 1 - 9, Feb, (1983)
35. Wilson, E.L., Bathe, K.J., amd Peterson, F.E., "Finite Element Analysis of Linear and Nonlinear Heat Transfer", **Nuclear Engineering and Design**, Vol.29., pp. 110 - 124, (1974)
36. Bathe, K.J., and Khoshgoftar, M.R., "Finite Element Formulation and Solution of Nonlinear Heat Transfer",**Nuclear Engineering and Design**, Vol.51., pp. 389 - 401, (1979)
37. Reddy, J.N., "**An introduction to the Finite Element Method** ", McGraw-Hill, New York, NY (1984)
38. Bathe, K.J., and Wilson, E.L., "**Numerical Methods in Finite Element Analysis**", Prentice - Hall, Inc., Englewood Cliffs, (1976)
39. Calius, E. and Springer, G.S., "Optimization of the Cure Window For A Large Filament Wound Case", **Report to the Chemical Research Projects Office**, NASA Ames Research Center, November (1984)
40. Mikhailov, M.D., and Ozisik, M.N., "**Unified Analysis and Solutions of Heat & Mass Diffusion**", John Wiley and Sons, New York (1983)
41. Heisler, M.P., "Temperature Charts for Induction and Constant Temperature Heating", **ASME Transactions** Vol.69, pp. 227 - 236, (1947)
42. Dahlgreen, S.D., "Variable Temperature CFRP Composite Cure Cycle Analysis", **18th International SAMPE Technical Conference**, Oct 7-9, (1986)
43. Gilliam, J.K., "Formation and Properties of Thermosetting and High Tg Polymeric Materials", **Polymer Engineering and Science**, Vol 26, No 20, pp. 1429 - 1433, Nov,(1986)

44. Ganani, E., Higgins, B.G., and Powell, R.L., "Monitoring the Initial Phase of Slow Curing Epoxy through Dynamic Viscoelastic Properties", **Polymer Engineering and Science**, Vol 26, No.22, pp. 1563 - 1567, Dec,(1986)
45. Hinrichs, R.J., and Thuen, J.M., "Control of Composite Cure Processes", in **"The Role of Polymeric Matrix in the Processing and Structural Properties of Composite Materials"**, (J.C.Seferis and L.Nicolais.eds), Plenum Press,(1981)
46. Mijovic, J., Kim, J, and Slaby, J., "Cure Kinetics of Epoxy Formulations of the Type Used in Advanced Composites", **Journal of Polymer Science**, Vol 29, pp. 1449 - 1462 (1984)
47. Bryson, Jr., A.E., and Ho, Yu-Chi, **"Applied Optimal Control: "**, Hemisphere, New York (1975)
48. Sage, A.P., and White, III, C.C., **"Optimum Systems Control "**, Prentice-Hall Inc, New York (1977)
49. Fraber, J.N., "Steady State Multiobjective Optimization of Continuous Copolymerization Reactors", **Polymer Engineering and Science**, Vol 26, No.7, April.(1986)
50. Hermes, H and Lasalle, J.P., **"Functional Analysis and Time Optimal Control"**, Academic Press, New York (1969)
51. Polak, K. **"Computational Methods in Optimization"**, Academic Press, New York, (1971)
52. Holliday, J.H., and Storey.C., "Numerical Solution of Certain Nonlinear Distributed Parameter Optimal Control Problems", **International Journal of Control**, Vol. 18, No. 4, pp. 817-825, Oct, (1973)
53. Goldwyn, R.M., Sriram, K.P. and Graham, M. "Time Optimal Control of Linear Diffusion Process", **Siam Journal of Control and Optimization** , pp. 295 - 308, Dec. (1966)
54. Glashof, K. and Weck, N., "Boundary Control of Parabolic Differential Equations in Arbitrary Dimensions Supermum Norm Problems", **Siam Journal of Control and Optimization** , Vol.14., No.4., pp. 662 - 681, July(1976)
55. Denham, W.F., **"Steepest Ascent Solution of Optimal Programming Problems"**, Ph.D Dissertation, Harvard, (1963)
56. Leondes, C.T., and Niemann, R.A., "On the Optimal Control Problem with Unrestricted Final Time", **Transactions of ASME Journal of Basic Engineering**, pp. 155 - 160, June, (1969)
57. Haftka, R.T., "Techniques for Thermal Sensitivity Analysis", **International Journal of Numerical Methods in Engineering**, Vol.17, pp. 71 - 80. (1980)
58. Hans, L.S., and Cosner, A.A., "Effective Thermal Conductivities of Fibrous Composites", **Journal of Heat Transfer**, Vol.13, pp. 387 - 392, May (1981)
59. Lapidus, L. **"Digital Computation for Chemical Engineers"**, McGraw - Hill Inc, New York, (1977)

60. Lee, C.W., "Composite Cure Process Control by Expert Systems", **Proceedings of the First Conference on Composite Materials**, American Society for Composites, (Oct 7 - 9, 1986), Dayton, OH.

Appendices

Appendix A. VARIATION OF REACTION RATE

In this appendix an empirical expression for the variation of the cure rate, $\frac{d\alpha}{dt}$, with time, t , and temperature, T , is presented. The expression for the cure rate was obtained by fitting an empirical model to the experimental data. In [39], the following expressions, were found to yield good agreement with data available for epoxy resins

$$\begin{aligned}\frac{d\alpha}{dt} &= K_0 (K_1 + K_2 \alpha^a) (B_1 - \alpha)^b (1.0 - \alpha)^c & \forall & \alpha \leq \alpha_c \\ \frac{d\alpha}{dt} &= K_3 (1.0 - \alpha)^d & \forall & \alpha > \alpha_c \quad (\text{A.1})\end{aligned}$$

The temperature dependent factors are given by

$$\begin{aligned}K_0 &= A_0 T + B_2 \\ K_1 &= A_1 e^{-\frac{\Delta E_1}{RT}} \\ K_2 &= A_2 e^{-\frac{\Delta E_2}{RT}} \\ K_3 &= A_3 e^{-\frac{\Delta E_3}{RT}}\end{aligned} \quad (\text{A.2})$$

where A_0 , is the linear factor, A_1 , A_2 and A_3 are pre-exponential factors, and ΔE_1 , ΔE_2 and ΔE_3 are the activation energies. R is the universal gas constant and T is the absolute temperature. B_1 , B_2 , a , b , c and d are constants of the reaction, independent of temperature. Table 6, gives the activation energies, pre-exponential factors and the constants used to characterize the variation of reaction rate, for the resin systems used as matrix material for this study

Table 6. REACTION RATE CONSTANTS FOR FIBERITE 976.

1. LINEAR FACTOR A_o

$$\begin{aligned} A_o &= 0.0044 \quad \forall \quad T < 480^\circ K \\ A_o &= 0.0000 \quad \forall \quad T > 480^\circ K \end{aligned}$$

2. PRE-EXPONENTIAL FACTORS A_1 , A_2 , and, A_3

$$\begin{aligned} A_1 &= 4400.00 \text{ 1/ sec} \\ A_2 &= 7050.00 \text{ 1/ sec} \\ A_3 &= \text{not applicable} \end{aligned}$$

3. ACTIVATION ENERGIES ΔE_1 , ΔE_2 , ΔE_3

$$\begin{aligned} \Delta E_1 &= 6250.00 \text{ Joule/mol} \\ \Delta E_2 &= 5680.00 \text{ Joule/mol} \\ \Delta E_3 &= \text{not applicable} \end{aligned}$$

4. HEAT OF REACTION FOR THE RESIN H_r

$$H_r = 530000.00 \text{ Joule/kg}$$

5. TEMPERATURE INDEPENDENT CONSTANTS B_1 , B_2 , a , b , c , d

$$\begin{aligned} B_1 &= 1.0 \\ B_2 &= -1.0 \quad \forall \quad T < 480^\circ K \\ B_2 &= 1.0 \quad \forall \quad T > 480^\circ K \\ a &= 1.03 \\ b &= 1.22 \\ c &= 0.00 \\ d &= \text{not applicable} \end{aligned}$$

Appendix B. CURE RATE DERIVATIVES

Consider the cure rate equation discribed in Appendix A. The partial derivatives of the cure rate with respect to the degree of cure at constant temperature and the partial of the cure rate with respect to the temperature at constant α , give the sensitivity of the rate expression to the changes in the state and co-state variables. They are very important regarding the optimal process control problem and play a significant role in determining the perturbation in the control

1. VARIATION OF $\frac{\partial \dot{\alpha}}{\partial T}$ DURING CURE.

$$\begin{aligned} \frac{\partial \dot{\alpha}}{\partial T} \Big|_{\alpha} = & A_o (K_1 + K_2 \alpha^a) (B_1 - \alpha)^b (1.0 - \alpha)^c \\ & + K_o \left(K_1 \frac{\Delta E_1}{R T^2} + K_2 \frac{\Delta E_2}{R T^2} \alpha^a \right) (B_1 - \alpha)^b (1.0 - \alpha)^c \quad \forall \quad \alpha \leq \alpha_c \quad (B.1) \end{aligned}$$

$$\frac{\partial \dot{\alpha}}{\partial T} \Big|_{\alpha} = K_3 \frac{\Delta E_3}{R T^2} (1.0 - \alpha)^d \quad \forall \quad \alpha > \alpha_c \quad (B.2)$$

The variation of $\frac{\partial \dot{\alpha}}{\partial T}$ gives an estimate of the change of the cure rate caused due to the changes in the temperature.

2. VARIATION OF $\frac{\partial \dot{\alpha}}{\partial \alpha}$ DURING CURE

The change in cure rate due to the variations of the co-state variable α (t) can be derived from the co-state equation Eq.(A.1) as

$$\begin{aligned} \frac{\partial \dot{\alpha}}{\partial \alpha} \Big|_T &= K_o (K_2 a \alpha^{a-1}) (B_1 - \alpha)^b (1.0 - \alpha)^c \\ &\quad - K_o (K_1 + K_2 \alpha^a) b (B_1 - \alpha)^{b-1} (1.0 - \alpha)^c \\ &\quad - K_o (K_1 + K_2 \alpha^a) (B_1 - \alpha)^b c (1 - \alpha)^{c-1} \quad \forall \quad \alpha \leq \alpha_c \quad (B.3) \end{aligned}$$

$$\frac{\partial \dot{\alpha}}{\partial \alpha} \Big|_T = - K_3 d (1.0 - \alpha)^{d-1} \quad \forall \quad \alpha > \alpha_c \quad (B.4)$$

It is to be noted that the above equations characterizing the sensitivity [57] of the reaction to the state and co-state behavior are empirical, being derived from the empirical relationship governing the reaction rate of the matrix resin being used.

Appendix C. VARIATION OF VISCOSITY

The resin viscosity as functions of the temperature and degree of cure and hence time are related by an empirical relationship given by

$$\mu = \mu_{\infty} \exp\left(\frac{U}{RT} + K_{\mu}\alpha\right) \quad (C.1)$$

where μ_{∞} is a constant, U is the activation energy for viscosity and K_{μ} is a constant independent of temperature relating the behavior of the degree of cure variations to the viscosity of the resin system.

Using Eq.(C.1), excellent correlation between data and prediction was shown in [7,8], for a few commonly used resin systems. Table 7 summarizes the constants for the resin system used in this study.

Table 7. VISCOSITY CONSTANTS FOR FIBERITE 976.

1. VISCOSITY CONSTANT μ_{∞}

$$\mu_{\infty} = 4.96 \times 10^{-7} \text{ Pa.sec}$$

2. ACTIVATION ENERGY ΔE

$$\Delta E = 4020.00 \text{ Joule/mol}$$

3. TEMPERATURE INDEPENDENT CONSTANTS K_{μ}

$$K_{\mu} = 19.3$$

Appendix D. CLASSICAL HEAT TRANSFER

The exact transient analysis, for regular geometries and isotropic systems have been carried out by various investigators. One of the primary methods used to solve the heat transfer problem is to apply fourier series as a solution to the transient heat transfer and estimate the coefficients of the series using Bessel's functions.

The classical solution for an infinitely long cylinder is based on the following assumptions

1. It is assumed that the body is at uniform temperature $T_i(r,0)$ at $t = 0$.
2. The surface of the body is suddenly exposed to a uniform convection environment, heat transfer coefficient h_o , and temperature of the surroundings of $T_\infty(t)$
3. The temperature varies with time and a single spatial variable r .

The non-dimensionalized governing equation for one dimensional, conduction heat transfer in an infinitely long cylinder, without heat generation is given by

$$\frac{\partial T}{\partial t} = \frac{\alpha}{r} \frac{\partial}{\partial r} \left[r \frac{\partial T}{\partial r} \right] \quad (D.1)$$

where α is the thermal diffusivity, r is the radial position, $T(r,t)$, is the temperature, and t is the time.

The boundary conditions for the heat transfer problem are written as

$$\frac{\partial T}{\partial r} = 0 \quad (D.2)$$

along the line of symmetry, and at the surface in contact with the fluid the flux boundary condition becomes

$$-K \frac{\partial T}{\partial r} = h_o (T - T_{\infty}(t)) \quad (D.3)$$

where h_o is the heat transfer coefficient of the fluid, $T_{\infty}(t)$, is the ambient temperature of the fluid in contact with the surface, and K is the thermal conductivity.

The initial condition governing all points at $t = 0$ is

$$T_i(r) = T(r,0) \quad (D.4)$$

The fourier series solution to the above problem have been presented in literature [29,30,40], as

$$T(r,t) = T_o + (T_i - T_o) + \sum_{l=1}^{\infty} C_l e^{(-\frac{\beta_l^2 \alpha t}{r_o^2})} J_o(\beta_l \frac{r}{r_o}) \quad (D.5)$$

The coefficients C_l are

$$C_i = \frac{2}{\beta_i} \frac{J_1(\beta_i)}{J_0^2(\beta_i) + J_1^2(\beta_i)}$$

and β_i are the roots of the algebraic equation

$$\beta_i \frac{J_1(\beta_i)}{J_0(\beta_i)} = B_i = \frac{h_o r_o}{k} \quad (D.6)$$

and J_1 and J_0 are the Bessel's functions of the first kind and B_i is the Biot number. The constants C_i can be calculated with the help of the Heisler charts. Heisler [41] recommends that for non - dimensional time $t^* > 0.2$, only the coefficient C_1 plays a significant part in contributing to the overall solution. Using this argument, and the centerline $r = 0$ as the reference, the temperature of the innermost point, (i.e., the point that takes the longest time to heat up) can be written as

$$T_c(r) = T_\infty + (T_i(r) - T_\infty) C_1 e^{-\beta_1^2 t^*} \quad (D.7)$$

Temperatures at all other radial locations in the domain are related to the centerline temperature through the expression

$$\frac{(T(r) - T_\infty)}{(T_i(r) - T_\infty)} = C_1 e^{-\beta_1^2 t^*} J_0(\beta_1 \frac{r}{r_o}) \quad (D.8)$$

Vita

Nagendra Somanath was born on the twenty second day of the month of October in the year Nineteen Sixty Two, Hassan, India. On graduation from Our Lady of Good Counsel High School in Bombay he entered the Indian Institute of Technology, Bombay as an Aeronautical Engineering major. He received his Bachelor of Technology degree on the 15'th of April 1985 and entered Virginia Polytechnic Institute and State University in September 1985 to work towards a Master of Science degree in Engineering Mechanics. On completion of his masters he intends to pursue his studies towards a doctorate at Virginia Tech.

Nagendra